TENNESSEE VALLEY AUTHORITY

CHATTANOOGA, TENNESSEE 37401

400 Chestnut Street Tower II

November 1, 1982

Director of Nuclear Reactor Regulation
Attention: Ms. E. Adensam, Chief
Licensing Branch No. 4
Division of Licensing
U.S. Nuclear Regulatory Commission
Washington, D.C. 20555

Dear Ms. Adensam:

In the Matter of) Docket Nos. 50-327
Tennessee Valley Authority) 50-328

We have provided, as Enclosure 1, our response to Thomas M. Novak's September 17, 1982 letter to H. G. Parris requesting additional information on hydrogen control for ice condenser plants. Also provided, as Enclosure 2, is our response to your October 1, 1982 letter to H. G. Parris requesting additional information on equipment temperature response to hydrogen burns. Also included in the response to the NRC question 2 of Enclosure 2 is a summary of the results of the Tayco igniter tests requested by NRC. This submittal responds to all of the outstanding NRC questions regarding hydrogen combustion and control and the associated hydrogen research program.

If you have any questions concerning this matter, please get in touch with J. E. Wills at FTS 858-2683.

Very truly yours,

TENNESSEE VALLEY AUTHORITY

L. M. Mills, Manager
Nuclear Licensing

Sworn to and subscribed before me
this 1st day of Nov. 1982

Bryant M. Lowery
Notary Public
My Commission Expires 4/8/86

B021

Enclosures
cc: U.S. Nuclear Regulatory Commission
Region II
Attn: Mr. James P. O'Reilly, Regional Administrator
101 Marietta Street, Suite 3100
Atlanta, Georgia 30303

ENCLOSURE 1

RESPONSE TO THOMAS M. NOVAK'S SEPTEMBER 17, 1982 LETTER TO H. G. PARRIS REQUESTING ADDITIONAL INFORMATION ON HYDROGEN CONTROL FOR ICE CONDENSER PLANTS

SEQUOYAH NUCLEAR PLANT

RESPONSE TO
REQUEST FOR ADDITIONAL INFORMATION
ON HYDROGEN CONTROL FOR ICE CONDENSER PLANTS

Question 1

A substantial number of laboratory tests were conducted as part of the ICOG-EPRI R&D Program for Hydrogen Control and Combustion. Test results were transmitted from the utilities to NRC as they became available. However, for several of the research programs, only selected test results were reported and organized compilations of all pertinent test information were not provided. This information is required to confirm the adequacy of the test program and assumptions made in the containment analyses. In this regard provide the following:

a) ACUREX

i) A table of droplet size and droplet density estimates for each of the fog/spray tests.

ii) A table of estimated flame speed for each test (flame speed should be calculable from thermocouple locations and ignition time data).

iii) Pressure and temperature traces similar to those depicted in Figures 4-2 of the December 1981 Acurex Project Report, but for tests 2.10, 2.11, and 2.12.

b) FACTORY MUTUAL

Results of ignition tests in which a glow plug was used in place of the ignition electrodes.

c) WHITESHELL

Tables summarizing pre- and post-burn conditions, igniter locations, maximum measured pressure rise, adiabatic pressure rise, completeness of burn, and estimated flame speed. These tables should be keyed to and cover all of the tests committed to in the test matrix (Tables 1-4 in Appendix A.1 of the fourth quarterly report on the TVA research program, June 16, 1981) plus any additional AECL tests conducted under this program. Of particular interest to the staff are the results of the 8.5% H_2 test with 30% H_2O and top ignition. Discuss your plans for conducting tests at steam concentrations above 30%, as committed to in previous quarterly reports.

d) HEDL

Figures depicting concentration gradients for each of the tests. Figures provided should permit better resolution than those included in the previous submittal.

Response 1

a)(i) The Acurex test vessel was not instrumented to measure either the droplet size or density during the fog/spray tests. An estimate of these parameters may be made from data obtained by Factory Mutual for the Acurex nozzles and reported in Appendix A.5 of TVA's Quarterly Report No. 5 submitted January 22, 1982. However, it should be recognized that differences in vessel geometry and nozzle number and arrangement between Factory Mutual and Acurex would affect the fog/spray conditions present during the Acurex tests.

(ii) The Acurex test vessel was not instrumented to measure localized flame speeds. An estimate of an "average" global flame speed may be calculated from the pressure rise data of the type reported in Appendix A.4 of TVA's Quarterly Report No. 5. Estimates of these "average" flame speed ranges were reported in section IV.D of the technical summary which was attached to TVA's executive summary report, submitted September 27, 1982.

(iii) Refer to Figures 1-1 through 1-6 for pressure and temperature responses from Acurex tests 2.10, 2.11, and 2.12.

b) The data from the Factory Mutual fog inerting tests, originally reported in Appendix A.5 of Quarterly Report No. 5, have been identified by igniter type in Tables 1-1 through 1-3.

c) Refer to Tables 1-4 through 1-6 for measured and calculated data from the Whiteshell CTF tests. The adiabatic pressure rises were not calculated and the flame speeds were not measured. However, the pressure rise time (t_{max}), which is the parameter of importance in estimating the speed at which the combustion event occurs, was measured and is included in the tables. The tables are keyed to the original numbers from TVA's Quarterly Report No. 4. Note that some tests were altered from the original list in Quarterly Report No. 4, submitted September 22, 1981, as the research progressed, e.g., the steam concentrations in series 2 were revised upward to include tests at 40 and 50 volume percent. The omission of test QR No. 1-19 (8.5% H_2, 30% steam, top ignition) was inadvertent. The test will be performed by early November (which is the earliest opportunity since other testing is currently underway at the Whiteshell facility). It should be emphasized that quite a few more CTF tests were actually performed than the number to which had been committed. In addition, numerous tests, including several with high steam concentrations in lean hydrogen mixtures, were performed in the Whiteshell small-vessel, igniter performance testing reported in Appendix A.2 of Quarterly Report No. 5.

d) Refer to Figures 1-7 and 1-8 for the maximum hydrogen (helium) concentration gradient transient data from each of the Hanford tests. The maximum difference reached a relatively steady state value during the release period for all tests. In addition, the maximum measured gradient during any test was less than 3 volume percent, except for tests HM-1A and HM-2. These two tests were performed with no recirculation flow from the simulated air return fans. Following termination of the helium-steam source, the lower compartment pressure decreased below the upper

Figure 1-1

Test 2.10

Centerline Temperature T2

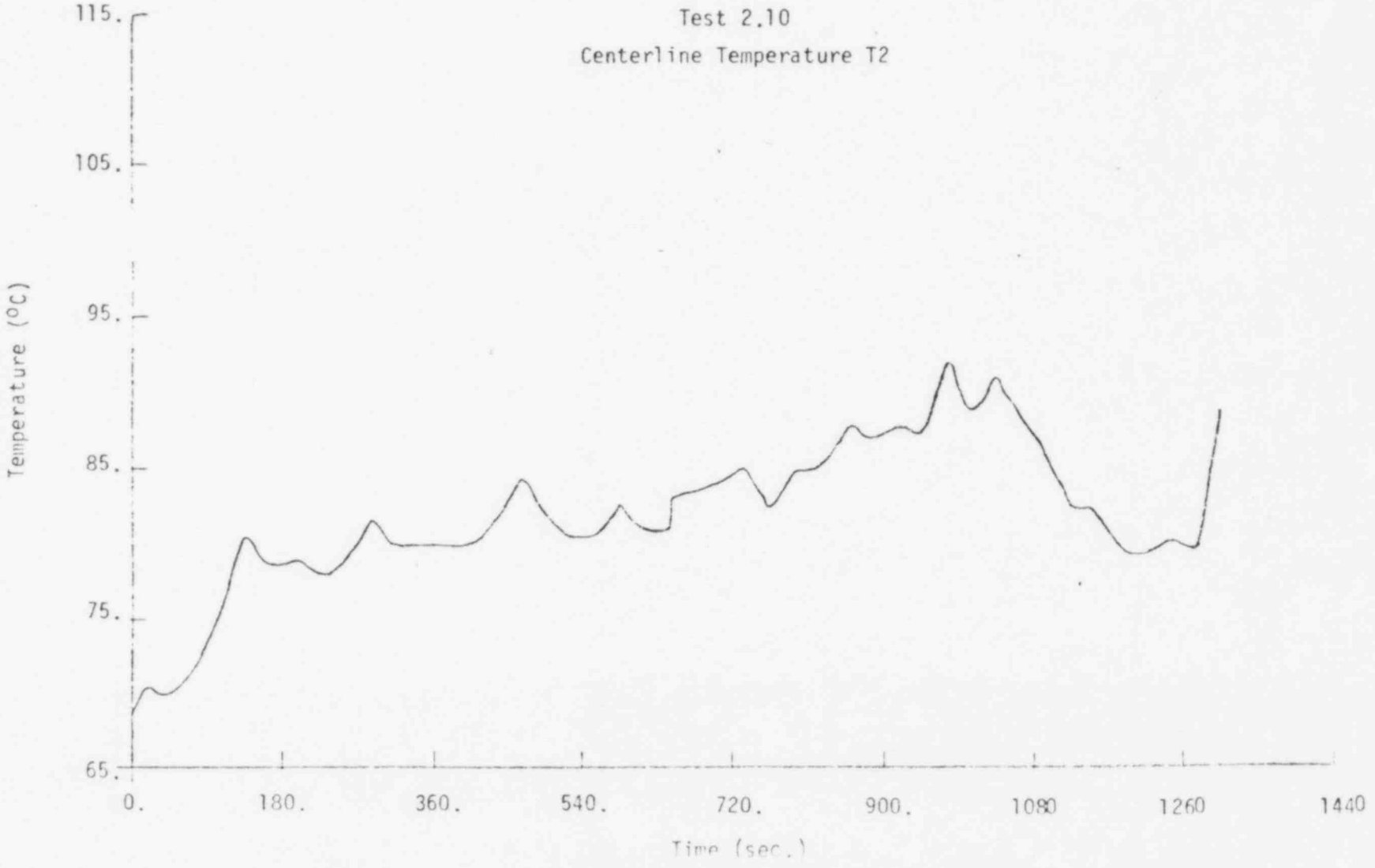

Figure 1-2

Test 2.10

Vessel Pressure P2

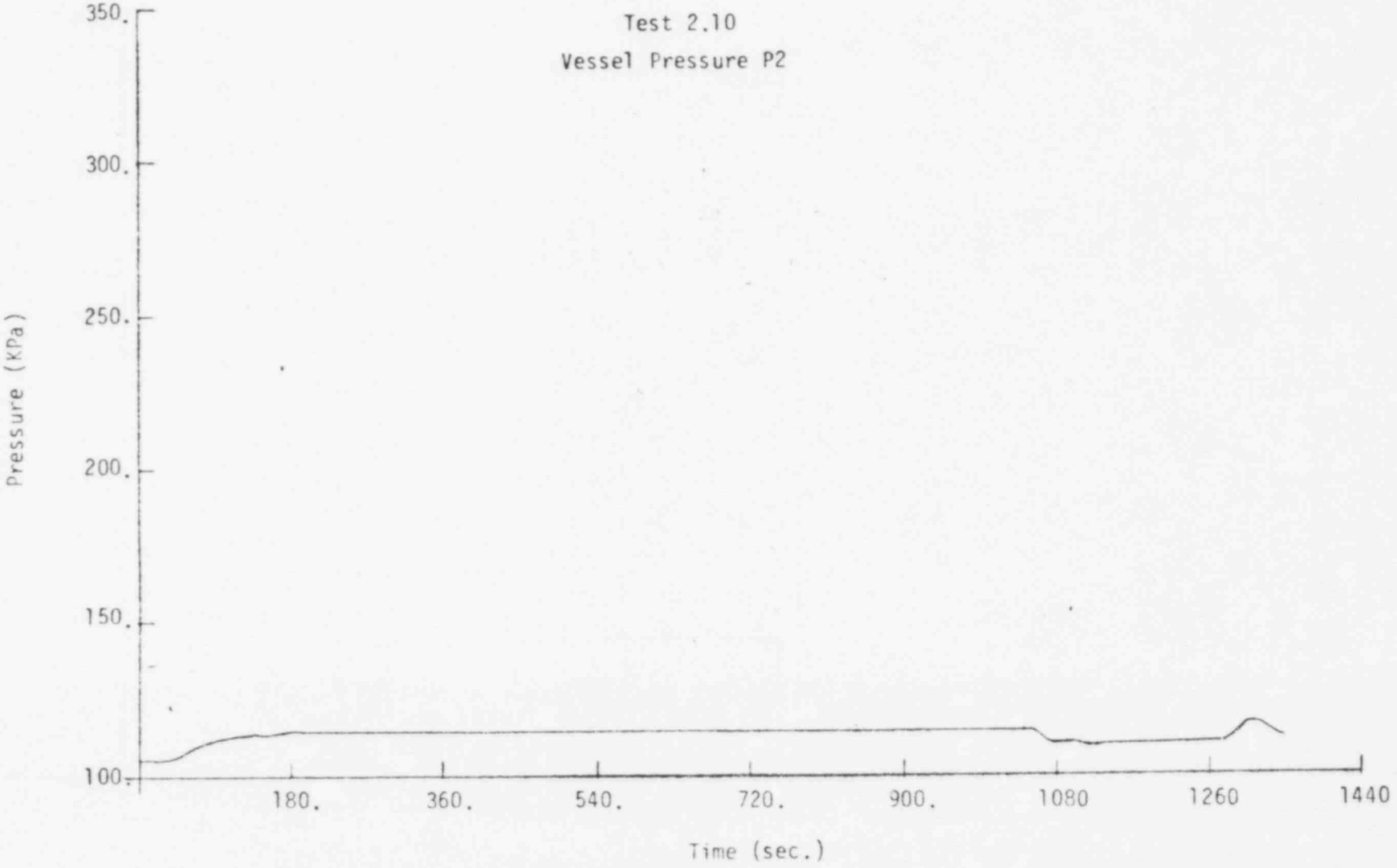

Figure 1-3

Test 2.11

Centerline Temperature T2

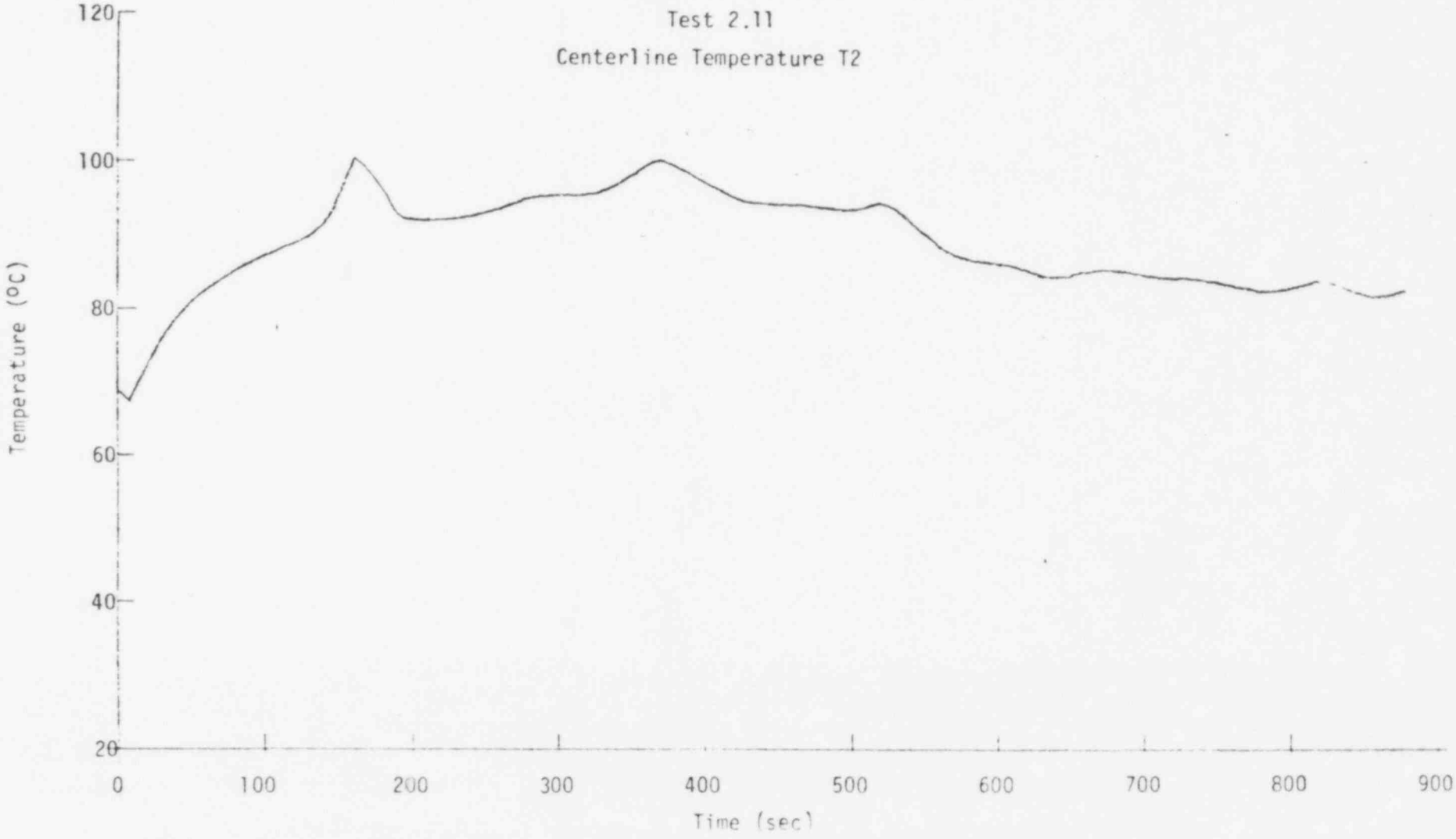

Figure 1-4

Test 2.11

Vessel Pressure P2

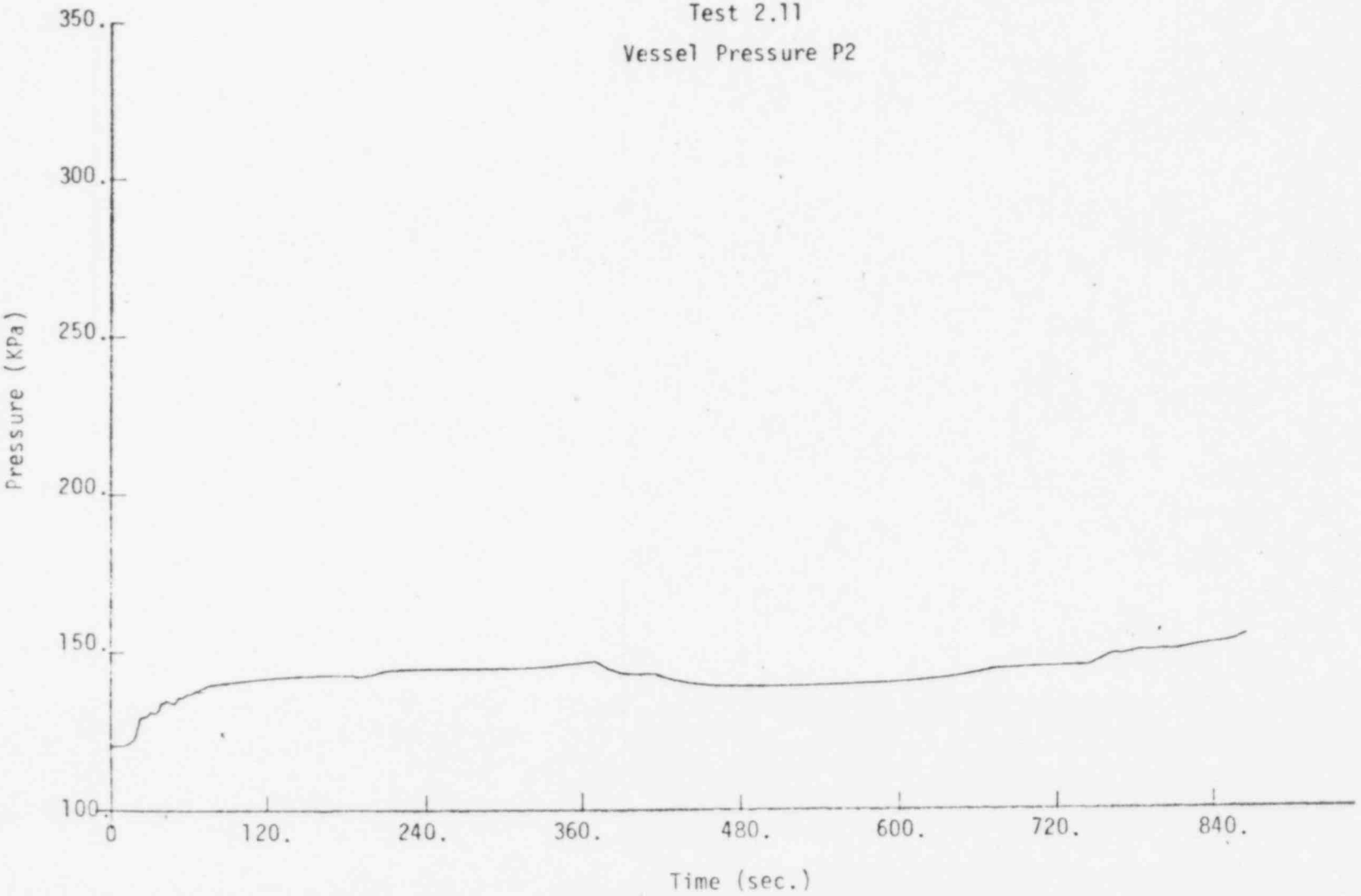

Figure 1-5

Test 2.12

Centerline Temperature T2

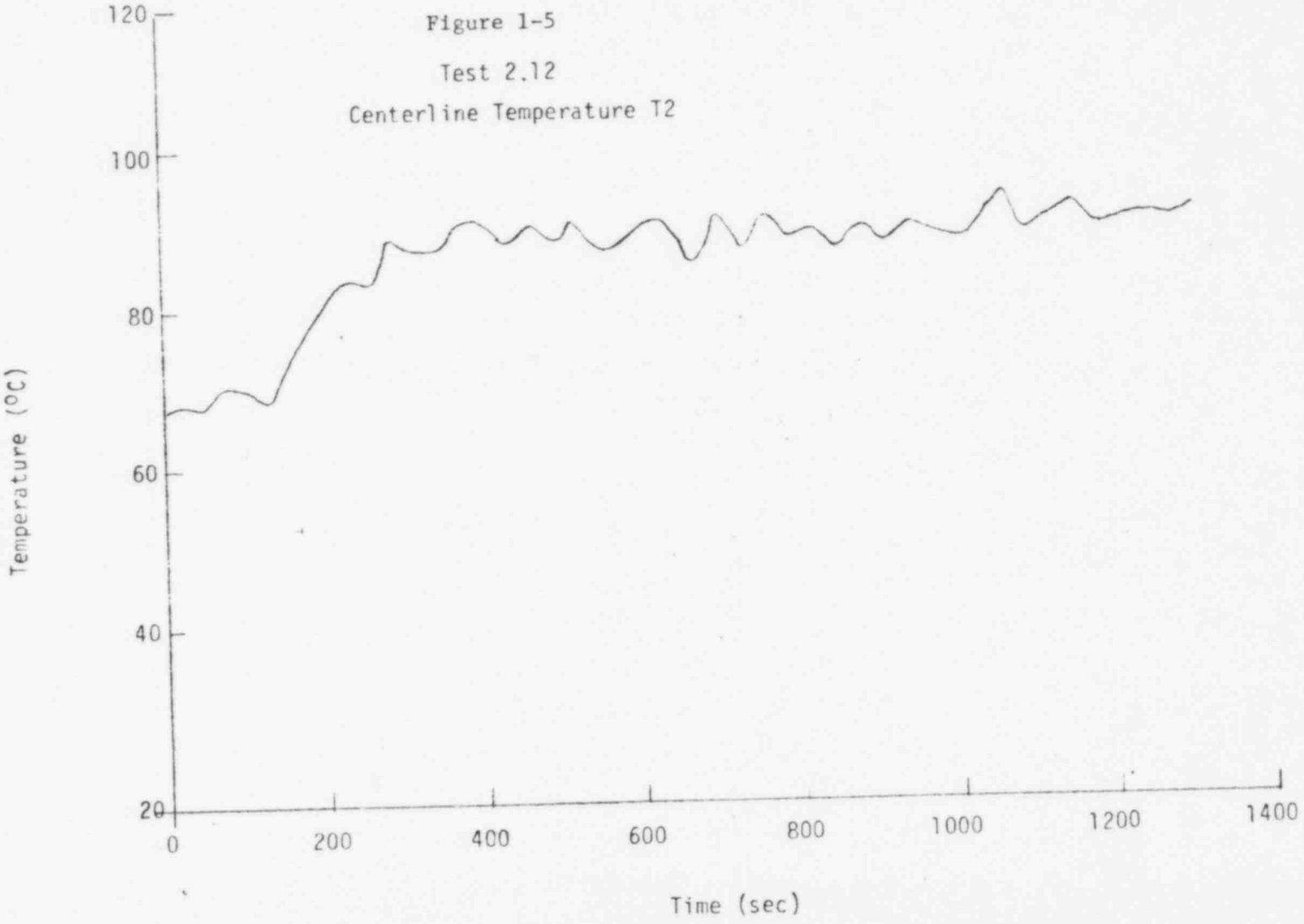

Figure 1-6

Test 2.12

Vessel Pressure P2

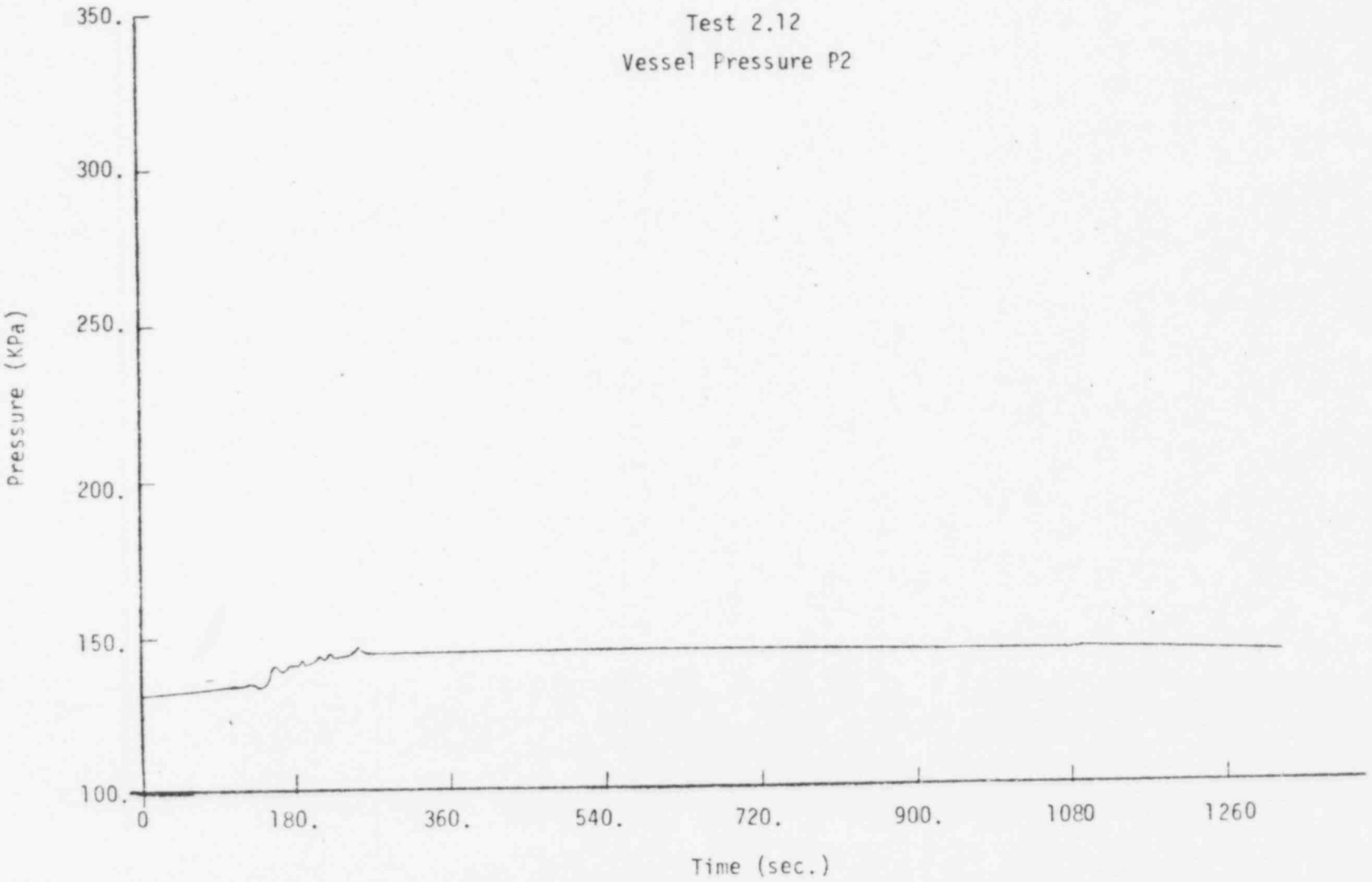

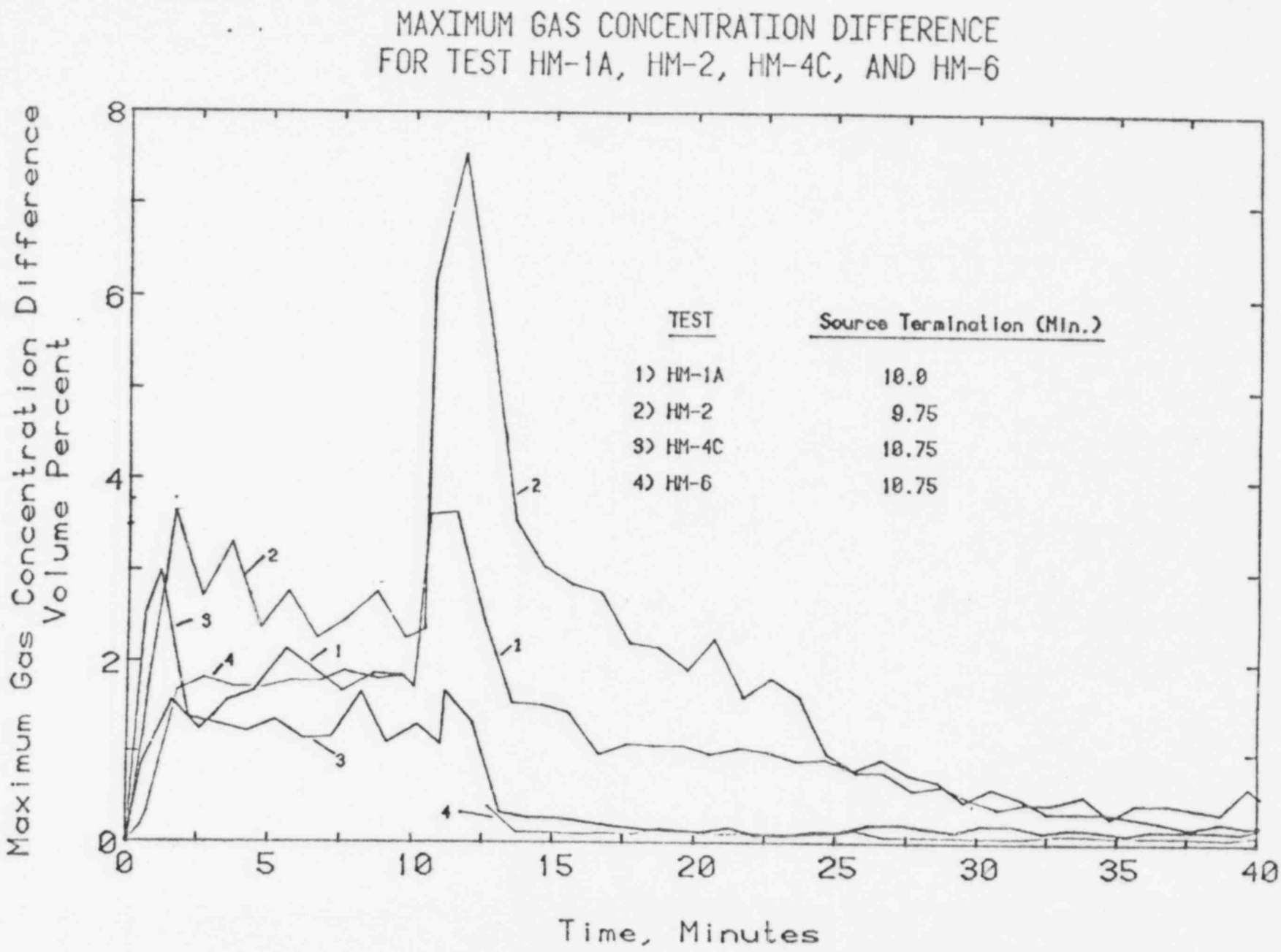
MAXIMUM GAS CONCENTRATION DIFFERENCE
FOR TEST HM-1A, HM-2, HM-4C, AND HM-6
Maximum Gas Concentration Difference
Volume Percent
Time, Minutes
0
2
4
6
8
0
5
10
15
20
25
30
35
40
TEST
Source Termination (Min.)
1) HM-1A
10.0
2) HM-2
9.75
3) HM-4C
10.75
4) HM-6
10.75
1
2
3
4

FIGURE 1-7

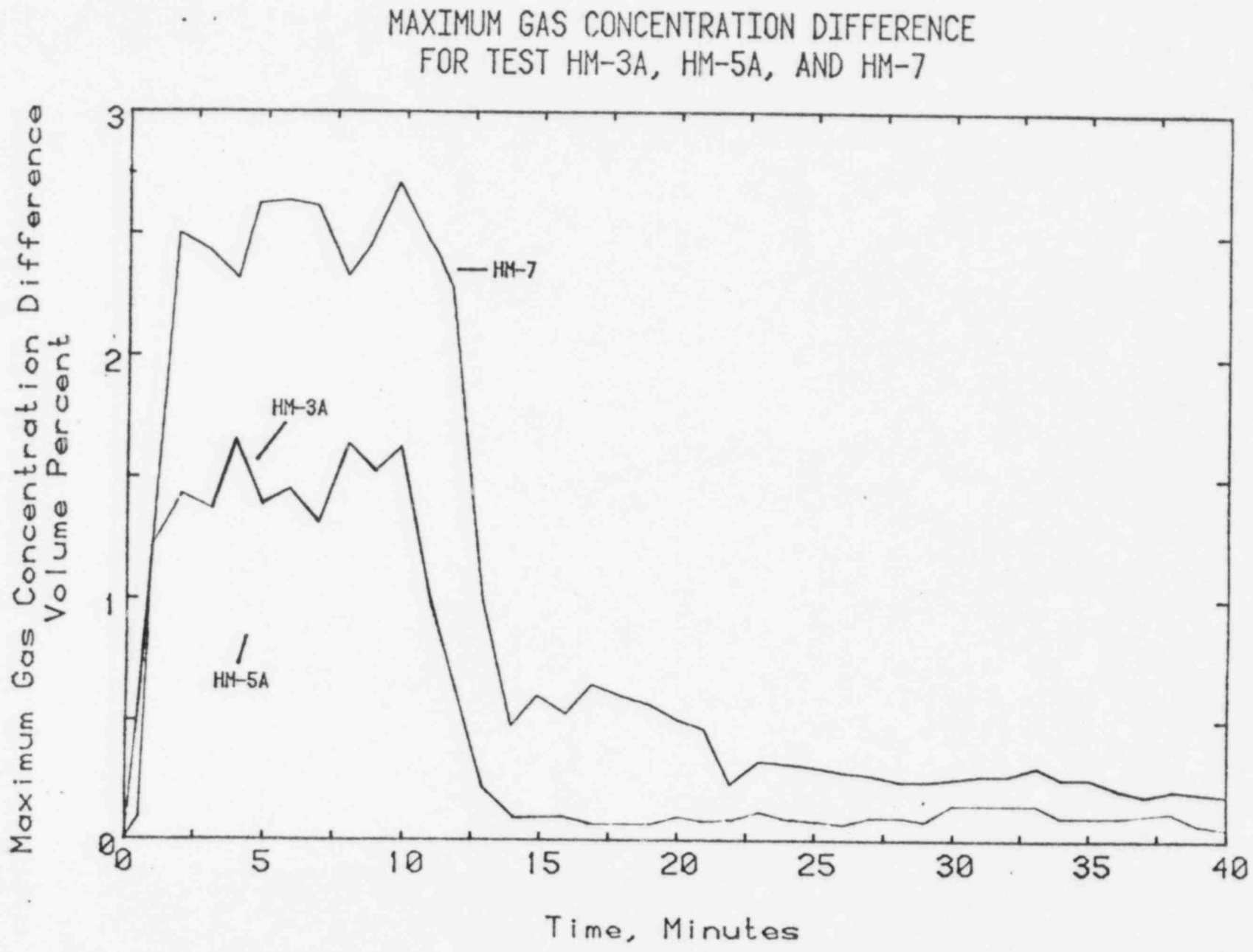
MAXIMUM GAS CONCENTRATION DIFFERENCE
FOR TEST HM-3A, HM-5A, AND HM-7
Maximum Gas Concentration Difference
Volume Percent
HM-7
HM-3A
HM-5A
0
1
2
3
0
5
10
15
20
25
30
35
40
Time, Minutes

FIGURE 1-8

TABLE 1-1

HYDROGEN-WATER FOG INERTING DATA AT 20°C

Nozzle	Pressure (psig)	Spray Angle (Full)	Drop Size Vol. Mean (Micron)	Drop Size No. Median (Micron)	Conc. $\frac{cm^3 H_2O}{cm^3 Mix}$	Igniter	Hydrogen LFL (vol %)
Spraco	10		111	9.8	8.1×10^{-4}	Spark	4.42 ± 0.11
2163-7604	20	~60°	54.5	4.7	3.8×10^{-4}	Spark	4.76 ± 0.31
~60°	25		44.1	3.8	2.7×10^{-4}	Spark	4.76 ± 0.31
	30	~60°	20.6	1.5	2.8×10^{-4}	Spark	4.72 ± 0.28
	30	~60°	20.6	1.5	2.8×10^{-4}	Glow Plug	5.0 ± 0.24
Spraco	10	61°	139	13	3.0×10^{-3}	Spark	4.64 ± 0.12
2020-1704	20		86.2	6.8	8.5×10^{-4}	Spark	4.76 ± 0.31
	25		58.4	4.8	2.9×10^{-4}	Spark	4.76 ± 0.31
	30	80°	35.7	5.6	1.5×10^{-4}	Spark	5.26 ± 0.1
Spraco	10		136	13	9.4×10^{-5}	Spark	4.40 ± 0.1
1806-1605	20		59.3	5	6.0×10^{-5}	Spark	4.76 ± 0.3
	25		66	4	5.7×10^{-4}	Spark	4.76 ± 0.3
	30	~40°	47.8	6.4	3.2×10^{-4}	Spark	4.65 ± 0.3
Spraco	10		136	14	4.5×10^{-3}	Spark	4.64 ± 0.1
1409-0604	20		110	10	2.2×10^{-2}	Spark	4.76 ± 0.
(20-30°)	25		114	11	2.7×10^{-2}	Spark	4.76 ± 0.
	30	20°	115	14	3.3×10^{-2}	Spark	5.26 ± 0.
Sonicore	20		-	5	1.1×10^{-3}	Spark	7.2 ± 0

03514

TABLE 1-2

HYDROGEN-WATER FOG INERTING DATA AT 50°C

Nozzle	Pressure (psi)	Drop Size Vol. Mean (Micron)	Drop Size No. Median (Micron)	Conc. $\frac{cm^3 H_2O}{cm^3 Mix}$	Igniter	Hydrogen LFL (vol %)
Spraco	40	33.1	5.2	1.4×10^{-4}	Spark	7.19 ± 0.22
2163-7604	30	21.4	4.2	8.1×10^{-5}	Spark	5.55 ± 0.11
	20	34.5	4.5	1.9×10^{-4}	Spark	5.55 ± 0.11
Spraco	40	24.5	3.8	9.3×10^{-5}	Spark	7.19 ± 0.22
2020-1704	30	27.1	4.2	1.1×10^{-4}	Spark	7.19 ± 0.22
	20	50.3	6.2	4.0×10^{-4}	Spark	6.32 ± 0.22
Spraco	10	-	-	-	Glow Plug	4.98 ± 0.22
1806-1605	20	43.2	-	9.7×10^{-5}	Glow Plug	5.22 ± 0.42
	30	15.2	-	1.6×10^{-5}	Glow Plug	5.44 ± 0.22
	40	11.2	3	1.9×10^{-5}	Glow Plug	5.18 ± 0.42
	40	11.2	3	1.9×10^{-5}	Spark	5.35 ± 0.42
Spraco	40	87.8	9.6	3.2×10^{-2}	Spark	5.55 ± 0.11
1405-0604	30	91.8	11.5	2.0×10^{-2}	Spark	5.55 ± 0.11
	25	115	14	1.7×10^{-2}	Spark	5.55 ± 0.11
Sonicore	25	24	2.4	1.1×10^{-3}	Spark	7.93 ± 0.23
035H	20	24.4	2.8	1.1×10^{-3}	Spark	7.19 ± 0.22

TABLE 1-3

HYDROGEN-WATER FOG INERTING DATA AT ~70°C

Nozzle	Press. (psi)	Igniter	Hydrogen LFL (vol %)
Spraco	10	Glow Plug	6.76 ± 0.22
2163-7604	20	Glow Plug	7.18 ± 0.22
	30	Glow Plug	7.62 ± 0.22
	40	Glow Plug	8.46 ± 0.22
Spraco	10	Glow Plug	5.88 ± 0.21
1405-0604	20	Glow Plug	6.32 ± 0.21
	30	Glow Plug	7.62 ± 0.21
	40	Glow Plug	7.62 ± 0.21

TABLE 1-4

CTF EXPERIMENTAL SERIES 1 AND 3

Q.R. No.	Exp. No. CTF-	Hydrogen (%)	Steam (%)	Air (%)	Fan	ΔP_m (kPa)	t_{max} (sec)	Burn (%)
1-1	101	5.0	0	95.0	off	13	9.5	~ 20
1-2	102	5.5	0	94.5	off	24	6.0	~ 26
1-3	103	6.0	0	94.0	off	27	5.0	~ 23
1-7	110	5.0	15	80.0	off	10	6.5	~ 20
1-8	111	5.0	15	80.0	off	8	7.0	~ 20
1-9	124 R	5.0	30	65.0	off	~7	7.0	~ 20
1-4	123	6.2	0	93.8	off	~47	6.0	30
3-1	105	5.5	0	94.5	on	105	1.5	~ 83
1-5	106	7.0	0	93.0	off	125	7.0	~ 100
3-2	107	7.0	0	93.0	on	161	1.2	100
1-10,11	125	6.0	15	79.0	on	87	1.5	60
1-13,14	126	6.0	30	64.0	on	65	1.6	50
1-6	108	8.0	0	92.0	off	146	4.2	100
1-12	113	8.0	15	77.0	off	126	4.9	100
1-15	116	8.0	30	62.0	off	38	5.0	38
3-3	109	8.0	0	92.0	on	187	0.8	100
1-16	117 (CI)	7.0	0	93.0	off	110	11.4	100
1-17	118 (CI)	7.0	15	78.0	off	45	4.5	~ 0
	118A (CI)	7.0	15	78.0	on	142	1.0	100
	119 (CI)	10.0	0	90.0	on	215	0.53	100
3-7	120 (CI)	14.0	0	86.0	on	290(?)	0.4	100
	CT 704 (TI)	11.0	0	89.0	on	225	0.6	100
	CT 701 (TI)	8.0	0	92.0	on	180	0.9	100
1-18	CT 702 (TI)	8.5	0	91.5	off	157	3.2	100
	CT 700 (TI)	7.0	0	93.0	on	145	1.1	100
	CT 703 (TI)	5.7	0	94.3	on	75	1.9	~ 72
	*CT 502	8.4	0	91.6	off	175	---	~ 100
	*CT 501	10.0	0	90.0	off	260	---	~ 100
	*CT 504	5.0	0	95.0	off	10	5.5	----
	*TST 10	6.0	0	94.0	off	175	---	----
	*TST 16	8.5	0	91.5	off	232	---	----
	*TST 13	7.5	0	92.5	off	20	---	----
	*TST 11	5.5	0	94.5	off	19	---	----

NOTES:

1. All experiments initially at 100°C except those indicated with an "*" were conducted at 28 ± 2°C.

2. Initial pressure 98 kPa.

3. All experiments are with bottom ignition except that those indicated with "CI" are with central ignition and those with "TI" are with top ignition.

TABLE 1-5

CTF EXPERIMENTAL SERIES 2 AND 3

Q.R. No.	Exp. No. CTF-	Hydrogen (%)	Steam (%)	Air (%)	Final H_2 (%)	ΔP_m (kPa)	t_{max} (sec)	Burn (%)
2-4	204	41.5	0.0	58.3	20.0*	403	0.07	56
	230	41.6	0.0	58.4	19.7*	424	0.06	59
	203	32.6	0.0	67.4	6.0*	452	0.06	84
	222	36.5	0.0	63.5	13.0*	434	0.06	70
	203A	31.0	0.0	69.0	2.4*	455	0.06	94
	223	27.0	0.0	73.0	0.0	441	0.07	100
2-3	236	29.6	0.0	70.4	0.0	469	0.05	100
2-17	217	15.0	0.0	85.0	0.0	303	0.11	100
2-2	202C	20.0	0.0	80.0	0.0	390	----	100
2-1	201R	10.0	0.0	90.0	0.0	215	0.87	100
	233	36.4	20.0	43.6	20.0*	331	0.12	50
	232	24.6	20.0	55.4	1.5*	369	0.12	93
	219	25.0	20.0	55.0	2.2*	359	0.18	92
2-12	212	35.5	20.0	44.5	19.0*	338	0.13	52
	231	29.5	0.0	70.5	0.0	462	0.05	100
2-5	205	11.0	10.0	79.0	0.0	216	0.72	100
2-7	237	30.0	10.0	60.0	5.5*	410	0.09	84
2-9	209	10.0	20.0	70.0	0.0	159	2.40	100
2-13	213B	10.0	30.0	60.0	0.0	148	3.20	100
	219B	10.0	40.0	50.0	0.0	112	6.10	100
2-10	210	16.0	20.0	64.0	0.0	293	0.27	100
	219C	10.0	50.0	40.0	10.0	0.0	----	0
	207	27.0	10.0	63.0	0.7*	407	0.15	98
2-11	211	28.0	20.0	52.0	7.0*	365	0.13	78
2-14	229	21.0	30.0	49.0	0.5*	321	0.22	98
	238	28.6	10.0	61.4	3.2*	407	0.07	90
	220(Bot Ign)	27.0	0.0	73.0	0.0	434	0.09	100
	221	25.4	0.0	74.6	0.0	434	0.075	100
2-16	216A	30.4	30.0	39.6	15.0*	255	0.45	55
	214	15.6	30.0	54.4	0.0	255	0.60	100
2-15	234	29.0	30.0	41.0	13.0*	283	0.24	59
	235	31.0	0.0	69.0	2.0*	463	0.05	94
2-18	218(Bot Ign)	20.0	0.0	80.0	0.0	386	0.14	100
	226	22.2	30.0	47.7	2.5*	300	0.27	90
2-6	224	25.0	10.0	65.0	0.0	407	0.08	100
	201R	10.0	0.0	90.0	0.0	210	0.80	100
3-8	207A (Fan)	27.0	10.0	63.0	0.5*	400	0.07	98
2-8	208	40.0	10.0	50.0	21.0*	345	0.11	53
3-10	310	20.0	0.0	80.0	0.0	359	0.09	100
3-6	308 (Fan)	7.0	0.0	93.0	0.0	145	1.50	100
3-4	306	6.0	0.0	94.0	3.0	55	5.50	51
3-9	309	15.0	0.0	85.0	0.0	283	0.24	100
	307B(Bot Ign)	10.3	0.0	89.7	0.0	179	1.25	100
	307A(Bot Ign)	11.5	0.0	87.9	0.0	186	1.00	100
3-5	307 (Bot Ign)	6.71	0.0	93.3	0.25	85	4.0	96

NOTES: (See second page)

NOTES FOR TABLE 1-5

* = Calculated

1. Initial temperature: 100°C

2. Initial pressure: 98 kPa

3. Unless stated, experiments are with central ignition

4. Experimental series 300 is with gratings

TABLE 1-6

CTF EXPERIMENTAL SERIES 4

Q.R. No.	Exp. No. CTF-	H_2(Pipe) (%)	H_2(Sphere) (%)	ΔP_m (kPa)	t_{max} (sec)	Burn (%)
	405 (EI)	10.0	10.0	248	6.75	100
	402A (EI)	8.0	8.0	210	14.75	100
	Fan on					
4-3	402A Fan off	8.0	8.0	10	16.0	~ 0
	404 (EI)	6.5	6.5	115	23.0	70
	Fan on					
	404 (EI)	6.5	6.5	2	24.0	~ 0
	Fan off					
4-4	401 (EI)	20.0	20.0	510	0.2	100
	Fan off					
4-1	407A (CI)	8.5	8.5	165	14.0	100
	Fan off					
	409 (CI)	10.0	10.0	225	1.8	100
	Fan off					
4-2	408 (CI)	20.0	20.0	500	0.15	100
	Fan off					
	410 (CI)	25.0	25.0	1300	.075	100
	Fan off					
	411 (EI)	10.0	10.0	260	5.5	100
	Constriction					
	412 (EI)	20.0	20.0	525	0.2	100
	Constriction					
4-5	418 (EI)	12.0	6.0	105p,135s	1.1	~ 0
	Burst Disk					
4-6	419 (EI)	15.0	6.0	115p,115s	.35p,.85s	70
	Burst Disk					
	416 (EI)	15.0	10.0	120p,325s	0.28p,.375s	100*
	Burst Disk					
	415 (EI)	15.0	20.0	120p,525s	0.32p,.4s	100*
	Burst Disk					

NOTES:

* = Assumed

1. All experiments at 24 $\pm$ 2°C, 98 kPa

2. s = sphere, p = pipe

3. EI = pipe end ignition

   CI = sphere central ignition

compartment pressure as the temperature decreased and the steam in the compartment condensed. The resulting low pressure caused a reverse migration through the slots simulating the ice condenser doors which, coupled with a lack of mixing from the fans or the source jet, created a maximum concentration difference of 3.5 volume percent for test HM-1A and 7.5 volume percent for test HM-2. The reverse flow condition which caused these high concentration differences was not prototypic of ice condenser containment conditions since the actual ice condenser is provided with doors which would simply close once the lower compartment pressure was no longer greater than the upper compartment pressure. Therefore, the post-release concentration differences in tests HM-1A and HM-2 are considered to be anomalous due to the simulation of the ice condenser doors in the test vessel design.

Question 2

The majority of the ICOG-EPRI tests which serve to demonstrate the validity of the deliberate ignition concept utilized a GMAC glow plug as the ignition source. TVA currently intends to install 120-V TAYCO igniters in the Permanent Hydrogen Mitigation System instead of the glow plugs. Although igniter durability tests have been completed by Singleton, additional testing of the 120-V igniter is required to show that it is an acceptable replacement for the GMAC igniter. Specifically,

a) Tests should be conducted to ensure that the igniter will continue to operate as intended in a spray atmosphere typical of that which would be expected in each region of containment where igniters are to be located.

b) Endurance tests should be conducted on a suitable sample size to assure adequacy and consistency of igniter surface temperature and lifetime.

Response 2

a) Tests have been conducted at TVA's Singleton Laboratory to ensure that the Tayco igniter assembly would continue to operate as intended in a typical containment spray atmosphere. The tests were conducted indoors in a room routinely used for spraying materials. The spray nozzle was a SPRACO hollow-cone nozzle (model No. 16711810) which was used in the utility-sponsored tests on the GM igniter at Fenwal, Inc. Several flow rates were tested at Singleton; the highest being 3.5 gal/min at 20 psid. The nozzle was oriented vertically downward and was located three feet above the igniter. The igniter was oriented horizontally and was mounted under a horizontal spray shield of the same configuration as the ones on the igniter assemblies to be installed in Sequoyah. The shield extended out over the igniter four inches from the mounting plate and was eight inches wide. The igniter extended about three inches out from the plate. In most of the tests, the igniter was mounted ten inches below the shield to correspond with the lowest relative position in any assembly in the plant.

   In the first test series, the initial igniter surface temperature varied between 1700-1730°F. When the spray nozzle was actuated, the igniter temperature dropped to between 1650-1690°F within about five minutes and remained relatively stable for the remaining 30 minutes of the test.

   In the second test series, a large room fan was placed about five feet from the front of the igniter facing it along its axis. This forced turbulence was intended to simulate a potentially turbulent local containment environment and increase the spray cooling effect. The local air velocity measured at the igniter location due to the fan was 400 ft/min $\pm$ 50. Again, the initial igniter surface temperature varied between 1700-1730°F. When the spray and fan were activated, the igniter temperature dropped to between 1600-1635°F within five minutes and remained stable for the remainder of the test.

   Even the 1600°F surface temperature with the fan-induced turbulence is well above the 1350°F surface temperature determined at Whiteshell to be the maximum required to ignite even lean hydrogen, rich steam mixtures. (Refer to TVA's summary of Tayco igniter testing submitted June 14, 1982.) Therefore, we believe that the Tayco igniter assembly would function effectively in a representative containment spray environment.

b) In addition to the single Tayco igniter that previously underwent endurance testing at Singleton, three additional igniters have been tested. These three were each subjected to a series of five tests consisting of endurance and cycling.

The first test consisted of energizing the igniters continuously for 24 hours in an open room at 120-V ac to initially determine their surface temperature capability. The minimum surface temperatures recorded following the initial warmup period ranged from 1715-1770°F.

Following the initial warmup test, the first of two endurance tests was performed. This test consisted of energizing the igniters for one week at 120-V ac to determine the surface temperature over an extended period. The average surface temperature of the three igniters during the test was between 1713-1742°F and the minimum temperature was between 1683-1732°F. The gradual decrease in measured igniter surface temperature during extended tests has been found to result from the use of spot-welded thermocouples as a measurement technique. When the thermocouples have been cleaned and re-welded to the igniter between test series, temperatures essentially the same as the initial temperatures are again measured. This indicates that some gradual deterioration of the thermocouple contact is probably occurring.

After the first endurance test, the third test consisted of cycling the igniters on/off 10 times each at 120-, 125-, 130-, and 135-V ac to assess their durability under thermal cycling. In each cycle the igniters were energized for five minutes and then allowed to cool to ambient. Surface temperatures in excess of 1700°F were reached within two minutes after the igniter was energized. The average peak surface temperature over ten cycles at 120-V ac varied from 1737-1773°F and over ten cycles at 135-V ac varied from 1838-1900°F.

The fourth test was the other endurance test in which the igniters were energized for one week at 135-V ac. During the seventh day of the test, one of the igniters failed to maintain an elevated temperature. The cause of failure has not been determined. The igniter had maintained an average surface temperature for more than 6 days of 1849°F and a minimum temperature of 1826°F before failure. The other two igniters continued to function satisfactorily with an average surface temperature during the test between 1797-1863°F and a minimum temperature between 1760-1841°F.

The final test was another cycling test similar to the first one with 10 cycles at each of the four voltages. The average peak surface temperature of the two igniters over 10 cycles at 120-V ac was between 1729-1774°F and over 10 cycles at 135-V ac varied from 1850-1905°F.

Two of the three additional Tayco igniters successfully survived all of the conditions to which they were subjected and continued to perform. The single failure occurred in the last day of a one-week test at 135-V ac. This voltage level is well above the normal expected voltage of 120-V ac which would be supplied at Sequoyah by the regulating transformer and, as such, is an extreme condition. In addition, the failed igniter successfully passed the initial 24-hour warmup test, the 7-day endurance test at the 120-V ac operating voltage, a set of thermal cycling tests at voltages up to and including 135-V ac, and over six days days of continuous operation at 135-V ac. Therefore, we believe that the Singleton tests on the additional Tayco igniters have shown that they are durable under endurance and cycling conditions.

Question 3

For the 120 V igniter system, describe the following:

a) Performance characteristics of the igniters including surface temperature as a function of voltage and age.

b) A comparison of surface area, power density, and other relevant parameters for the original and currently proposed igniters.

c) Igniter mounting provisions.

d) Proposed preoperational and surveillance testing. If surveillance testing will be based on comparisons of measured voltage/current to preoperational values, specify the range for acceptance.

e) Power distribution system for the igniters, in particular, the location of the breakers in the system and the number of igniters on a breaker.

Response 3

a) Igniter surface temperatures measured as a function of voltage and age were reported in Attachment B of TVA's "Summary of Testing to Determine Suitability of Tayco Igniter for Use in the PHMS at Sequoyah and Watts Bar," submitted June 14, 1982. In addition, refer to response 2 of the present submittal.

b) Relevant parameters for the GM and Tayco igniter relate to performance - the ability to ignite lean mixtures - and to durability. As reported in the submittal referenced in response 3(a), testing at Whiteshell showed that both the GM and Tayco igniters had the ability to ignite lean mixtures at their operating voltages. The two igniter types possessed similar lower ignition limits. The Tayco igniter minimum surface temperature required for ignition was measurably lower than the GM surface temperature. Also as reported in previous submittals and in response 2, testing at Singleton has shown that both the GM and Tayco igniters are sufficiently durable.

   The GM igniter has a heated surface area of about 0.61 in^2 and a power at 12-V ac of 99 watts for a "calculated surface power density" of 162 $watts/in^2$. The Tayco igniter has a heated surface area of about 10.9 in^2 and a power at 120-V ac of 519 watts for a power density of 48 $watts/in^2$. The calculated surface power density for the Tayco igniter is lower due to the difference in heating element configuration of a coil compared to a rod. Based on the Whiteshell results discussed above, surface power density must not be closely related to igniter performance capability.

c) As shown in Figure 1 and described in the text of the submittal referenced in response 3(a), the Tayco igniter will be mounted in a NEMA type 4 enclosure with the heating element protruding. The igniter body is threaded to accept a washer and nut to allow secure mounting in the enclosure. All electrical connections are made within the enclosure. The entire assembly will be seismically supported.

d) Preoperational and surveillance testing for the PHMS was described in response 1 of our December 1, 1981, submittal. Preoperational testing will consist of energizing the system, measuring the surface temperature of each individual igniter, and recording the voltage and current in each igniter circuit. Later, during surveillance testing, the voltage and current of each circuit will be measured and compared with the readings previously recorded during the preoperational test. Since there are only two igniters in each circuit, the current measured during the surveillance test would drop by about half if one of the two igniters had failed. Such a major drop in current would be outside the range for acceptance in the test.

e) The power distribution system for the PHMS was described in Response 1 of our December 1, 1981, submittal. In each train, power from the 480/120 V ac regulating transformer is routed to the 120 V ac distribution panel located on elevation 759 of the auxiliary building. The distribution panel for each train contains 16 separate circuits, each providing power to two igniters and including a circuit breaker.

Question 4

Provide details regarding the number and location of permanent igniters in containment. Discuss the influence of considerations such as volume served per igniter and preferred flame direction on the design of the permanent system.

Response 4

A description of the number and location of igniters in the PHMS was provided in Response 1 of our December 1, 1981, submittal. Since that time, the location of the igniters in the ice condenser upper plenum has been changed to allow the assemblies to be seismically mounted. The upper plenum igniters on the crane wall side will be located at elevation 785 and the igniters on the containment wall side at about elevation 792.

As discussed in previous submittals, igniters are distributed throughout the major regions of containment in which hydrogen could be released or to which it could flow in significant quantities. No specific consideration was given to the "volume served" per igniter. Igniters in both the upper and lower compartment are located at intermediate as well as high elevations to allow the partial burning that would accompany upward flame propagation.

Question 5

Recent tests conducted at McGill indicate that flame accelerations accompanied by large pressure increases, and detonations can occur at hydrogen concentrations as low as 13%. Although remote, the possibility of flame accelerations and local detonations occurring around obstacles and in confined regions of containment cannot be entirely dismissed. Further analysis of the probability and consequences of these events are thus warranted. In this regard:

a) Discuss the chain of events and conditions required to cause flame accelerations and detonation in containment, and the probability that such conditions might exist. Identify the locations in containment at which flame acceleration/detonation would most likely occur.

b) Provide quantitative estimates of the extent and magnitude of flame acceleration in containment and the resulting pressure increase and loads on structures and equipment.

c) Provide the results of a calculation (pressure versus time curve) for the largest conceivable local detonation which could occur in your containment. Demonstrate that the effects of such a detonation could be safely accommodated by structures and essential equipment. Also, provide an estimate of the limiting size of a cloud of detonable gas with regard to the structural capability of the containment shell.

Response 5

The issues of local detonation and transition to detonation have been addressed in previous submittals. Refer to:

- Sequoyah Nuclear Plant Hydrogen Study, Volume II, Revision in Response to NRC Questions (letter from J. L. Cross to R. L. Tedesco dated December 11, 1980).

- Additional Information Requested by NRC (letter from J. L. Cross to R. L. Tedesco dated December 17, 1980).

- Resolution of Equipment Survivability Issue for the Sequoyah Nuclear Plant (letters from L. M. Mills to E. Adensam dated June 2, 1981, and June 3, 1981).

- Response to Additional NRC Questions on Hydrogen Control System (letters from L. M. Mills to E. Adensam dated December 1, 1981, and January 5, 1982).

- Executive Summary Report (letter from L. M. Mills to E. Adensam dated September 27, 1982).

The reference McGill tests were performed in laboratory-scale apparatus with specialized features such as large length/diameter ratios, uniaxial flame propagation, regularly spaced obstacles, etc., which are designed to promote the detonability of test mixtures. The McGill test conditions would not exist in the Sequoyah containment. Four major areas of difference that have been addressed at length in the referenced submittals include the available

hydrogen concentration, the available ignition source strength, the confined geometry with a large length/diameter ratio, and the presence of regular obstacles. We agree that the possibility of transition to detonation and local detonation is remote and believe that further analysis of the consequences of these events is thus unwarranted.

a) The conditions associated with flame acceleration and detonation in the laboratory have been discussed in relation to the Sequoyah containment in the referenced submittals. The probability of those conditions is judged to be extremely remote. No locations were identified in the containment at which flame acceleration/detonation would occur.

b) Since significant flame acceleration in the containment is so improbable, the resulting pressure increase and loads on structures and equipment would be hypothetical.

c) As stated in previous submittals, we cannot conceive of a local detonation occurring in the Sequoyah containment. However, at the request of the NRC, TVA provided a calculated pressure versus time curve from a hypothetical local detonation in our submittal of December 17, 1980, referenced above. An analysis of the containment shell response to this load was provided in our submittal of June 2, 1981, referenced above. This analysis demonstrated that a margin of safety of three existed before material yield would be reached. The effect of a hypothetical local detonation on equipment has not been analyzed. However, as stated in our submittal of December 11, 1980, referenced above, the effect of such a hypothetical local detonation would be attenuated greatly by distance. It is probable that redundant equipment would have enough physical separation to avoid damage to both trains.

Question 6

The analysis provided to date concerning the survivability of air return fans and hydrogen skimmer fans neglects any fan overspeed or motoring which occurs as a result of postulated hydrogen combustion in the upper plenum and upper containment. Describe how the fans will react to the differential pressure associated with hydrogen combustion, and justify the assumptions concerning fan overspeed. Describe the effects of combustion in the lower compartment (e.g., fan stalling).

Response 6

Analyses have been submitted previously addressing the survivability of the air return fans under both pressure and temperature effects during hydrogen combustion postulated to occur in the upper compartment. No burns were predicted by CLASIX to occur in the upper compartment for the base case parameter assumptions. However, some of the sensitivity studies that were performed did result in upper compartment burns. In the analyses done previously to address the pressure effect on the fans, any overspeeding of the fans was neglected for simplicity. This is believed to be a reasonable assumption because the pressure differential during the burns is neither very great or very extended and because the pressure loading condition used in the analysis was so conservative. This pressure load was assumed to be a constant 50 psid force acting downward on the fan blades and was assumed to occur in addition to all the loads the fan experiences during operation at its normal speed. The static load of 50 psid is very conservative since it exceeds even the worst peak transient differential pressures during a burn. For example, in the sensitivity case where the hydrogen ignition limit in the upper compartment and the dead-ended region was assumed to be 6 volume percent with 60% burn completeness, the duration of an upper compartment burn pressurization was about 12 seconds and the peak differential pressure was about 7.5 psid. The integrated load would only be about 36 psi-seconds. A transient load of this magnitude is not believed to have a potential for causing significant overspeeding of the fan.

A previous submittal has also addressed air return fan survivability during postulated lower compartment burns. During the period of lower compartment combustion and pressurization, the backdraft dampers above the fans would close and prevent significant differential pressure loads on the fans. These dampers were designed to withstand pressurization during a design basis LOCA which would cause a higher differential pressure than calculated in any of the burn sensitivity studies. The air return fans have been operated during a test with the dampers closed and experienced no damage such as from stalling.

Question 7

With regard to the equipment survivability analysis, the level of conservatism implicit in the temperature forcing function is developed for the lower containment and upper plenum is not apparent and quantifiable. Additional analyses should be conducted to provide a base line or "best estimate" of equipment response, and to ensure that temperature curves assumed in the analyses embody all uncertainties in the accident sequence and combustion parameters. Accordingly, provide analyses of equipment temperature response to:

1) The base case transient assumed in the containment analyses.

2) The containment transient resulting from a spectrum of accident scenarios.

3) The containment transients resulting under different assumed values for flame speed and ignition criteria for the worst case accident sequence. The range of these combustion parameters assumed for the equipment survivability anlayses should include but not necessarily be limited to the values assumed in the containment sensitivity studies, ie., 1-12 ft/sec speed and 6-10% hydrogen for ignition.

Response 7

1) In our response of December 1, 1981, we provided equipment survivability results for 8 v/o-85% hydrogen burns with a flame speed of 1 ft/sec. At that time we also performed HEATING5 analyses for a flame speed of 6 ft/sec for all the equipment analyzed in the 1 ft/sec submittal. The 1 ft/sec results showed higher equipment temperatures in every instance than the 6 ft/sec analyses. For that reason, we submitted only the 1 ft/sec results.

2) The S_2D case is a reasonable upper bound scenario for the Sequoyah Plant. The maximum hydrogen release rate and the total amount of hydrogen released prior to core slump, as predicted by MARCH, bounds other accident scenarios believed to be high contributors to risk at Sequoyah. In our December 1, 1981, submittal, we provided maximum release rates for several scenarios. The S_2D maximum release rate was 1.1 lb/sec. An S_1D had the highest peak release rate at 1.3 lb/sec. The S_2D event oxidized 75% of the core. The next highest scenario involved approximately 35% of the core. While S_1D has a slightly higher release rate than S_2D, it is not high enough to result in oxygen inerting during burns, prevent a rapid reduction in hydrogen concentration in the burn compartment during a burn, nor produce higher atmospheric and flame temperatures for a given ignition criteria than the S_2D case. The much larger total amount of hydrogen released in the S_2D case results in more burns and thus higher equipment temperatures.

The S_2D scenario used for the equipment survivability evaluations produces higher equipment temperatures than would be produced by other scenarios reviewed. The S_2D results, therefore, conservatively bound the other scenarios.

3) As stated in our response to item 1 of this question, flame speeds of 1 ft/sec produced higher temperatures than 6 ft/sec speeds. The comparison of the cases showed that the longer burn duration seen at the lower speeds input more energy to the equipment and was more important than the change in peak temperature. Evaluations using flame speeds that are faster than those studied will not, therefore, result in higher equipment temperatures than those previously reported. In our response to question 3 of your October 1, 1982, request for additional information we have provided the results of thermal analyses of equipment for burn criteria of 6 v/o-60% (CLASIX case 1C). The analyses showed the peak equipment temperatures are essentially the same as reported in our previous submittals. There are still large margins between the calculated values and the survivable temperatures.

Question 8

For the survivability analysis, it is our understanding that the current thermal model assumes radiation from the flame to the object only during a burn, with convection occurring at all times outside the burn period. In an actual burn, radiation from the cloud of hot gases following the flame front can account for a substantial portion of the total heat transfer to the object. An additional heat flux term or a combined radiation-convection heat transfer coefficient should be used to account for this radiant heat source. In this regard, clarify the treatment of heat transfer following the burn and justify the approach taken.

Response 8

The equipment survivability analysis submitted on December 1, 1981, utilized thermal models which assumed radiative heat transfer only during a burn. The radiative heat transfer during the burn included the radiation from the cloud of hot gases following the flame front. Radiative heat transfer from the hot gas cloud for all thermal models was evaluated at the adabatic flame temperature. Additional analyses have shown that radiative heat transfer from the atmosphere to the equipment after burn termination produced changes in the equipment surface temperature response of about 10°F. The CLASIX temperature profile was used as the temperature forcing function for the radiative heat transfer after the burn was completed. Gas and surface emissivities of 1.0 (i.e., black body) and view factors of 1.0 were used in the post burn period for conservatism.

Question 9

HEDL containment mixing tests conducted as part of ICOG/EPRI R&D program indicate that spatial hydrogen concentration gradients of as much as 2 to 7% can be expected to exist within containment at a given time. If such a gradient were to exist within the volume of a hydrogen cloud in which combustion has just been initiated, the volume-average hydrogen concentration for the cloud can conceivably be significantly higher than the hydrogen concentration at the point of ignition. In light of this, discuss the influence of hydrogen concentration gradients on the concentration requirement for ignition that is input to CLASIX, and justify the ignition concentration value used in the CLASIX containment analyses.

Response 9

The results of the Hanford containment mixing test were described in Appendix A.6 of TVA's Quarterly Report No. 5 and in section IV.E of the technical summary attached to TVA's executive summary report. The maximum spatial hydrogen concentration gradients measured during any of the tests were less than three volume percent with two exceptions. These exceptions occurred during tests HM-1A and HM-2 which revealed test vessel design details which were not prototypic of actual ice condenser containment conditions as discussed in Response 1(d). We believe that the maximum test gradients of less than 3 percent indicate that relatively rapid and uniform mixing would occur during postulated hydrogen release scenarios in the plant. Assuming that gradients of this magnitude (less than 3%) could exist in the plant before ignition, the volume of such a cloud with a higher concentration away from the point of ignition could not be significant due to the number of igniters distributed throughout each region. The sensitivity of containment response to the hydrogen lower ignition limit has been analyzed with CLASIX. The existence of potential nonuniformities of the magnitude discussed here would not be expected to yield a significantly different response.

Question 10

Describe in detail the fog formation study cited in response to Question 9 of the July 21, 1981, Request for Information. Include in this description the analytical development of the models for fog formation and removal, methods for solution, assumptions, and input parameters. Provide plots of fog concentration and size as a function of time assuming various spray removal efficiencies, and mean droplet diameters.

Question 11

Describe in detail the analyses of fog effects on hydrogen combustion cited in response to Question 9 of the July 21, 1981, Request for Information. Include in this description the analytical development of the combustion kinetics and heat transfer models, and quantitative comparisons between the theoretical results and data obtained from the Factory Mutual Tests. Provide plots of fog droplet size and concentrations required to inert at various hydrogen concentrations under typical post-LOCA containment conditions.

Response 10 and 11

Refer to the attachment, "Fog Inerting Analysis for PWR Ice Condenser Plants," for the information requested in questions 10 and 11.

Question 12

In the CLASIX spray model it is not clear whether the mass of spray treated in a time increment is assumed to be only that amount of spray mass which is introduced in a single time step, or the mass of droplet accumulated in the atmosphere over the fall time period. Clarify the spray mass accounting used in CLASIX and the mass of spray treated in a single time step. Discuss the significance of any errors introduced by the apparent assumption that only one time increment of spray mass is exposed to the containment atmosphere during a single time step.

Response 12

The mass of spray treated in a time increment by the CLASIX spray model is the amount of spray introduced in a single time step and not the mass of droplet accumulated in the atmosphere over the fall time. The CLASIX spray model model operates in a different time domain than the compartment. The compartment conditions are frozen in time and the compartment response to the spray is determined as if the mass of spray introduced during the time step completed its fall during the time step. The compartment mass and energy balance is updated at the end of each time step to reflect the spray interaction. The spray interaction is determined by a classical transient technique which is fully described in responses 10 (c,d) and 11 (a,b) in our October 18, 1982, submittal. Based on the discussions provided, we believe the CLASIX spray model provides an appropriate treatment of spray and containment atmospheric behavior for hydrogen burn transients.

Question 13

CLASIX spray model analyses provided to date have been limited to the comparison of pressure, temperature, and integrated heat removal for the purpose of evaluating the effect of the spray operating in a separate time domain. Additional information is needed, however, to confirm the adequacy of the heat and mass transfer relationships and assumptions implicit in the CLASIX spray models, especially in treating a compartment in which hydrogen combustion is taking place. In this regard:

a) Provide a quantitive description of the spray heat and mass transfer under containment conditions typical of a hydrogen burn. Include in your response plots of containment temperature, spray heat transfer, spray mass evaporation, and suspended water mass as a function of time for both the CLASIX spray model and a model in which the spray mass is tracked throughout the fall (and allowed to accumulate in the containment atmosphere).

b) Provide analyses of spray mass evaporation and pressure suppression effects for an upper compartment burn.

c) Justify the drop film coefficient value assumed in the spray model analyses (20 Btu/h $ft^{2}{}^{o}F$) and discuss the effect of using a constant value throughout a burn transient.

Response 13

a) The CLASIX Topical Report includes a comparison of the CLASIX spray model to a finite difference spray model for atmospheric temperature over $700^{o}F$ (see figure D-1). The temperatures used in this comparison are consistent with the temperatures resulting from an upper compartment hydrogen burn. We believe this figure augmented by our response to questions 10 and 11 of your August 9, 1982, request for additional information on CLASIX will adequately address your concerns. Our response to the August 9, 1982, letter was submitted October 18, 1982.

b) Sensitivity studies of various spray parameters were provided December 15, 1980, in our Sequoyah Nuclear Plant Core Degradation Program Volume II report. Refer to Table 10 of Appendix U for a summary of these studies.

c) Refer to CLASIX case JV906 of our December 15, 1980, submittal. In this case the spray heat transfer coefficient was reduced from 20 $BTU/hr\text{-}ft^{2}\text{-}{}^{o}F$ to 2. For burns in the upper compartment based on an 8 v/o ignition criteria and 50% burn completeness, the temperature in the upper compartment increased $80^{o}F$ due to the heat transfer coefficient reduction. This shows the results are not particularly sensitive to the heat transfer coefficient chosen.

Question 14

Concerning the CLASIX containment response analyses:

a) Justify the burn time and burn propagation delay times used (reported burn times for Sequoyah an cGuire differ by a factor of 2 to 3).

b) Justify the radiant heat transfer beam lengths used (a beam length of 59 ft for the lower compartment in Sequoyah seems high - 20 to 30 ft may be more appropriate).

c) The base case and majority of S_2D sensitivity studies assume that combustion occurs at an 8% hydrogen concentration with an 85% completeness of burn. Available combustion data for hydrogen/dry air mixtures indicate that lean mixtures of approximately 8% H_2 and below are prevented from reacting completely and adiabatically due to buoyancy, diffusion and heat loss effects. Only as hydrogen concentration is increased to about 8.5% will the reaction begin to approach adiabaticity. While arguments for an 8% ignition concentration may be valid, provide the results of additional CLASIX analyses to indicate the effect of an increase in ignition concentration from 8% to 8.5-9%.

d) Provide the results of CLASIX analyses for flame speeds of 10 and 100 times the present value.

e) To assess the effect of igniter system failure or ineffectiveness, provide the results of sensitivity studies in which the lower and dead-ended compartments are effectively inerted, and the upper plenum igniters burn with low efficiency or not at all. Assume combustion in the upper compartment at 9-10% hydrogen.

Response 14

a) Refer to our response to question 4a of your letter dated August 9, 1982. Our response was submitted October 18, 1982.

b) We agree. The beam length value used in all of our analyses provided since mid 1981 was 25 feet for the lower compartment. The value provided in Table 11 of our December 1, 1981, submittal is in error.

c) The purpose of providing results at 6, 8, and 10 v/o was to preclude running a multitude of cases at slightly varied hydrogen concentration values as a criteria for ignition. These runs are believed to be sufficient to evaluate igniter performance. Additionally, Duke Power submitted results for their McGuire plant based on an 8.5 v/o and 100% burn completeness. We recommend you refer to their results. Their results show there is not a substantial difference between 8 and 8.5 v/o ignition criteria.

d) We believe additional flame speed sensitivity analyses are unwarranted. We provided results for an order of magnitude shift in the flame speed. A two order of magnitude shift in flame speeds for some of the values provided would result in supersonic flames and would not be physically achievable in our plant.

At present, as supported by all transient test data, the pressures seen in vessels with a pre-energized igniter system are well below adiabatic for the 6, 8, or 10 v/o ignition criteris used to analyze Sequoyah. There is no question the faster the rate of energy addition, the closer the pressures will approach the adiabatic pressure for a given hydrogen concentration. In the limit, if the energy addition rate is sufficiently high (i.e., high flame speed), venting through the ice condenser doors will not occur and the pressure in the burn compartment will behave as a perfectly insulated single volume vessel. The increase in differential pressure that would be obtained in this instance would be approximately 33 lb/in^2 at 6 v/o, 45 lb/in^2 at 8 v/o, and 60 lb/in^2 at 10 v/o for complete burns.

e) Refer to case JV903 in Appendix U of our December 15, 1980, submittal where the results for the requested case were provided. The case was based on 10 v/o ignition criteria and no air return fan operation. The results show an upper compartment burn producing in a peak pressure of 92 lb/in^2a.

RESPONSE TO
REQUEST FOR ADDITIONAL INFORMATION ON
EQUIPMENT SURVIVABILITY

Question 1

In response to Item 2 in your letter dated April 6, 1982, you have provided only one example to indicate that the temperature reached by the equipment during a hydrogen burn is below the qualification temperature for that equipment. Confirm that you have performed analysis for all the equipment required for the hydrogen burn and provide the qualification testing of these equipment. Also provide the reference to individual Summary Component Evaluation Worksheets (SCEWS) which were submitted in the EQ submittal in response to NUREG-0588, so that the staff can make an independent evaluation of the subject analyses.

Response 1

In our submittals on equipment survivability dated June 2, 1981, December 1, 1981, and April 6, 1982, TVA provided the results of testing or analysis of five pieces of equipment for hydrogen burns. Detailed evaluations were not provided for all components on the equipment list provided in our earlier submittals. Justification of our approach in evaluting only selected items was also provided in our December 1, 1981, and April 6, 1982, submittals. "Qualification testing" for hydrogen burns was not performed nor is it required.

The following list provides the requested reference to the SCEWS provided in our Electrical Equipment Environmental Qualification Report in accordance with NUREG-0588 for unit 1 at Sequoyah. The items listed below are included in Table 3.11-4 with the page number for easy reference. The equipment list is taken from Table 2.2-1 of our December 1, 1981, submittal.

Item	Page
LT-2-148, -156, -164, -171, -172 -173, -174, 175	7
Air Return Fans	8
FCV-43-201, -202, -207, -208	22
LT-63-176, -177, -178, -179	17
FCV-63-172	12
LT-68-320, -355A	14
TE-68-1, -24, -43, -65	13
TE-68-18, -41, -60, -83	13
Electrical Penetrations	10
Containment Isolation Valves	1,2,3,5,6,11,12,18, 19,22,23,26,27,28,29

E72293.04

ENCLOSURE 2

RESPONSE TO OCTOBER 1, 1982 LETTER

FROM E. ADENSAM TO H. G. PARRIS REQUESTING ADDITIONAL INFORMATION

ON EQUIPMENT SURVIVABILITY

SEQUOYAH NUCLEAR PLANT

The hydrogen igniters for the Interim Distributed Ignition System (IDIS) and the Permanent Hydrogen Mitigation System (PHMS) are not Class 1E and are thus not included. The ice condenser doors and seals, flanged penetrations, equipment hatch, and air locks are not Class 1E components and thus do not have SCEWs. The hydrogen analyzers are listed in Table 2.2-1 but are located outside containment and are thus not subjected to hydrogen burns. The core exit thermocouples are not Class 1E equipment. The reactor vessel level thermocouples and the vessel vent valves have not been added to the plant at this time. When they are, the NUREG-0588 report will be updated to include these components.

Question 3

In your response to item 3 in your letter dated April 6, 1982, you indicated that for Case 1C the burns are of a much shorter duration and the ambient temperature is lower. The staff recognizes that the burns are of a shorter duration, but in addition to this duration between burns is also of much shorter duration which allows less time for the equipment to cooldown. Also, if the licensee wants to demonstrate the blowdown sensitivity studies (case JJ1) that containment integrity is maintained even for three times the mass flow rate used in S_2D scenario then it should also be demonstrated that equipment will survive for that scenario. Hence, provide the equipment temperature for these two cases.

Response 3

The results of the thermal anlaysis of the cable in conduit for a burn criteria of 6 v/o-60% (CLASIX Case 1C) is provided on Figure 1. The response of the cable in conduit is provided as it is the most responsive to environmental changes of any of the equipment analyzed. The analysis shows that the maximum surface temperature is essentially the same as shown for the same 8 v/o-85% case on Figure 2-2.14 of our December 1, 1981, submittal. This analysis of CLASIX Case 1C very conservatively includes radiative heat transfer from the hot gas cloud during the burn at the adiabatic flame temperature and radiative heat transfer based on the CLASIX profile at all times during the transient. This essentially doubles the radiation heat transfer during the burn. In addition, to adding more conservatism the radiation term utilizing the CLASIX profile used gas and equipment surface emissivities of 1.0 (i.e., black body radiation) and view factors of 1.0. Natural convection was also included in the same manner as presented in the analysis discussed in our December 1, 1981, submittal. Even with these gross conservatisms the same large margins in our earlier analyses still remain assuring the survivability of our equipment.

The S_2D scenario used for equipment survivability analysis utilized a maximum hydrogen release rate of 1.1 lb/min. As can be seen by our response to Item 2 of Question 7 and from the table on scenarios in section C of our December 1, 1981, submittal, the S_2D release rate is most appropriate for all plant transients. We provided a discussion of why equipment analysis for CLASIX Case JJ1 is not required in our April 6, 1982, submittal. The containment transients based on the S_2D release rates provide a conservative environmental profile for equipment survivability analysis.

Question 4

In your submittal of December 1, 1981, you indicated that the analysis of the teflon wire which was melted during Fenwal testing also indicated that teflon will completely melt in 1.4 seconds. Provide the melting point for the teflon used in the analysis. Also using the same model provide the results of the analyses predicting the surface temperature of the exposed thermocouple and RTD cable.

Response 4

The melting point of teflon used to determine if the insulation on the thermocouple wire in our analysis was 617°F. This value was obtained from the Omega Temperature Measurement Handbook, 1982 edition. The calculated insulation surface temperature in our analysis was 990°F.

Analyses of the RTD and thermocouple cable were not performed. Testing was done in lieu of analysis. Because of the temperatures reached during the tests (1368°F for the thermocouple cable) the tests were adequate representations of hydrogen burns in the lower compartment where this cabling is located. Analyses would not provide additional information and were therefore not performed. Additional justifications are provided in our December 1, 1981, submittal.

Question 2

Since the probability of local detonation exists, provide the analyses or experimental results to demonstrate the survivability of essential equipment for the local detonation predicted.

Response 2

Refer to response 5 of Enclosure 1, "Response to Request for Additional Information on Hydrogen Control for Ice Condenser Plants" for a discussion of local detonation and equipment survivability.

Question 5

Sandia, based on the experimental results, is predicting that scaling may have a big impact on the analytical model used to predict equipment temperature. Tests results performed in small chamber may not be used to demonstrate the equipment survivability in the contianment. Based on this, demonstrate how the analytical model used for Sequoyah takes into account the scaling factor. If the analytical model does not consider the scaling factor, provide the basis for eliminating this factor.

Response 5

We agree with Sandia that scaling effects must be carefully considered in not only small tests but any tests that do not accurately model the plant. Because of this, all the analyses performed for Sequoyah were based on full scale. No small scale test data was used which would require extrapolation up to plant conditions. All scale factors for the CLASIX and HEATING 5 analyses are therefore 1.0.

FIGURE 1

SQN H2 STUDIES

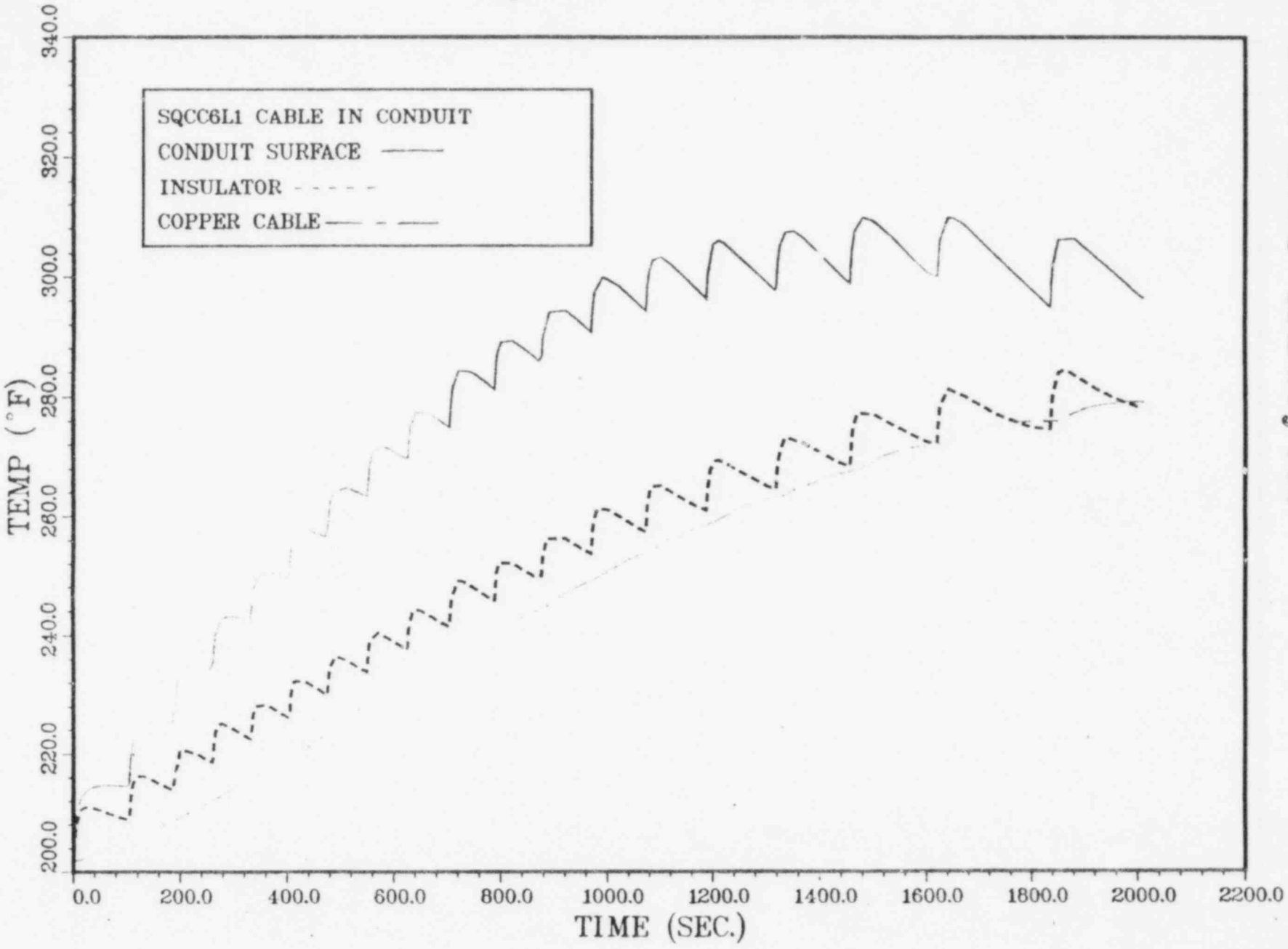

ATTACHMENT

FOG INERTING ANALYSIS FOR PWR ICE CONDENSER PLANTS

CORE AND CONTAINMENT ANALYSIS
NUCLEAR SAFETY DEPARTMENT
WESTINGHOUSE ELECTRIC CORP.

OCTOBER 1982

ABSTRACT

The recent hydrogen burn test conducted at the Lawrence Livermore National Laboratory has raised the NRC and the ice condenser plant owners concern about fog inerting probability and consequences in ice condenser plants. The present investigation is aimed at resolving this fog inerting issue. In this report, major fog formation and removal mechanisms that could exist in the post-accident ice condenser containment are identified and quantified. Methodologies have been developed for predicting fog formation and removal rates and for predicting fog concentrations in various compartments in an ice condenser containment.

This methodology employs the Hijikata-Mori boundary layer fog formation theory, and calculates the fog formation rates due to boundary layer and bulk stream condensation. Next, the mass conservation equations for fog droplets are solved and the fog concentrations in various compartments are calculated. The methodology has been used to predict fog concentrations in the Sequoyah, McGuire, and D. C. Cook containments, using the CLASIX output data for an S_2D accident sequence.

In order to utilize the calculational results from the study, a fog inerting criterion has been established. This criterion uses the hydrogen concentration, volume mean drop size, and fog concentration to define the fog inerting regime. For a given hydrogen concentration, the minimum fog inerting concentration (in mass/volume) was found to vary with the square of the volume mean drop diameter. This criterion has been verified by the recent Factory Mutual fog inerting test data.

The application of the fog inerting criterion to the three ice condenser plants shows that fog inerting would not exist in the upper and lower compartments. Some slight elevation of the lower flammability limit in the ice condenser upper plenum may be possible due to the presence of fog but the present calculations show that hydrogen concentrations of 8-8.5 percent in the upper plenum are still flammable. Previous CLASIX analyses have shown that the containment response to burning 8-8.5 percent hydrogen mixtures would be acceptable.

ABSTRACT

The recent hydrogen burn test conducted at the Lawrence Livermore National Laboratory has raised the NRC and the ice condenser plant owners concern about fog inerting probability and consequences in ice condenser plants. The present investigation is aimed at resolving this fog inerting issue. In this report, major fog formation and removal mechanisms that could exist in the post-accident ice condenser containment are identified and quantified. Methodologies have been developed for predicting fog formation and removal rates and for predicting fog concentrations in various compartments in an ice condenser containment.

This methodology employs the Hijikata-Mori boundary layer fog formation theory, and calculates the fog formation rates due to boundary layer and bulk stream condensation. Next, the mass conservation equations for fog droplets are solved and the fog concentrations in various compartments are calculated. The methodology has been used to predict fog concentrations in the Sequoyah, McGuire, and D. C. Cook containments, using the CLASIX output data for an S_2D accident sequence.

In order to utilize the calculational results from the study, a fog inerting criterion has been established. This criterion uses the hydrogen concentration, volume mean drop size, and fog concentration to define the fog inerting regime. For a given hydrogen concentration, the minimum fog inerting concentration (in mass/volume) was found to vary with the square of the volume mean drop diameter. This criterion has been verified by the recent Factory Mutual fog inerting test data.

The application of the fog inerting criterion to the three ice condenser plants shows that fog inerting would not exist in the upper and lower compartments. Some slight elevation of the lower flammability limit in the ice condenser upper plenum may be possible due to the presence of fog but the present calculations show that hydrogen concentrations of 8-8.5 percent in the upper plenum are still flammable. Previous CLASIX analyses have shown that the containment response to burning 8-8.5 percent hydrogen mixtures would be acceptable.

TABLE OF CONTENTS

TABLE OF CONTENTS (Continued)

LIST OF TABLES

LIST OF FIGURES

LIST OF FIGURES (Continued)

LIST OF FIGURES (Continued)

1.0 BACKGROUND

The incident at Three Mile Island has demonstrated that a significant amount of hydrogen could be generated during core degradation. This experience raised NRC concern about the safety of nuclear power plants, in terms of their capability to control hydrogen during severe accidents. Since ice condenser plants have a relatively small volume and low containment design pressure, the NRC has requested the ice condenser plant owners to study hydrogen control methods for use in their plants. In this regard, the Tennessee Valley Authority (TVA), Duke Power and American Electric Power (AEP) have installed glow plug igniters at various locations inside their ice condenser containments to ignite hydrogen at low concentration.

Recently, the NRC requested Lawrence Livermore National Laboratory (LLNL) to carry out experiments on these igniters to determine their effectiveness. In these experiments, two tests with high steam concentration failed to achieve ignition even after enough steam condensed to yield a theoretically combustible mixture. One explanatory hypothesis was that substantial fog formation could occur when saturated steam is discharged into a unheated vessel and under some conditions- og could effectively preclude hydrogen from combustion[1].

The LLNL tests raised some doubts about the effectiveness of glow plug igniters under fog formation conditions. In a recent review of hydrogen related issues for ice condenser plants,[2] the NRC has raised several questions concerning the probability and consequences of fog formation and steam supersaturation in ice condenser plants.

TVA, AEP, and Duke established experimental and theoretical analysis programs to study the effects of fog and spray on igniter performance. The experimental program was contracted to Factory Mutual. The experiments were designed to test the glow plug igniter's performance under different fogging conditions. In response to the NRC questions, the plant owners requested Westinghouse to perform fog inerting analyses for the Sequoyah, McGuire, and D. C. Cook plants. This report presents the results of the Westinghouse studies.

2.0 INTRODUCTION

From the post-test analysis of the LLNL hydrogen burn tests, it appears that substantial fog formation could have occurred inside the test vessel. Generally, fog droplets are only a few microns in diameter. These sizes of droplets have the potential to prevent a flammable gas mixture from combustion or quench a propagating flame. This is because these sizes of droplets vaporize very fast (on the order of milliseconds), absorbing an enormous amount of the heat released from combustion if a substantial quantity of these droplets is present in the atmosphere. In comparison, large water droplets in the range of few hundred microns or larger (e.g. spray droplets) have no inerting effect on combustion[20] and hence have insignificant effect on glow plug igniter's performance. Therefore, the present analysis will be concentrated on the generation and removal of fog (mist), and its impact on the glow plug igniter system.

There are a number of potential fog generation and removal mechanisms present in a post-accident ice condenser containment atmosphere. The fog generation mechanisms include fog generated by the break flow (if it is two-phase), fog formation near the ice and structural heat sink surfaces (since the surface temperatures could be well below the dew point), and fog generation due to homogeneous and heterogeneous nucleation in condensing bulk streams. The fog removal mechanisms include gravitational settling, agglomeration, vaporization and removal by spray droplets. In order to estimate the post-accident fog concentrations in ice condenser containments, these competing mechanisms must be studied, and evaluated. To solve this problem, it requires a numerical integration of the mass conservation equations for the mist droplets in the various containment subcompartments. By making some simplifying assumptions, the transient fog concentration in the various subcompartments has been estimated.

The analysis presented here considers all the fog removal and generation mechanisms previously described except agglomeration. In addition, it

considers the fog entrainment in the intercompartmental flows (including fan flows) in the fog mass conservation equations. CLASIX results for an S_2D event were used as boundary conditions to the problem.

In addition to calculation of fog concentrations in various containment compartments, it was necessary to establish a fog inerting criterion. A fog inerting criterion has been proposed by Berman et al., which predicts the minimum fog concentration required to inert a given hydrogen concentration and given volume mean fog drop size. This criterion seems to overpredict the minimum fog inerting concentration, when compared with experimental data. A more realistic fog inerting theory is presented in the present study.

The fog inerting methodology, analysis, and results are presented in the following sections of this report. Sections 3 and 4 present the methodology for calculating the fog formation and removal rates. Section 5 gives the fog inerting criteria, and Section 6 presents the results.

3.0 FOG GENERATING MECHANISMS IN AN ICE CONDENSER CONTAINMENT

The inerting capability of fog droplets depends on their sizes and concentration in the containment atmosphere, as well as the hydrogen concentration. This section is intended to identify various fog generation mechanisms present in an ice condenser containment and to determine the drop sizes and the rates of fog generation from these mechanisms. Three fog generation mechanisms are discussed in this section and the dominant fog generation mechanisms are identified.

3.1 FOG GENERATED BY BREAK FLOW

The post-LOCA containment atmosphere is most likely to be a drop-laden atmosphere. The large-scale simulated LOCA experiments conducted to date have directly or indirectly confirmed the presence of two-phase atmospheres. For example, Marvikken[3] and Battelle - Frankfurt[4] experiments were instrumented to measure fluid densities and water levels in various parts of the containment. Therefore, fog generation by the break flow cannot be neglected. The following discussion of this phenomenon pertains to small LOCAs.

In the early stage of a small LOCA transient, a substantial portion of the primary coolant discharged from the break will remain as liquid. Because of the superheat and high velocity, this liquid will be framented by aerodynamic forces and homogeneous nucleation mechanisms into small droplets. These droplets are expected to be entrained by the intercompartmental and fan flows and spread to other parts of the ice condenser containment. During their travel throughout the containment, the fog droplets will be removed by gravitational settling, sprays, and vaporization. The fog generation period lasts until the water level in the reactor vessel falls to the break elevation and the break flow is no longer two-phase. For the particular S_2D sequence analyzed by MARCH and previously used as the basis for the performance of a containment

analysis by CLASIX,[5] this period lasts for about 36 minutes and about 4.2×10^5 lbs of water has been discharged into the lower compartment during this period of time.[7]

After the water level in the reactor vessel falls below the break elevation, the break flow rate is substantially reduced. The flow is essentially steam and no fog droplets will be generated. As a result, the lower compartment becomes superheated afterward. Fog droplets may vaporize during their travel through this compartment and substantial removal of mist droplets is expected.

Large suspended drops generated by the break flow will be removed very quickly by gravitational settling and impingement. For the drops larger than 20 μ, the removal rate is high and complete removal only takes a few seconds. For the smallest drops (less than 1 μ) the terminal velocity is so small that they virtually remain suspended in the atmosphere indefinitely. The only effective removal mechanisms for these sizes of drops are vaporization, and collision with larger spray drops. The weight fraction of these sizes of drops is estimated to be below 1 percent[13] of the total drop population. The population of these small drops can increase if nucleation of embryos occurs in a saturated atmosphere.

3.1.1 AMOUNT OF FOG GENERATED BY BREAK FLOW

As discussed previously, the existence of a two-phase drop-laden regime has been observed experimentally. In a small LOCA, flashing of primary coolant at the break and subsequent vaporization of blowdown liquid represent a series of changes of thermodynamic states. Since the reactor coolant pressure is high, the break flow will be choked. The acceleration of primary coolant to the break location is essentially an isentropic process, in which the pressure decreases to the point at which substantial homogeneous nucleation occurs. When the flow leaves the break, the liquid is fragmented by both the aerodynamic forces and the nucleation mechanism into small fog droplets. These fog droplets continue to vaporize, because of the superheat in the droplets, until a thermodynamic equilibrium state is reached. Because of the high superheat and large aerodynamic forces, it is expected that the fog droplets generated are very small.[8] This vaporization process is essentially isenthalpic.

The existence of a two phase drop-laden regime can also be explained by use of a T-S diagram for steam as shown in Figure 3.1 (Figure 1 of Reference 6). It is shown in this figure that the blowdown liquid goes through a series of thermodynamic states, starting from the subcooled liquid state B_0. The liquid expands isentropically from the subcooled state B_0 to the state B_1 at the break, where a two-phase critical flow is developed. At the same time, temperature changes from T_0 to T_1. After leaving the break, the droplets continue to vaporize because of excessive superheat until finally an equilibrium state B_2 is reached at which the droplets are in thermal equilibrium with their surroundings. This vaporization process is essentially isenthalpic. At this time, the droplet temperature drops to T_2 and the atmospheric temperature also rises to T_2. For a small LOCA, the equilibrium temperature varies with time. According to the CLASIX analysis of the Sequoyah plant, the lower compartment gas temperature rises quickly from 100°F to approximately 200°F and then stays at this temperature for an extended period of time. Using these temperatures as final equilibrium

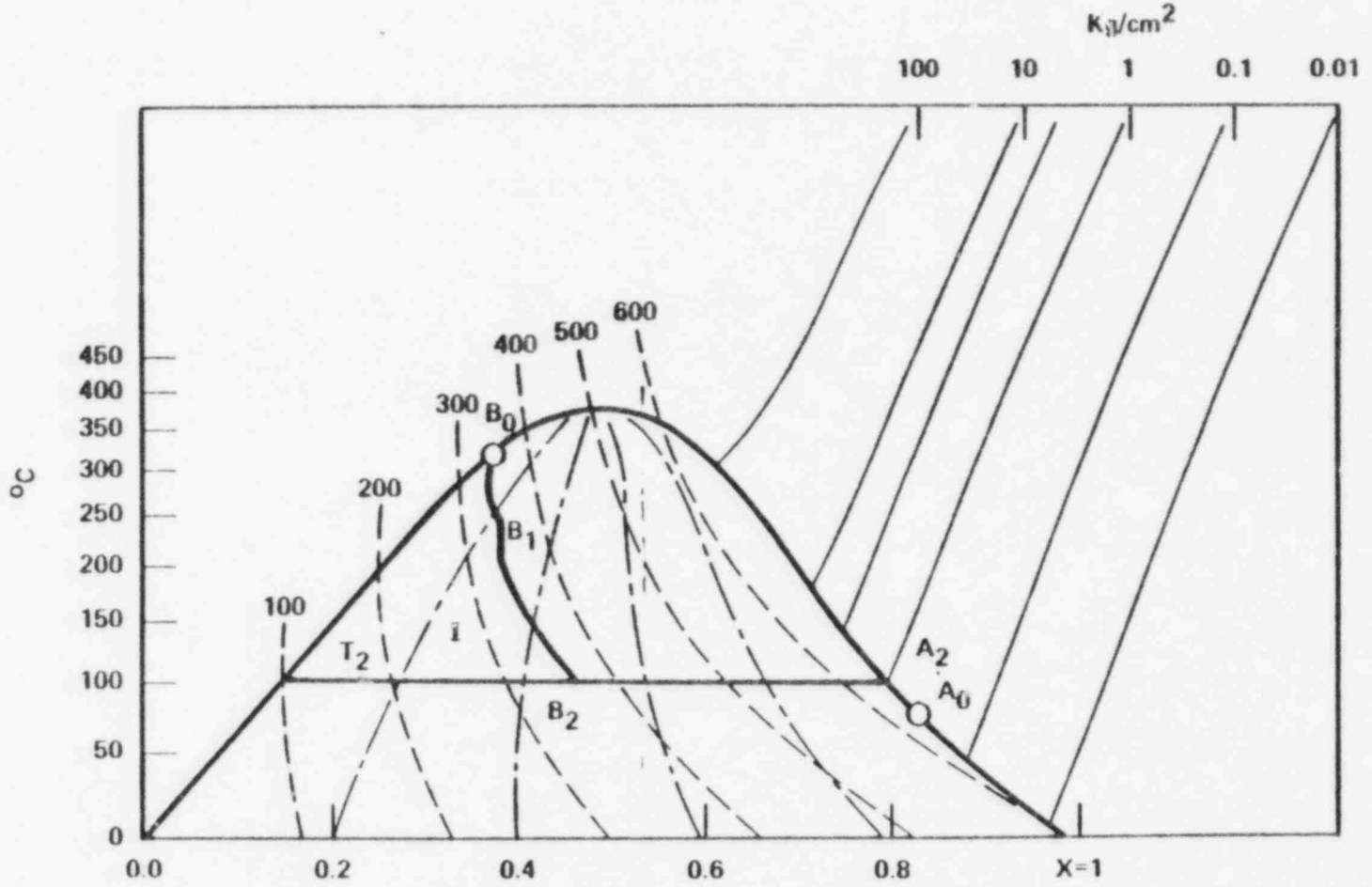

FIGURE 3.1 T-S DIAGRAM FOR REACTOR COOLANT DISCHARGED FROM BREAK

temperatures for water droplets, the weight fraction of water droplets in the break flow is approximately 50 percent, which is consistent with the MARCH calculations[7] of the break flow rate and its energy release rate.

The discussion given above is valid only when the initial state of the break flow is subcooled or saturated liquid. After the water level inside the reactor vessel falls below the break elevation, the break flow will be steam. The moisture content of the steam will be very low, even though isentropic expansion may lead to homogeneous nucleation and subsequent condensation in the vapor stream. Depending on the supersaturation that can be achieved in this isentropic expansion, a condensation shock is possible when critical supersaturation is reached. However, it is believed that the amount of fog droplets generated by homogeneous nucleation in this supersonic jet is negligible as compared to other fog generating mechanisms. Hence, it will be neglected in this present analysis. Therefore, the fog generation by the break flow is considered possible only when the water level in the reactor vessel is above the break elevation.

According to the MARCH[7] calculation at 2172 seconds into the accident, the water level inside the reactor vessel falls below the break elevation for the S_2D case analyzed in Reference 7. By this time approximately 421,000 lbs of water has been discharged from the break. It is calculated from MARCH break flow energy and mass output that 56 percent of this discharged fluid, i.e., 236,000 lbs, will be discharged as liquid droplets. However, most of these droplets will be quickly removed by gravitational settling and impinging on the structures and floor.

3.1.2 DROP SIZES GENERATED BY BREAK FLOW

The flashing jet experiment conducted by Brown and York[8] has indicated that the drop sizes produced by flashing liquid are small. They derived a correlation for the linear mean drop size based on the test data. The correlation shows that the mean drop size is inversely proportional to the Weber number and it decreases linearly with increasing

superheat. However, this correlation is applicable for liquid superheat less than 75°F and it can not be extrapolated to the large superheat of the reactor coolant. However, some conclusion concerning the drop sizes produced by blowdown of the reactor coolant can be drawn for this condition. The break flow has much larger superheat and Weber number than those used in this experiment; therefore, the drop sizes produced by the break flow should be much smaller than ~50μ observed in this experiment.

Gido and Koestel[9] have developed a method for estimating the drop size leaving the fragmentation/evaporation zone of a blowdown jet. This model is based on the assumption that drops with an internal temperature difference of less than 5°K will escape fragmentation. This model has been verified by the low superheat data of Brown and York. Application of this method to the LOCA condition shows that the maximum attainable drop size is 7μ (this means that any drop size larger than 7μ will not escape fragmentation by homogeneous nucleation). The corresponding mean drop size is about 4μ, based on the observation of the largest drop size and mean drop size in the experiment reported in Reference 8. Since the droplets are generated by the break flow before 2172 seconds, most of these droplets will be removed by containment sprays before hydrogen starts to release into containment (~ 3800 seconds). At this time, most of suspended droplets are formed by condensation. Therefore, this volume mean drop size of 4μ is not used in the present analysis; instead, the present analysis uses 10μ volume mean drop diameter, which is the nominal drop size for cloud and fog drops formed by condensation..

3.2 NUCLEATION OF FOG DROPLETS IN CONTAINMENT ATMOSPHERE

Nucleation of water embryos from the homogeneous vapor phase plays an important role in fog generation in containment. Nucleation is a process by which tiny water embryos or condensation nuclei are formed from a pure vapor phase at a rapid rate. In incipient homogeneous nucleation, the local gas temperature drops below the dew point corresponding to the local steam partial pressure and some degree of local supersaturation is needed. The degree of supersaturation needed to

start nucleation depends on the number of condensation nuclei present in the containment. These condensation nuclei could be very small water droplets or dust particles. If sufficient number of condensation nuclei exist, the required supersaturation could be small.

This section is devoted to the discussion of fog formation by homogeneous and heterogeneous nucleation. The classical nucleation theories are used to explain the nucleation phenomenon.

3.2.1 NUCLEATION THEORIES

The process of nucleation of an embryo water drop is important in understanding the mechanism of fog formation in ice condenser plants. Two types of nucleation process, namely, homogeneous and heterogeneous nucleations, and their theories will be discussed in Section 3.2.1.

3.2.1.1 CLASSICAL THEORY OF HOMOGENEOUS NUCLEATION

When an embryo droplet, usually assumed spherical, is formed from condensation of water vapor molecules, its free energy changes. The change of free energy can be expressed as

$$\Delta G = 4\pi r^2 \sigma - (4/3)\, \pi r^3 n_L KT \ln (P/P_o) \qquad (3.1)$$

where σ is the surface free energy per unit area, or surface tension, r is the drop radius, P is the vapor pressure, P_o is the saturation pressure at the droplet temperature, n_L is number of molecules per unit volume, K is the Boltzman constant, and T is the drop temperature. The supersaturation S, is defined as P/P_o.

Equation (3.1) represents a free energy barrier to the growth of the drops at a given supersaturation. At maximum ΔG, the critical radius r* can be obtained from Equation 3.1 as

$$r^* = \frac{2\sigma}{n_L KT \ln (P/P_o)} \qquad (3.2)$$

The drops of the critical size can be considered as condensation nuclei since at this size the drops will grow with no change in free energy. This critical size represents an equilibrium size at which a supersaturated vapor at vapor pressure P is in equilibrium with this critical drop at a lower saturation pressure P_o. However, this equilibrium mode is unstable. For example, if a drop of the critical size originally in equilibrium with the surrounding vapor suffers a sudden small increase in size due to condensation, then (if the drop temperature does not change), Equation 3.2 shows that the equilibrium pressure, P, on its surface will decrease. Therefore, the actual vapor pressure will then be greater than the equilibrium value and further condensation will occur. This is why the drop of this critical size is called condensation nucleus.

The nucleation rate of critical-sized embryos can be obtained from the kinetics of a nonequilibrium distribution of embryos. The classical nucleation theory[10] shows that there is a very sudden increase in the nucleation rate when past a certain critical value of supersaturation. An extensive validation of the nucleation theory was conducted by Volmer and Flood[11] in an experiment in which a number of vapors were expanded to visible condensation in a cylinder. The observed critical supersaturations agreed suprisingly well with theory in nearly all cases, including water vapor.

Critical condensation nuclei sizes typically range from 10 to 100 atoms. These sizes are considerably smaller than the mean free path of the vapor molecules and therefore the rates of mass and heat transfer at the drop surface cannot be predicted by bulk transport theories. In this case, the kinetic theory of gas should be used to predict the rates of mass and heat transfer at the drop surface.

Starting from the kinetic theory of gas and the energy conservation equation, the rate of growth of a condensation nucleus was obtained by Hill et al.[10] It was found that the growth rate is on the order of 10^{-3} ft/sec. Therefore, it takes only about 1 millisecond for the condensation nucleus to grow to a fog droplet size of 1 μ.

3.2.1.2 HETEROGENEOUS NUCLEATION THEORY

Another mechanism of forming embryos is heterogeneous nucleation on foreign particles that could suspend in the containment atmosphere. These particles may serve as nucleation sites for vapor and thus enhance the nucleation rate. The source of foreign particles in the containment following core degradation could come from fission product aerosols and dust particles. The size distribution of these particles are important because the supersaturation required to form embryos depends on particle sizes.

A typical size distribution of atmospheric aerosols is that of Junge[12], taken from surveys made near Frankfurt A.M., Germany. The surveys found that the size range of dust particles is from 0.01 to 1 μ. In the range from 0.01 to 0.5 μ, there are between 100 and 10,000 particles per cubic centimeter. A majority of particles have sizes smaller than 1 micron. At the smallest size of 0.01 μ, the critical supersaturation is about 1.02 and at the largest size the supersaturation is only 1.001.

The atmospheric aerosols consist of particulates of various sizes, various chemical components, and various electrostatic charges. The aerosol particulates could be soluble or insoluble in water. All these properties could affect the required supersaturation for nucleation.

In the case of insoluble particulates, the contact angle, ϕ, between the embryo and the particle surface is important. If the particle is completely wettable, $\phi = 0$, it forms a base on which a small amount of water can form a drop of large radius of curvature and thus satisfy the Helmholtz equation (Eq. 3.2) at a much lower supersaturation than would be the case if same number of molecules form a drop with a particle core. Fletcher[15] developed a relationship between the supersaturation and drop radius for several values of contact angle, assuming that the particle is spherical. Competely wettable, a particle of 1 micron or so, when covered with a film of water, is theoretically at the critical radius, and it needs only 1.001 critical supersaturation.

The other source of aerosol particulates is fission products. During normal operation, the primary coolant contains very little fission products. During core uncovery a release of fission products, such as the gap release, could occur at about the same time the hydrogen releases. The amount of fission products released to the containment is insignificant before core melting. The size distribution of fission products in the containment can be extrapolated from the CSE experiments[14]. These experiments indicated that soon after fission product release, the mean particle diameter was 15 μ. A few hours later, the mean diameter decreased to about 5 μ because of settling of large particles onto the floor. These sizes are substantially larger than those of dust particles and therefore, critical supersaturation is even smaller than values quoted above for the dust particles.

3.2.2 FOG FORMATION CONDITIONS

Fog formation in a mixture of vapor and noncondensible gases has been of interest to meteorologists, and turbine and condenser designers. Fog is formed by homogeneous or heterogeneous nucleation as a result of temperature drop below the dew point (sometimes with concommitant pressure drop). During the temperature drop, a local gas element will go through a series of thermodynamic states. Eventually, a state is reached at which incipient fog formation occurs. Some degree of vapor supersaturation is needed to precipitate fog formation. The vapor supersaturation at which rapid nucleation of vapor first appears is called critical supersaturation. The critical supersaturation, in general, is a function of temperature, vapor properties, mixing time (if a mixing process is involved), and concentration and sizes of foreign particles. The critical supersaturation data for water has been given in Reference 15.

Fog formation in an ice condenser containment as a result of homogeneous or heterogeneous nucleation could occur: (i) inside the thermal boundary layer near a cold surface, (ii) in adiabatic or nearly adiabatic expansion of vapor jet, and (iii) in mixing of a hot vapor stream with another cooler gas.

Surface cooling may create a region of local supersaturation within the thermal boundary layer, even though the bulk stream is still superheated. If the local supersaturation reaches the critical supersaturation, incipient fog formation will commence. This condensation mechanism may exist in any compartment within the containment especially in the ice condenser where ice temperature is well below the dew point.

When a high speed vapor - noncondensible gas mixture jet goes through an adiabatic or nearly adiabatic expansion, the gas mixture temperature and pressure will drop rapidly such that condensation may occur somewhere in the expansion process. This is the case when a hydrogen-steam mixture jet exits from a break at a supersonic speed. The jet experiences a rapid expansion and if critical supersaturation is reached, condensation shock may occur somewhere within the expanding jet. This condensation mechanism can only occur in a compartment in which the hydrogen-steam mixture jet exists.

Condensation in a fast expanding vapor - noncondensible gas jet is a localized phenomenon. Since the jet expands into a superheated environment in the lower compartment at the later time of the transient, little moisture would be generated in the expansion process even if a condensation shock does exist. Therefore, the present study does not attempt to treat the condensation shock as a source of fog formation.

The third mechanism, condensation due to mixing, may exist in a compartment where a hot hydrogen-steam mixture mixes with a relatively cold containment atmosphere. During the mixing process, local critical supersaturation within the mixing gas could be reached and condensation would ensue. This mechanism could exist in the lower compartment in which relatively cold gas from the upper compartment is returned by the deck fans and mixed with the hot humid air.

Thus, the mixing of cold and hot vapor streams will be treated in the present study. However, only bulk condensation is considered. That is, it is not intended to compute the temperature profile to predict the

local condensation rate. Instead, the bulk gas is assumed at one uniform temperature, and bulk condensation will occur when mixing results in saturation conditions. This is consistent with the CLASIX code assumption of uniform gas temperature.

Before entering into the discussion of the methodology to calculate the fog formation rates from various fog formation mechanisms, a discussion of fog formation conditions is necessary. Since the bulk condensation approach for the mixing process has been adopted, the fog formation conditions for the mixing process are simply that critical supersaturation is reached in the bulk stream. For practical purposes, the critical supersaturation is assumed to be 1.0 since it is likely that plenty of condensation nuclei exist in the atmosphere before mixing condensation takes place.

3.2.3 CONDITIONS FOR FOG FORMATION NEAR A COLD SURFACE

Fog starts to form at a fast rate near a cold surface when local vapor supersaturation reaches the critical supersaturation. Near the cold surface, a thermal boundary layer is formed, within which local vapor pressure and saturation pressure vary. Typical vapor pressure and temperature profiles, when the incipient homogeneous nucleation first appears, are shown in Figure 3.2. It is seen in this figure that when the local vapor pressure reaches the critical vapor pressure there is a sudden appearance of fog in the boundary layer due to the fast nucleation rate. Rosner and Epstein[11] have derived fog formation conditions near a cold surface, assuming that the local vapor pressure curve is tangent to the critical vapor pressure curve at the fog incipient point. A more general fog formation criterion given by Hijikata and Mori[17] is

$$\frac{\Delta W}{\Delta T} > \left(\frac{dW}{dT}\right)_{wall} \tag{3.3}$$

where $\Delta W = W - W_w$

$\Delta T = T - T_w$

and the weight fraction of condensing vapor, W, can be related to the partial pressure of the condensing vapor P_v as

$$W = \frac{(P_v/P)\,(M_v/M_g)}{1 - (P_v/P)\,(1 - M_v/M_g)} \tag{3.4}$$

where P = total pressure

M_v = vapor molecular weight

M_g = noncondensible gas molecular weight

Equation (3.3) may be rewritten as

$$n > 2 \tag{3.5}$$

where

$$n \equiv 2\,\frac{\Delta W}{\Delta T} \Big/ \left(\frac{dW}{dT}\right)_{wall}$$

The parameter n is used in the following section to calculate the fog formation rate. It will be demonstrated that when $n < 2$, no fog formation is possible.

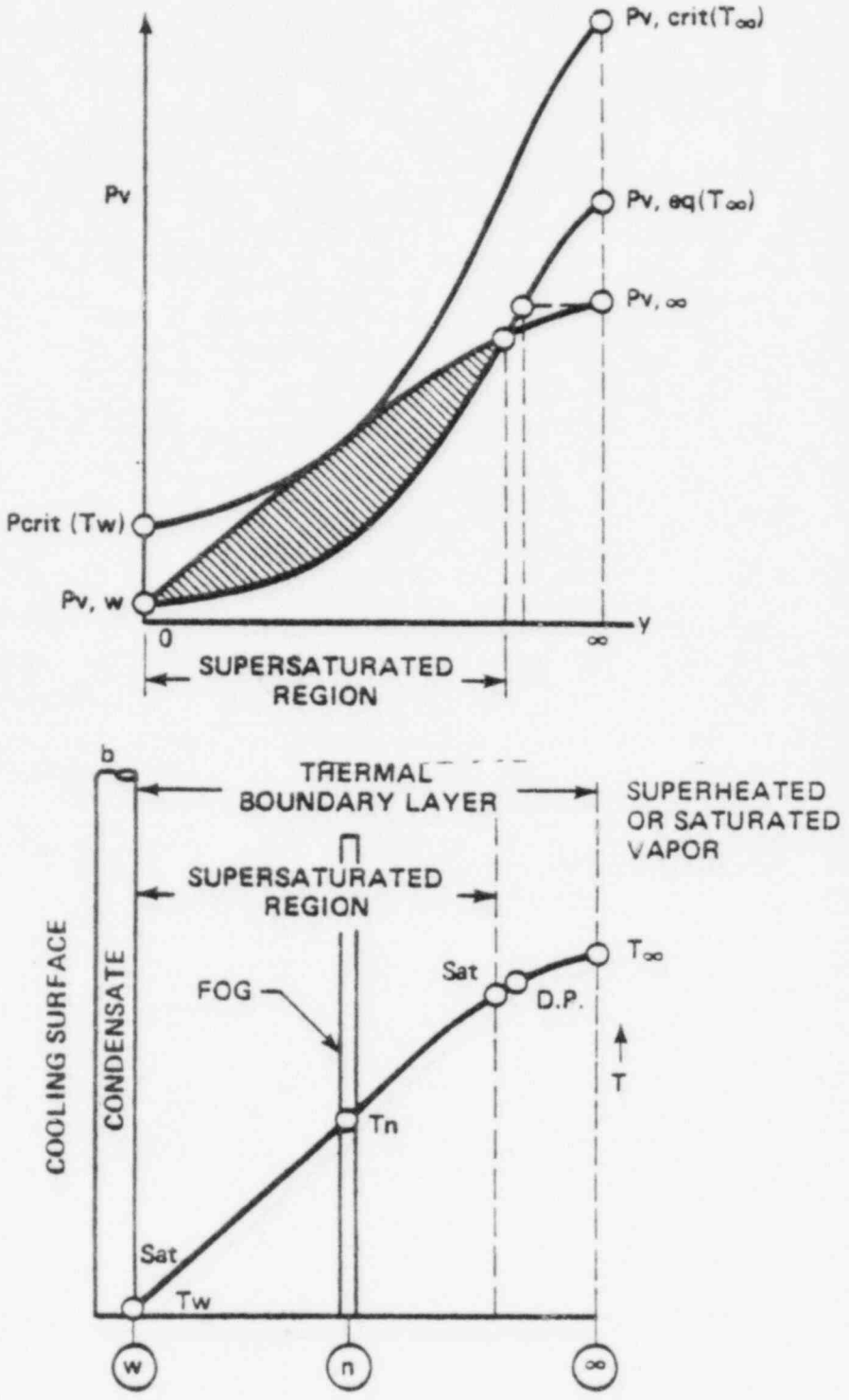

FIGURE 3.2 VAPOR PRESSURE AND TEMPERATURE PROFILES NEAR A COLD SURFACE

3.2.4 RATE OF FOG FORMATION NEAR A COLD SURFACE

As has been discussed in Section 3.2.3, fog will form near cold surfaces (e.g., in the ice condenser early in the transient.) As discussed in Section 3.2.1, once water embryos are formed it takes only a few milliseconds for them to grow to the micron size. After these micron size fog droplets are formed, it needs very little supersaturation for further growth. Therefore, in the present analysis, it is assumed that vapor and droplets are in thermal equilibrium and local vapor pressure is equal to the local saturation pressure. This section is concerned with the transport of these micron-size fog droplets within the thermal boundary layer.

The boundary layer fog formation rate can be determined using the Hijikata-Mori theory[17] of fog formation in the thermal boundary layer. It was assumed that a thin liquid film, having a thickness of δ_ℓ on a cold surface, coexists with a gas-droplet flow in a two-phase boundary layer of thickness δ outside the liquid film as shown in Figure 3.3.

It was further assumed that the saturation condition exists within the two-phase boundary layer and the boundary layer approximation is applicable. Numerical solutions were obtained for the mass fraction of fog droplets, Y_o, at the gas-liquid film interface. The fog droplet flow rate at a distance X along the plate may be expressed in terms of Y as

$$\dot{m}_f = L \rho \int_0^\delta Y u dy \qquad (3.6)$$

where Y = mass fraction of fog droplets in the boundary layer

ρ_ℓ = fog droplet density

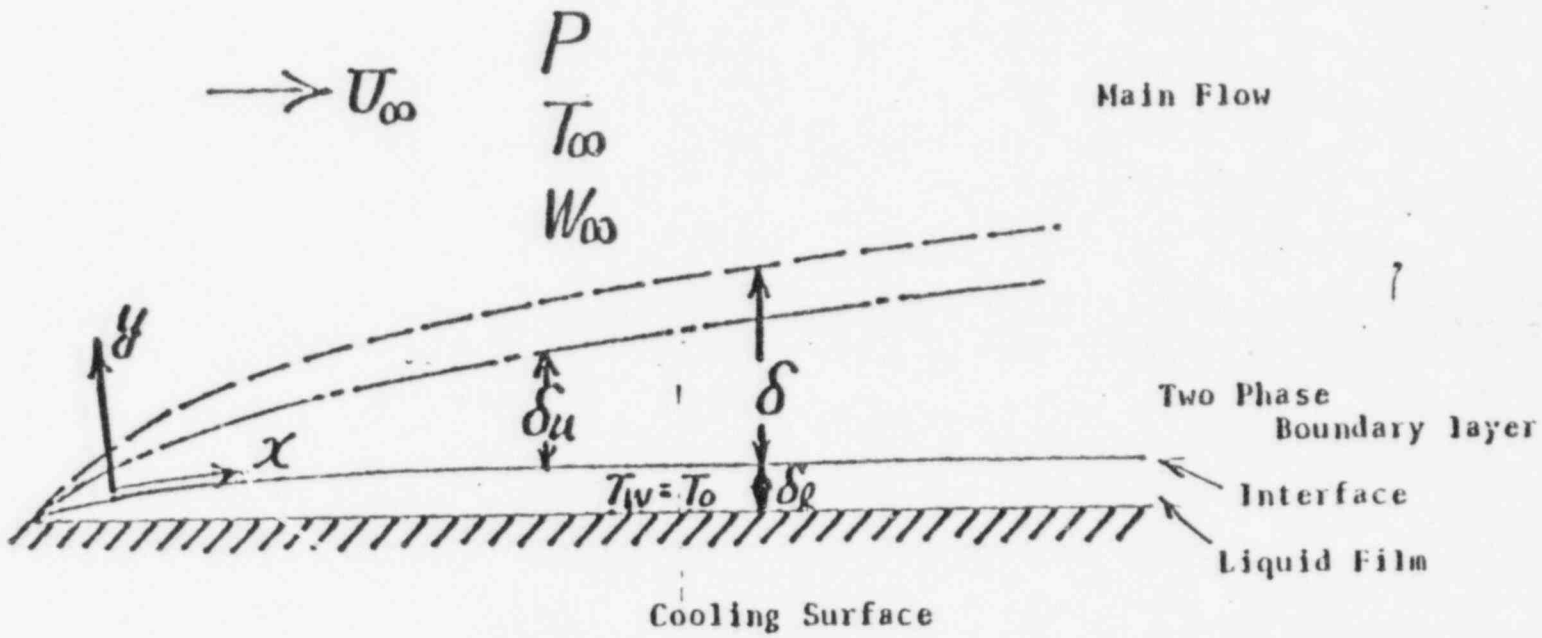

FIGURE 3.3 FORMATION OF FOG NEAR A COLD SURFACE

ρ_v = vapor density

ρ_g = noncondensible gas density

Y_0 = mass fraction of fog droplets at the wall

y = coordinate perpendicular to the plate

δ = fog boundary layer thickness

L = width of boundary layer

ρ = $\rho_v + \rho_g$

Using the boundary layer approximations

$$Y = Y_0 (1 - y/\delta) \tag{3.7}$$

$$u = U \left\{ \frac{3}{2} \left(\frac{y}{\delta_u} \right) - \frac{1}{2} \left(\frac{y}{\delta_u} \right)^3 \right\} \tag{3.8}$$

$$\delta (x) = a\, x^{1/2} \tag{3.9}$$

$$\delta_u = \delta (x) (1 - \xi) \tag{3.10}$$

where a = known constant

ξ = known constant

U = free stream velocity

Substituting Eqs. (3.7) through (3.10) into Eq. (3.6), we have the rate of fog formation

$$\dot{m}_f = \rho L \delta Y_o U_\infty \left\{ \frac{0.25}{1 - \xi} - \frac{0.025}{(1 - \xi)^3} \right\} \qquad (3.11)$$

Derivation of expressions for a, Y_o, and ξ is given in Appendix A. Even though boundary layer fog formation may occur in any containment subcompartment, the fog formation rate is likely to be small except in the ice condenser. For fog formation in the ice condenser, L is the total length of the periphery of ice baskets and x is the height of the ice bed.

During fog formation in the boundary layer, heat transfer to the cold surface will decrease the bulk fluid temperature. If the bulk fluid temperature drops below the dew point corresponding to the free stream vapor pressure, then bulk stream condensation could occur. In this case, it is assumed that the boundary layer thickness, δ, will grow so thick that $L\delta U_\infty$ becomes the gas volumetric flow rate Q through the condensing compartment. This is a very conservative assumption in terms of the fog formation rate. Under this assumption Equation (3.11) becomes

$$\dot{m}_{cond} = \rho Q Y_o \left\{ \frac{0.25}{1 - \xi} - \frac{0.025}{(1 - \xi)^3} \right\} \qquad (3.12)$$

where $\dot{m}_{cond}$ is the sum of boundary and bulk stream fog formation rates.

3.2.5 FOG DROP SIZES

As mentioned earlier, when homogeneous nucleation commences, a large number of condensation nuclei are formed and they grow to the micron size within a few milliseconds. In heterogeneous nucleation, fog droplets grow on aerosol particles, which are usually less than 1 μ. In any case, the final drop sizes are determined by the atmospheric conditions with which the drops are in thermal equilibrium.

Neiburger and Chien[18] studied the growth of cloud drops by condensation and calculated droplet size distribution based on a cloud cooling rate of 6°C/hr. The initial size distribution of condensation nuclei (sodium chloride) were chosen to correspond to available observations as shown in Figure 3.4 (designated as 0 second). The calculated drop size distributions at 3000 and 6000 seconds are shown in Figure 3.4. It is seen that the diameters of fog droplets range from 0.01 μ to 20 μ. The volume mean drop diameters are 8 μ and 12 μ at 3000 and 6000 seconds, respectively. In the present study, a mean value of the volume mean drop sizes, i.e. 10 μ, is chosen for fog deposition and inerting calculations. This is consistent with the observation of valley fogs of volume mean drop diameters ranging from 9 to 14 μ[30].

3.3 FINE MIST DROPLETS FROM CONTAINMENT SPRAYS

The containment sprays produce fairly large drop sizes. A typical containment spray nozzle, e.g., Spraco 1713 nozzle, produces the size distribution as shown in Figure 3.5, using a pressure difference of 50 psi across the nozzle[19]. It is seen that water droplets produced from containment spray range from 100 μ to 2000 μ. These large drops have little potential for raising the lower flammability limit, as already demonstrated in the Fenwal tests[20] and more recent tests at Factory Mutual[21]. To affect the flammability limit of a hydrogen mixture, the drop sizes have to be smaller than about 20 μ, namely in the fog drop size ranges. Since containment sprays essentially do not produce drops in this size range, containment sprays will not be considered as a means to produce fog droplets. Rather, it will be considered as a means to remove the fog droplets.

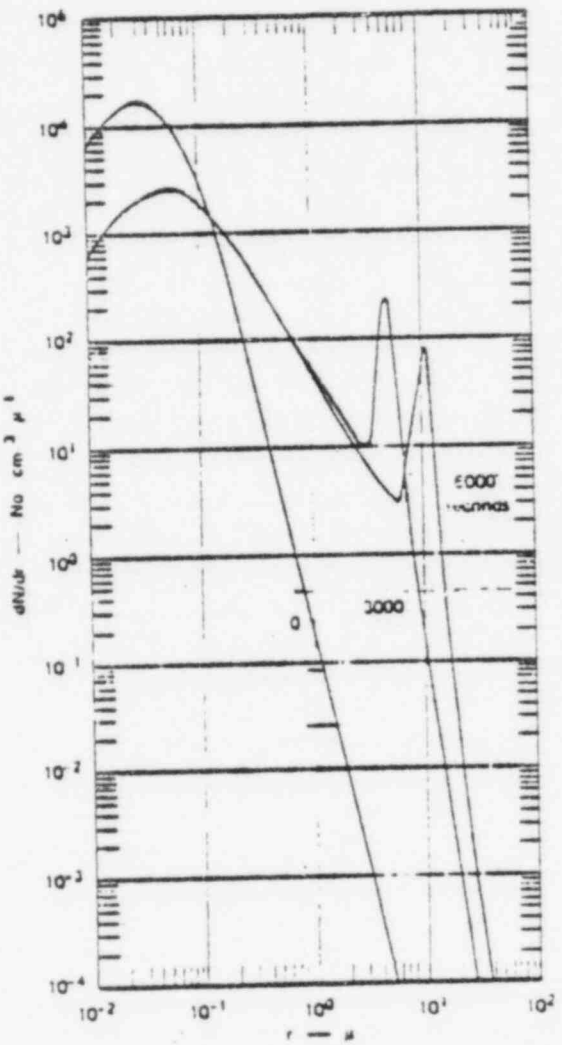

FIGURE 3.4 CLOUD DROP SIZE DISTRIBUTION
PREDICTED BY NEIBURGER AND CHIEN

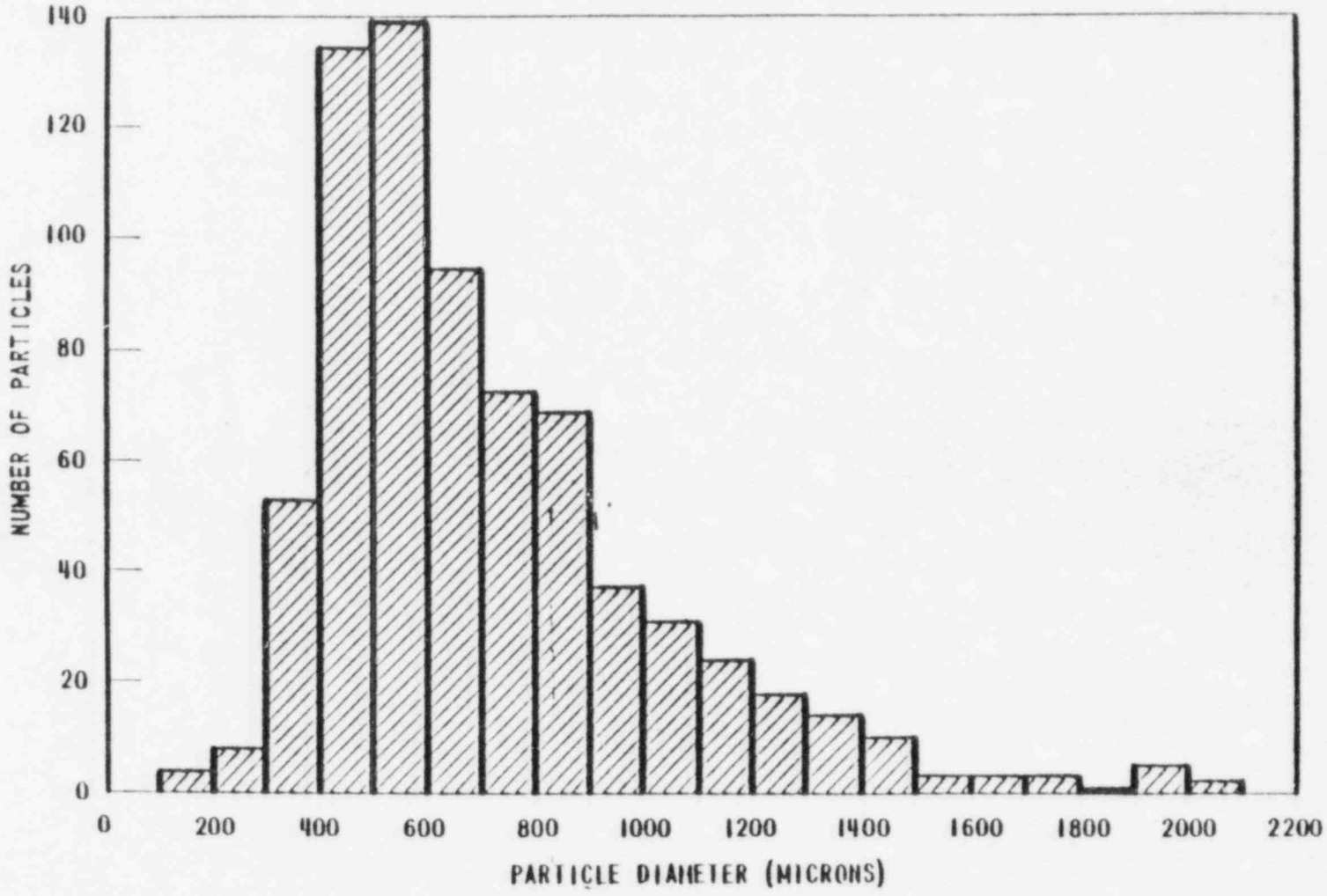

FIGURE 3.5 PARTICLE SIZE DISTRIBUTION FOR 50 PSI PRESSURE DROP ACROSS NOZZLE NO. 1713

4.0 FOG REMOVAL MECHANISMS IN AN ICE CONDENSER CONTAINMENT

In Section 3, the mechanisms of generating fog droplets were discussed. After these droplets are generated, they can be removed from the containment atmosphere by gravitational settling, vaporization, containment sprays, and impingement on structures. They can also coalesce with other drops during collision and form bigger drops. These bigger drops could easily settle out of the atmosphere under gravity. These fog droplet removal mechanisms will be discussed in this section.

4.1 SETTLING DUE TO GRAVITY

Drop removal rates due to gravitational settling depend strongly on drop radius. The removal rate increases linearly with drop terminal velocity, drop concentration, and settling area. The relationship may be expressed as

$$\dot{m}_{set} = V_t \, n \, A \qquad (4.1)$$

where n is the mass of mist droplets per unit volume, and A is the settling area.

The terminal velocity, V_t, is a strong function of drop radius and the relationship is shown in Figure 4.1 (Figure 5 of Reference 6). For a 1000 μ drop, its terminal velocity is above 1 m/s, while for a 10 μ drop, which is the typical fog drop size, its terminal velocity is only about 1 cm/s. Therefore, there is very little removal by gravity for fog droplets.

4.2 AGGLOMERATION

After the fog droplets are produced, the droplets will undergo changes in the number density and size distribution with time, when drops collide with each other and coalesce. The agglomeration rate (No. of particles per unit volume per unit time) has been found to be proportional to the square of the drop population density and the coagulation mechanisms dependent rate constant K[22].

For drops larger than 1 μ, the dominant mechanism is the difference in velocities between drops in adjacent streamlines. This is usually termed the velocity gradient coagulation. For drops smaller than 1 μ, the velocity gradient effect becomes small, and drops are brought together by Brownian motion. This leads to greatly different agglomeration rates for different initial drop sizes. A typical agglomeration rate as a function of drop size in a moderately turbulent atmosphere is shown in Figure 4.2. In Figure 4.2, the sharp rise of the agglomeration rate with drop diameter larger than 1 μ implies that the larger drops agglomerate quickly to the maximum stable size supported by the atmospheric turbulence. The agglomeration rates for drops less than 1 μ are very small. Since most of the fog droplets are in micron size ranges, the agglomeration rate is not large. It is assumed in the present analysis that the initial 4 μ blowdown mean drop size will grow to 10 μ (See Section 3.2.5). Agglomeration as a separate mechanism for fog growth has been conservatively neglected.

4.3 VAPORIZATION

Fog droplets suspended in the containment atmosphere are considered to be in thermodynamic equilibrium with the surrounding gas. When the surrounding atmosphere becomes superheated or when the droplets are entrained into a superheated subcompartment, they can undergo vaporization or condensation.

In the present analysis, it is assumed that water vapor and mist droplets are in thermal equilibrium at all times. Therefore, the amount of vaporization or condensation will be determined by the thermal equilibrium state reached by the vapor and drops. In other words, it is not intended to model heat transfer between the drops and the surrounding gas, and thus determine the vaporization rate. This is a good assumption for the small fog drop sizes.

4.4 REMOVAL BY SPRAY DROPS

As mentioned above, the containment spray droplets range from 100 μ - 2000 μ, which are substantially larger than the fog droplets. If fog droplets enter the spray zone, they will probably be removed by the spray droplets by colliding with them, since the spray drop volume is much larger than the fog drop volume. A simple analytical model is used in the present study which assumes that all the fog droplets residing in the spray zone will be swept by the sprays to the floor with the spray drop removal efficiency E. The spray removal rate may be expressed as

$$\dot{m}_{sp} = E\, Q_{sp}\, M_c / \eta_{sp}\, V \qquad (4.2)$$

where E = spray drop removal efficiency

Q_{sp} = volumetric flow rate of sprays

η_{sp} = volume fraction of spray droplets in the spray zone

M_c = mass of fog in compartment volume V

4.5 OTHER REMOVAL MECHANISMS

Another similar mechanism for fog removal is the formation of droplets in the ice condenser. These droplets which would be generated in the ice bed when the ice melts, would fall through the ice bed, and remove fog droplets from the flow through the ice condenser. This large quantity of water would be effective in removing fog droplets. However, due to difficulty in modeling this removal mechanism, it is conservatively neglected in the present analysis.

In addition to the removal mechanisms mentioned above, fog can also be removed by impacting structural surfaces. Due to the inertia of fog droplets, substantial fog removal by impacting structural surfaces could occur when the drop-laden mixture flow passes through long, narrow, curved paths, such as ice basket flow paths, and fan ducts. Moreover, the centrifugal force exerting on the fog droplets, when they pass through the fans, could cause the fog droplets to impact the blade surfaces or other parts of the fans. These removal mechanisms are believed to be significant; however, they are conservatively neglected in the present analysis. It is, therefore, believed that the present analysis is very conservative.

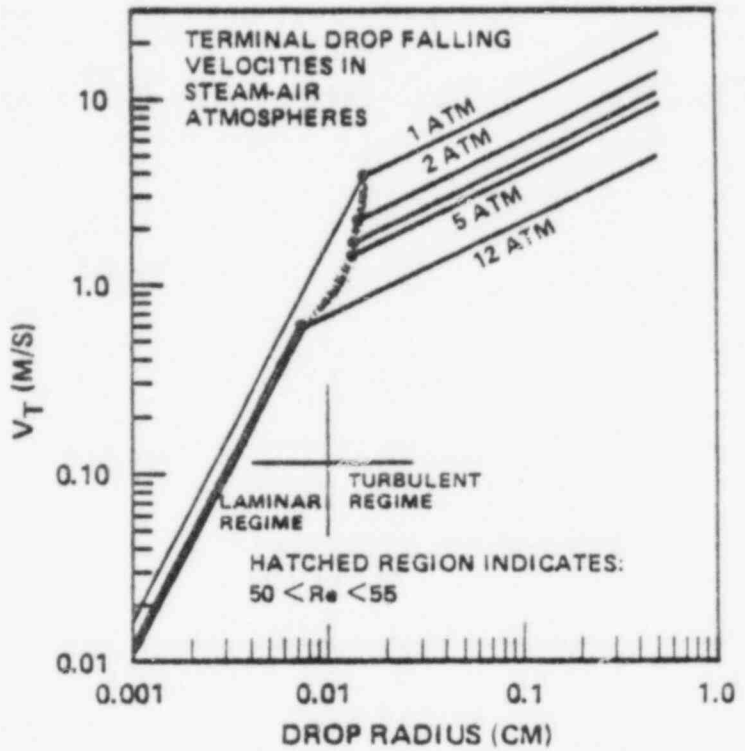

FIGURE 4.1 TERMINAL VELOCITY AS A FUNCTION OF DROP RADIUS IN STEAM-AIR ATMOSPHERE

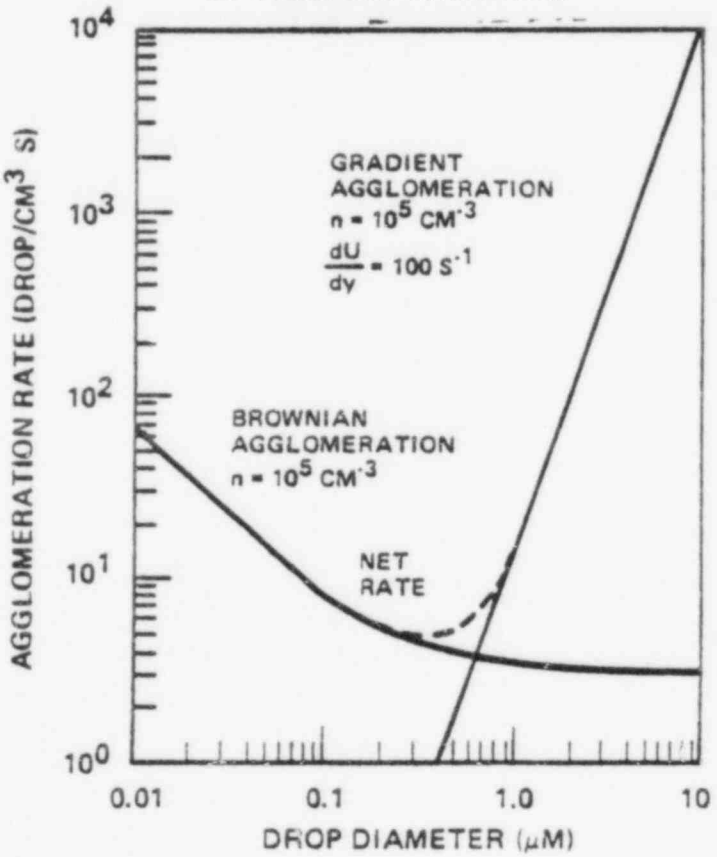

FIGURE 4.2 AGGLOMERATION RATES IN AIR BETWEEN EQUAL-SIZED DROPS

5.0 FOG INERTING CRITERIA

Recent hydrogen burn experiments conducted at Lawrence Livermore Laboratory indicated that substantial fog formation could occur when saturated steam is discharged into an unheated vessel. It appeared that this fog prevented a glow plug igniter from successfully igniting the hydrogen mixture in the vessel. The ability of fog in inhibiting and quenching of hydrogen combustion can be explained as follows. The fog droplets suspended in the hydrogen-air-steam mixture act as a heat sink that could absorb a large amount of combustion heat, greatly reducing the pressure and temperature rises resulting from hydrogen combustion. If droplets are sufficiently small such that they could vaporize inside the thin (1mm) flame front, the flame may be quenched or inhibited. For a flame speed of 2 m/s, the drop residence time is of the order of 0.5×10^{-3} seconds.[24] In such a short period of time, the droplets of initial radius less than about 4 μ will vaporize entirely in the flame front.

The quenching of a propagating flame is also governed by the distance between droplets. As the droplets become closely packed, the total droplet surface area available for energy loss increases. A critical spacing between droplets exists such that a large fraction of the heat released is absorbed, thus preventing flame propagation. This critical spacing is known as the "quenching distance", which is usually determined by propagating flames in tubes.

5.1 PREVIOUS WORK

The effectiveness of fog droplets in inhibiting or quenching a flame depends on its quenching distance, was determined by Berman et al.[24] as

$$d_q = [4V/S]_{crit} \tag{5.1}$$

where V is the gas volume and S is the heat transfer surface area. For various hydrogen-air mixtures, the data on the quenching distance is

shown in Figure 5.1. In the suspended fog droplets, this volume-to-surface ratio (i.e., V/S) is equal to

$$\frac{1}{6} \frac{d\,(1 - \eta)}{\eta}$$

where d is the mean droplet diameter and η is the volume fraction of water. When four times this ratio approaches the quenching distance, a critical droplet diameter can be obtained as

$$d_c = \frac{3}{2} \frac{\eta d_q}{1 - \eta} \qquad (5.2)$$

Using this criterion for quenching a flame, for a given volume fraction of water and gas composition, d_q can be determined. The critical droplet diameter then can be determined from the above equation. The drop sizes less than the critical drop size are capable of quenching a flame.

A plot of Eq. (5.2) for two hydrogen concentrations is shown in Figure 5.2

5.2 PRESENT THEORY

The previous theories do not model the heat transfer and combustion processes occurring between the burned gas and the suspended droplets. A new theory has been developed, which models the heat loss and combustion.

Consider a hydrogen/air/steam/mist droplets mixture in which a flame is propagating. The flame may be divided into three zones: heating zone, reaction zone, and post-reaction zone as shown in Figure 5.3. The unburned gas at temperature T_u moves in the reaction zone with the laminar burning velocity S_u. If the unburned gas density is ρ_u, then the constant mass flow rate m is equal to $\rho_u S_u$. The unburned gas is heated to ignition temperature T_i and burned in the reaction

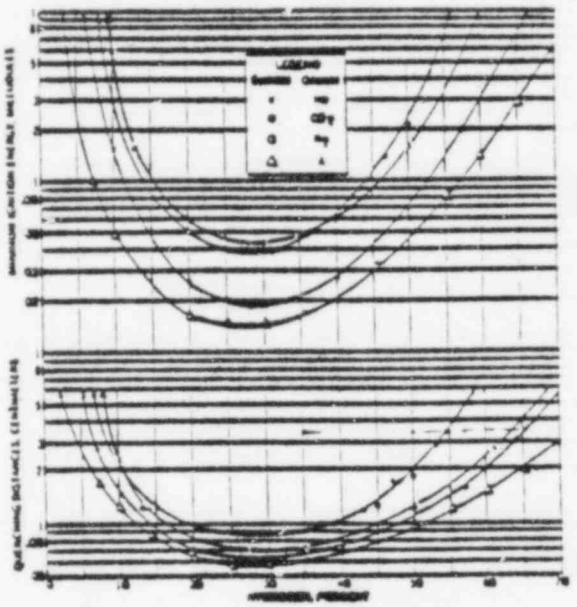

FIG. 5.1 MINIMUM IGNITION ENERGIES AND QUENCHING DISTANCE FOR HYDROGEN-OXYGEN INERT GAS MIXTURES AT ATMOSPHERIC PRESSURE

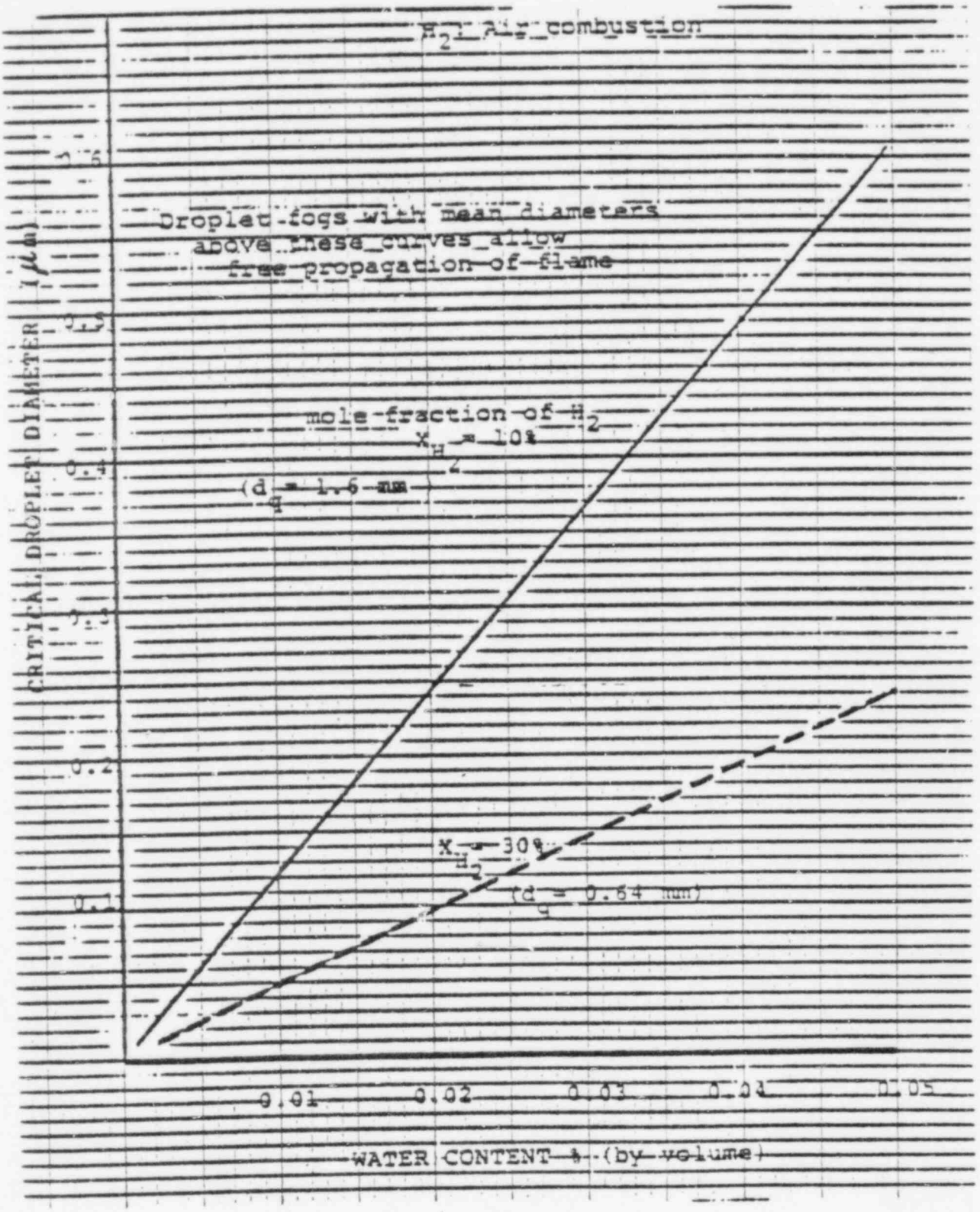

FIGURE 5.2 THE EFFECT OF DROPLET SPACING ON FLAME QUENCHING

zone to reach the flame temperature T_f. The fog droplets will act as a heat sink that reduces the flame temperature. The problem has been formulated and solved by von Karman[25]. In his formulation, three energy equations, which incorporate the heat loss terms, were written for the three zones described above. The solution to these equations yields the following relationship

$$2 K\theta_i = \left\{1 - \exp\left(-\frac{1}{2}\mu^2\right)(Y_u - Y_f)\right\} \times \left[1 + \sqrt{1 + (4K/\mu)^2}\right] \left\{ \times \left\{1 - \frac{1}{\sqrt{1 + K/\mu^2}}\right\} \right. \tag{5.3}$$

where $\theta_i = \bar{C}_p (T_i - T_u)/q$

$$\mu = \sqrt{\bar{C}_p / \bar{\lambda} w}\, m$$

$K\theta_i = (S/\bar{C}_p w)\, \theta_i$

= the ratio of heat loss rate per unit volume to the heat release rate by chemical reaction per unit volume

q = heat of combustion

$\bar{C}_p$ = mean specific heat

$\bar{\lambda}$ = heat conductivity

w = reaction rate (mass of fuel consumed per unit time per unit volume)

Y_u = hydrogen mass fraction in the heating zone

Y_f = hydrogen mass fraction in the reaction zone

m = $\rho_u S_u$

A plot of Eq. (5.3) is shown in Figure 5.4. It is seen that for a given $K\theta_i$, there is a minimum value of $(Y_u - Y_f)/\theta_i$. Below this minimum value, there is no solution for the $\sqrt{\theta_i}\ \mu$. Therefore, this value is considered as the flammability limit. At the flammability limit, the value of $K\theta_i$ can be determined from Figure 5.4 or from Eq. (5.3) as

$$(K)_{crit}\ \theta_i = f\ ((Y_u - Y_f)/\theta_i) \tag{5.4}$$

A plot of $(K)_{crit}\ \theta_i$ as a function of $(Y_u - Y_f)/\theta_i$ is shown in Figure 5.5. Equation (5.4) may be expressed as

$$\frac{n}{d^2} = \frac{q\ \bar{C}_p\ \rho_u^2\ Su^2\ (Y_u - Y_f)\ f\left(\frac{Y_u - Y_f}{\theta_i}\right)}{12\ \bar{\lambda}^2 (T_i - T_u)} \tag{5.5}$$

Detailed derivation procedure for Eq. (5.5), is given in Appendix B. Using the data on S_u from Reference (26) we can calculate the right hand side of Eq. (5.5) for a given composition and initial gas temperature.

5.3 VERIFICATION OF THEORIES BY EXPERIMENTS

Experiments have been conducted at Factory Mutual to study the effects of water fog density, droplet diameter, and temperature on the lower flammability limit of hydrogen-air-steam mixtures[21]. The results indicated that most of the fog nozzles tested at 20°C only changed the limit from 4.03 volume percent to 4.76 percent, corresponding to fog concentration in the range of 0.028-0.085 volume percent, and volume mean drop size ranging from 45-90 microns. For the 50°C case, the lower

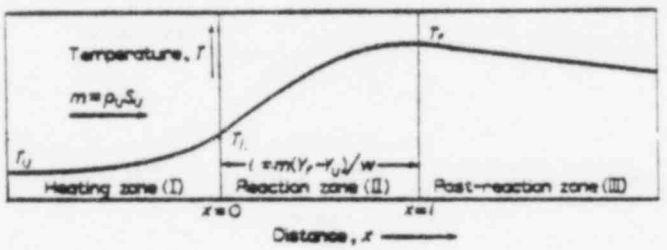

FIGURE 5.3 SCHEMATIC REPRESENTATION OF TEMPERATURE PROFILE THROUGH THE FLAME FRONT

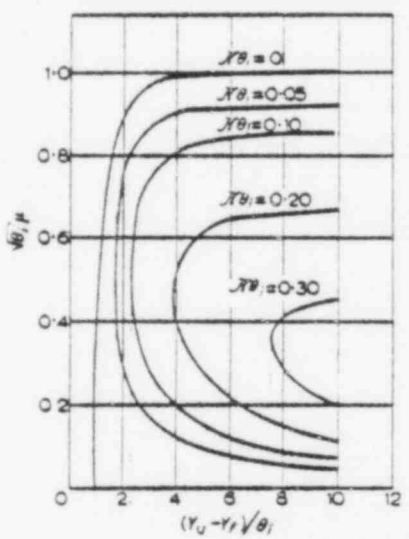

FIGURE 5.4 THE PARAMETER $\sqrt{\theta_i}\ \mu$ AS A FUNCTION OF $(Y_u - Y_p)/\theta_i$ FOR DIFFERENT VALUES OF $K\theta_i$

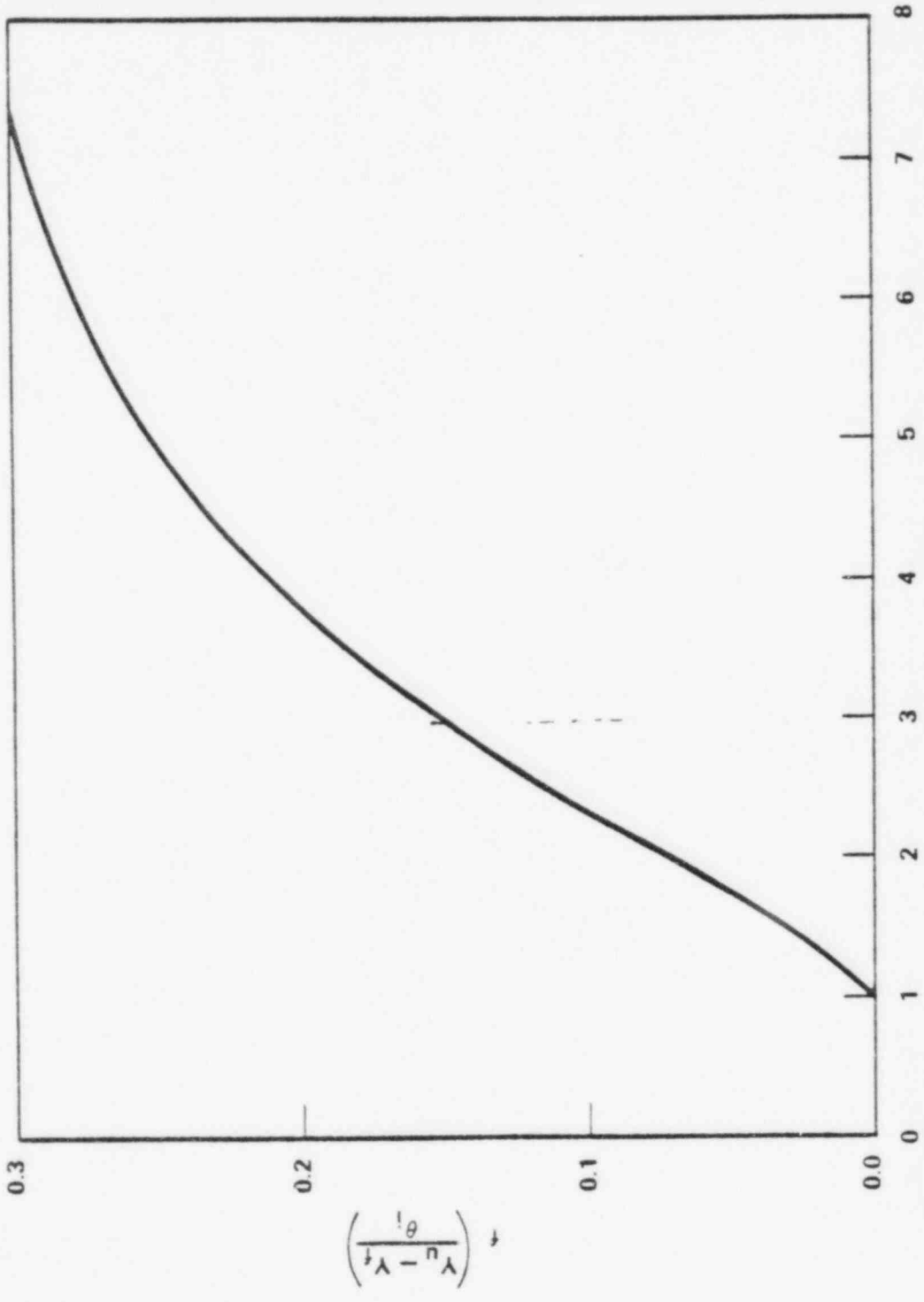

FIGURE 5.5 $(K)_{crit}$ θ_i AT THE FLAMMABILITY LIMIT AS A FUNCTION OF $(Y_u - Y_f)/\theta_i$

flammability limit increases to 7.2 percent, corresponding to 0.01-0.04 volume percent of fog and 20-50 micron volume mean drop sizes. The results demonstrated that the fog inerting effect is more pronounced at small drop sizes.

Figures 5.6 through 5.8 show the comparison between the test data and the theoretical predictions. For this comparison, the present theory used the free stream temperature to calculate the thermodynamic properties used in Equation (5.5). This yielded somewhat higher fog concentrations than those calculated by use of the mean of the flame and free stream temperatures. In Figures 5.6 and 5.7, the data suggests a linear relationship between the volume concentration and volume mean drop size on the log-log plot. It also suggests that the minimum fog inerting concentration varies approximately with the square of the volume mean drop size. In this regard, the present theory seems to be more consistent with the data than the Berman et al. theory.

The present theory is in good agreement with the Factory Mutual data at 4.76 percent H_2; however, it overpredicts the minimu fog inerting concentration at 7.2 percent H_2. The cause of this discrepancy is still unknown. The discrepancy may be caused by the uncertainty of the data. The following discussion supports this claim. The fog droplets are very small and they vaporize very fast in a flame. Therefore, the fog droplets behave as steam except for their larger heat absorption capability. When the fog droplets vaporize, they absorb the heat of vaporization which is much larger than the steam sensible heat. Typically, the heat of vaporization of water is about 1000 Btu/lb and the average specific heat of steam in the temperature range of interest is about 0.48 Btu/lb. It is well known that a hydrogen flame cannot propagate in steam higher than about 64 percent in a steam-air mixture. At 7.9 percent H_2, the adiabatic flame temperature is about 1240°F and therefore the increase of the steam sensible heat is about 540 Btu/lb. Consequently, for the same amount of fog droplets and steam, the fog droplets heat absorption capability is about 1.9 times higher. This means that the fog concentration which is equivalent to 22.1 percent steam in steam and air is capable of inerting 7.9 percent H_2. This

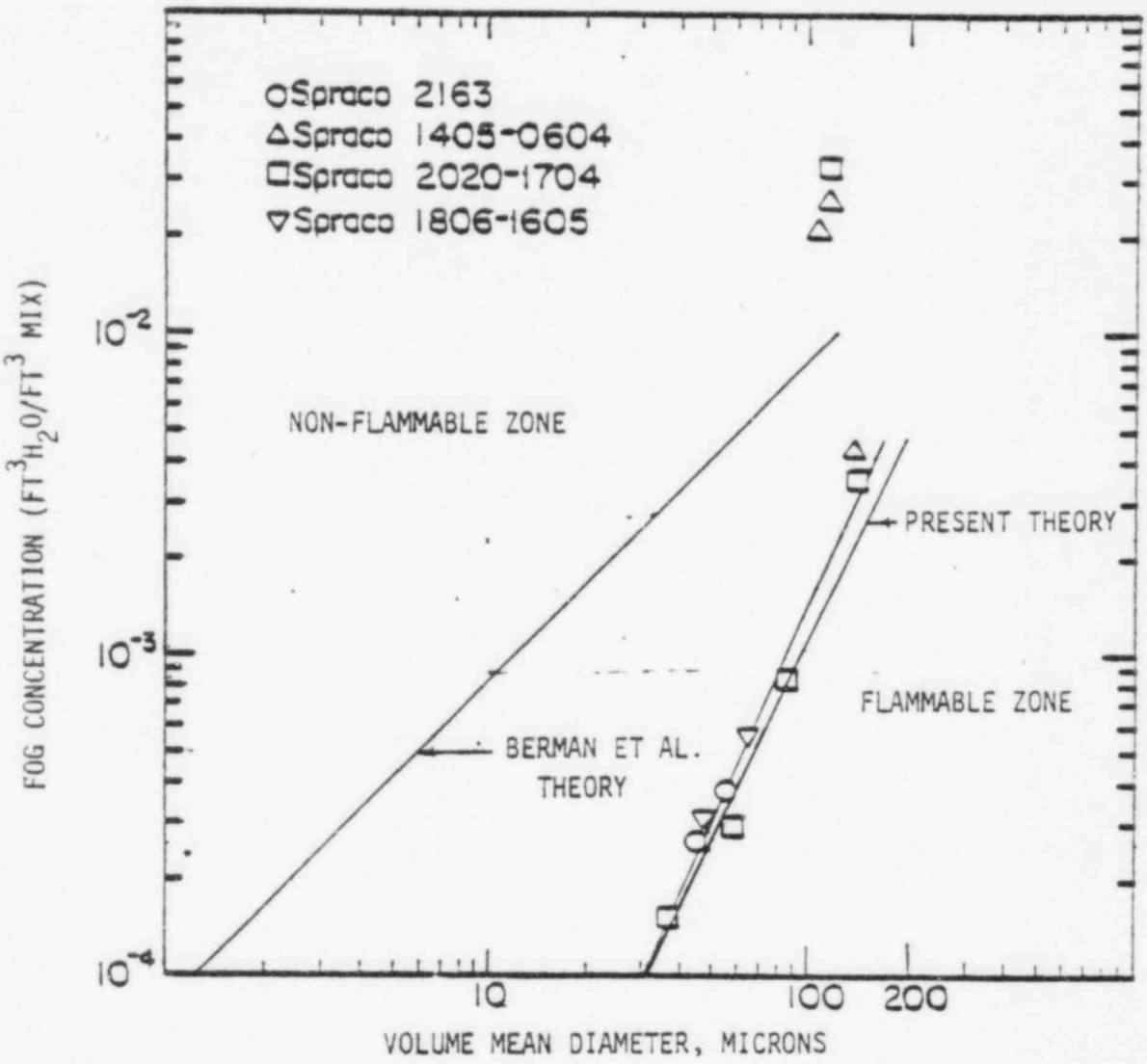

FIGURE 5.6 COMPARISON BETWEEN THEORIES AND FACTORY MUTUAL FOG INERTING EXPERIMENTS ON 4.76 PERCENT H_2

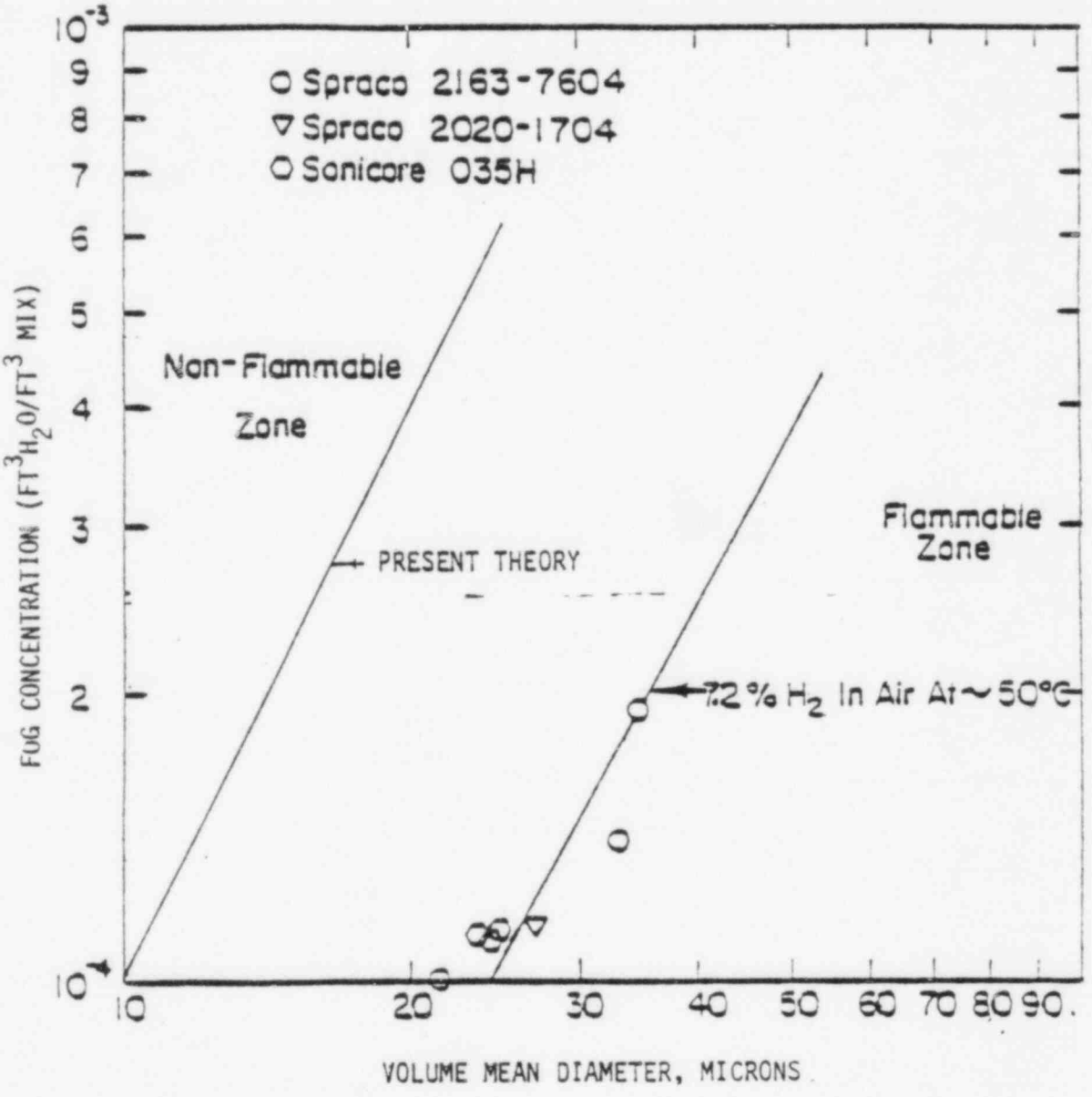

FIGURE 5.7 COMPARISON BETWEEN THE PRESENT THEORY AND FACTORY MUTUAL FOG INERTING EXPERIMENTS ON 7.2 PERCENT H_2

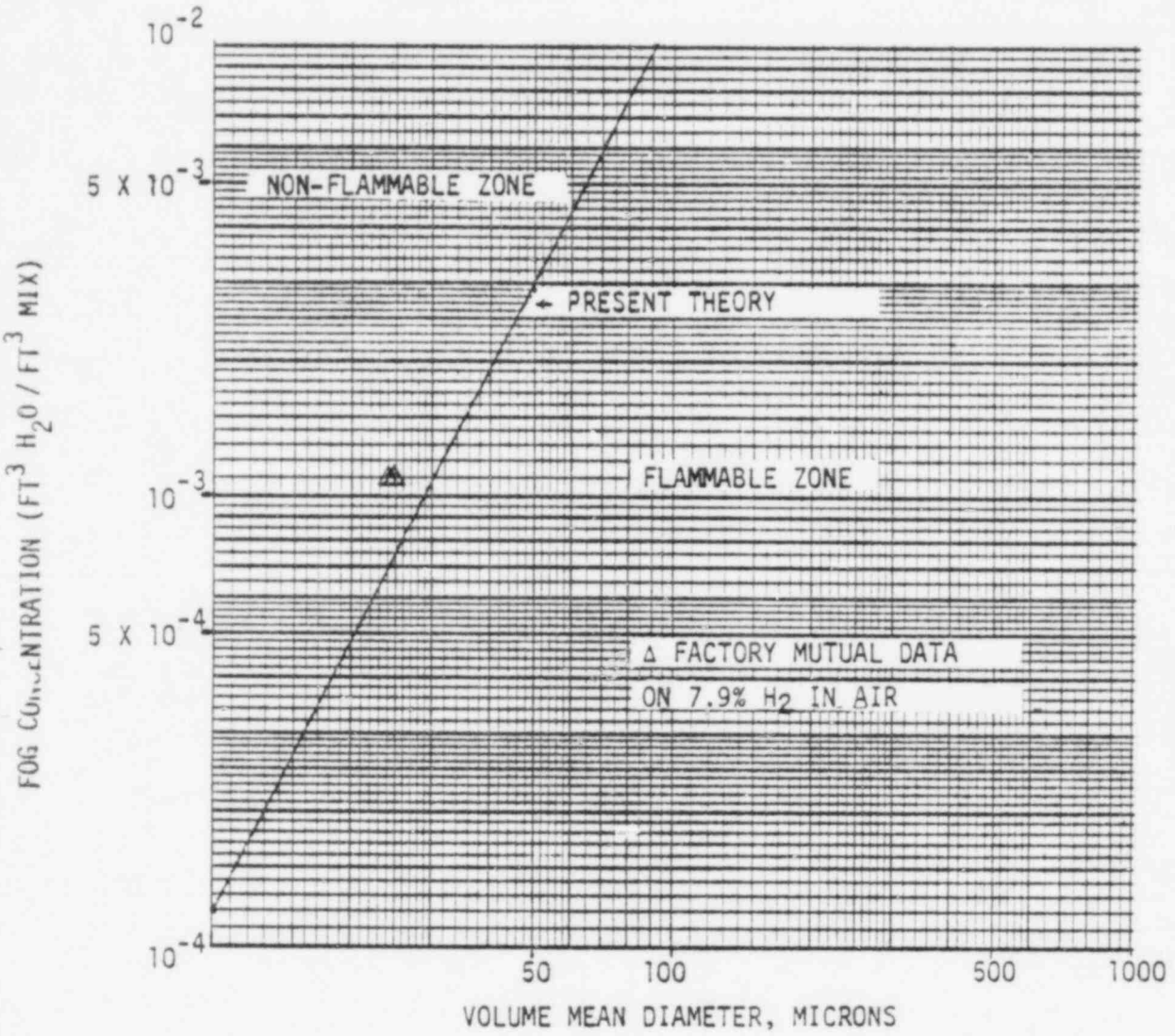

FIGURE 5.8 COMPARISON BETWEEN THE PRESENT THEORY AND FACTORY MUTUAL FOG INERTING EXPERIMENTS ON 7.9 PERCENT H_2

fog inerting vomumetric concentration was calculated to be 1.61×10^{-4} ft^3 H_2O/ft^3 mix. To inert 7.2 percent H_2, a minimum fog concentration which corresponds to about 21.3 percent steam in steam and air is required. This gives a minimum fog inerting concentration of 1.56×10^{-4} ft^3 H_2O/ft^3 mix for 7.2 percent H_2 . These estimates show that the present predictions are reasonable and conservative. The estimates are consistent with Factory Mutual data on 7.9 percent H_2 but not on 7.2 percent H_2.

It should be noted that in the tests three fog concentration measuring techniques were used. These three techniques gave substantially different results. The discrepancy is at least one order of magnitude difference. The fog concentration data presented in Figures 5.6 through 5.8 were obtained from one of the techniques. In view of the uncertainty of the data, care must be exercised in using them for inerting analysis purposes. They should be used in conjunction with the present fog inerting criterion in the assessment of fog inerting potential in the ice condenser plants. Some uncertainty also exists in the present fog inerting theory. The maximum uncertainty associated with the underprediction of the heat loss and temperature dependence of the thermophysical properties is estimated to be ± 63 percent.

It should also be pointed out that the Factory Mutual data and the present theory can only predict the minimum fog inerting concentration. Estimates of burn completeness in just-flammable fog mixtures were not within the scope of the present effort.

6.0 ASSESSMENT OF FOG INERTING PROBABILITY IN ICE CONDENSER CONTAINMENTS

As discussed in the previous sections, there exist several mechanisms of generating and removing fog droplets from the ice condenser containment. In addition, fog droplets are also transported from one subcompartment to another by entrainment in the gas stream. The fog entrainment rate is difficult to assess without knowing the velocity field and drop size distribution. For simplifying purposes, it is presently assumed that the mass fraction of mist droplets in the intercompartmental and fan flows is the same as that within the subcompartment from which the flows are originated. This is a good assumption since the fog droplets are small. The amount of fog droplets in a subcompartment depends on all these mechanisms.

The total amount of fog droplets is important in determining the volume fraction of suspended condensate in a subcompartment. This volume fraction, in turn, is used in the fog inerting criteria to determine whether a particular hydrogen mixture composition formed in a subcompartment at any time is flammable or not. In other words, by knowing the hydrogen concentration and the mean fog drop size, we can determine whether the calculated volume fraction of fog droplets is high enough to prevent the mixture from combustion.

6.1 DETERMINATION OF VOLUME FRACTION OF MIST DROPLETS IN ICE CONDENSER CONTAINMENTS

Consider a subcompartment in the ice condenser containment as shown in Figure 6.1. There exist several mechanisms by which mist drops can be generated or removed. Fog droplets can be generated by homogeneous or heterogeneous nucleation in the thermal boundary layer and/or in the bulk stream and they can increase in size by condensation or decrease in size by vaporization. The rate of generation of mist droplets by condensation and their continued growth (or shrinkage due to vaporization is represented by $\dot{m}_{cond}$. The other mechanism of generating mist droplets considered in this analysis is the primary coolant discharge from the break and the rate of generating fog droplets from this mechanism is

represented by $\dot{m}_{break}$. Two fog droplet removal mechanisms are considered in this analysis: one is gravitational settling and the other is removal by containment spray. The fog droplet removal rate by gravitational settling is represented by $\dot{m}_{set}$ and that by spray is represented by $\dot{m}_{sp}$. In addition to the generating and removal mechanisms discussed above, the mist droplet concentration in a subcompartment is also affected by the intercompartmental and fan flows. In the intercompartmental and fan flows, the mass fraction of fog droplets entrained is η and the gas mixture flow rate is $\dot{m}$. Therefore the rates of fog droplets mass into and out of a subcompartment are $\Sigma\eta_{in}\,\dot{m}_{in}$ and $\Sigma\eta_{out}\,\dot{m}_{out}$, respectively. It should be noted that $\Sigma\eta_{in}\,\dot{m}_{in}$ and $\Sigma\eta_{out}\,\dot{m}_{out}$ include the fog mass entrainment rates in all the intercompartmental and fan flows into and out of a subcompartment.

The mass conservation equation for the fog droplets in a subcompartment may be expressed as

$$\frac{dM_c}{dt} = \Sigma\eta_{in}\,\dot{m}_{in} - \Sigma\eta_{out}\,\dot{m}_{out} + \dot{m}_{break} + \dot{m}_{cond} - \dot{m}_{set} - \dot{m}_{sp} \qquad (6.1)$$

where Σ is a summation over all the flow paths. In Eq. (6.1), if $\dot{m}_{cond}$ is negative, then it becomes the rate of vaporization. Eq. (6.1) can be integrated to give the total mass of condensate at time t

$$M_c(t) = \int_0^t (\Sigma\eta_{in}\,\dot{m}_{in} - \Sigma\eta_{out}\,\dot{m}_{out} + \dot{m}_{break} + \dot{m}_{cond} - \dot{m}_{set} - \dot{m}_{sp})\,dt$$

$$= \sum_i (\Sigma\eta_{in}^{\,i}\,\dot{m}_{in}^{\,i} - \Sigma\eta_{out}^{\,i}\,\dot{m}_{out}^{\,i} + \dot{m}_{break}^{\,i} + \dot{m}_{cond}^{\,i} - \dot{m}_{set}^{\,i} - \dot{m}_{sp}^{\,i})\,\Delta t_i \qquad (6.2)$$

The present analysis will employ the CLASIX calculations of containment transient during a small LOCA. In the CLASIX analysis, the entire ice condenser containment is usually divided into five or six subcompartments for analysis purposes. Temperatures, total pressure, steam partial pressures, and intercompartmental flow rates are calculated by CLASIX during transients. This information is used in Eq. (6.2) to determine fog droplet mass.

When applying Eq. (6.1) to each individual subcompartment, we have the following fog mass conservation equations in finite difference form:

Upper Compartment

$$M_{UC}(t+\Delta t) = M_{UC}(t) + \left(\Sigma n_{in}\, \dot{m}_{in}(t) - \Sigma n_{out}\, \dot{m}_{out}(t) + \dot{m}_{UC,cond}(t) - \dot{m}_{UC,set}(t) - \dot{m}_{UC,sp}(t) \right) \Delta t \qquad (6.3)$$

Lower Compartment

$$M_{LC}(t+\Delta t) = M_{LC}(t) + \left(\Sigma n_{in}\, \dot{m}_{in} - \Sigma n_{out}\, \dot{m}_{out} + \dot{m}_{LC,break}(t) - \dot{m}_{LC,cond}(t) - \dot{m}_{LC,set}(t) - \dot{m}_{LC,sp}(t) \right) \Delta t \qquad (6.4)$$

Ice Condenser Upper Plenum

$$M_{UP}(t + \Delta t) = M_{UP}(t) + \left(\Sigma \eta_{in} \dot{m}_{in}(t) - \Sigma \eta_{out} \dot{m}_{out}(t) + \dot{m}_{UP,cond}(t) - \dot{m}_{UP,set}(t)\right) \Delta t$$

Ice Condenser Lower Plenum

$$M_{LP}(t + \Delta t) = M_{LP}(t) + \left(\Sigma \eta_{in} \dot{m}_{in}(t) - \Sigma \eta_{out} \dot{m}_{out}(t) + \dot{m}_{LP,cond}(t) - \dot{m}_{LP,set}(t)\right) \Delta t \quad (6.5)$$

Dead Ended Region

$$M_{DE}(t + \Delta t) = M_{DE}(t) + \left(\Sigma \eta_{in} \dot{m}_{in}(t) - \Sigma \eta_{out} \dot{m}_{out}(t) \pm \dot{m}_{DE,cond}(t) - \dot{m}_{DE,set}(t)\right) \Delta t \quad (6.6)$$

Fan/Accumulator Rooms*

$$M_{FA}(t + \Delta t) = M_{FA}(t) + \left(\Sigma \eta_{in} \dot{m}_{in}(t) - \Sigma \eta_{out} \dot{m}_{out}(t) + \dot{m}_{FA,cond}(t) - \dot{m}_{FA,set}(t) - \dot{m}_{FA,sp}(t)\right) \Delta t \quad (6.7)$$

In the present analysis, the fog concentrations in the intercompartmental and fan flows are assumed to be the same as those in the compartment from which the flows are orginated.

---

* These rooms were analyzed only for the D. C. Cook plant (See Figure 6.9).

In the equations given above, the intercompartmental and fan flow rates $\dot{m}_{in}$ and $\dot{m}_{out}$ are provided by CLASIX calculational results. The procedures of calculating fog droplets generating and removal rates are based on the discussions in the previous sections and the details are given in the following sections.

6.1.1 CALCULATION OF $\dot{M}_{BREAK}$

To date little experimental data is available to estimate the amount of fog droplets generated by the break flow. For a large LOCA, Almenas and Marchello[3] estimated that 13 percent of the total blowdown drop population (by weight) has drop radius range from 1 μ to 20 μ and only 1 percent less than 1 μ. This estimate is somewhat larger than the 4 μ mean drop size sited in Section 3.1.2, which is believed to be conservative.

Since we are only interested in fog drops smaller than 20 μ, and only these drops can remain suspended in air until the time when the hydrogen is released, we assume that the estimate of Almenas and Marchello is applicable in small LOCAs and 14 percent of the suspended liquid are fog droplets which have a potential inerting effect.

The fraction of reactor coolant discharged from the break that remains as suspended liquid has been determined in Section 3. Knowing the break flow rates from a computer code such as MARCH, we can calculate the amount of liquid suspended in the atmosphere. Then from the drop size distribution we can calculate the amount of fog droplets suspended in the atmosphere.

Defining the blowdown rate as $\dot{m}_b$, the liquid fraction of the break flow as ξ_b, the fraction of fog droplets smaller than 20 μ as f_b, we have

$$\dot{m}_{break} = f_b \dot{m}_b \xi_b \tag{6.8}$$

In the present analysis f_b = 0.14 is used. f_b becomes zero when the water level in the reactor vessel falls below the break elevation.

6.1.2 CALCULATION OF $\dot{M}_{COND}$

As discussed previously, m_{cond} is the rate of formation of mist droplets by nucleation, condensation, or vaporization. Nucleation of fog droplets can take place in the thermal boundary layer and in the bulk fluid. We conservatively assume that little supersaturation is needed for nucleation in the bulk stream and fog will form when the bulk stream steam partial pressure reaches the saturation steam pressure corresponding to the gas stream temperature. Therefore, the bulk stream fog formation rates can be determined from the equilibrium thermodynamic states of the gas mixture.

The boundary layer fog formation rate can be determined using the Hijikata-Mori theory[17] of fog formation in the thermal boundary layer as discussed in Section 3.2.4. The fog formation rate in the thermal boundary layer and the bulk stream is given by Eq. (3.12). Boundary layer and bulk stream fog formation rates will be calculated for the ice condenser and lower compartment. The volumetric gas flow rate, gas and wall temperatures, total pressure, and steam partial pressure were obtained from the CLASIX output.

6.1.3 CALCULATION OF $\dot{M}_{SET}$

The rate of settling of the fog droplets depends on their terminal velocity, concentration and compartment cross sectional area. The droplet terminal velocity is a function of drop size. In the present study, Equation (4.1) will be used to calculate the fog gravitational settling rate.

6.1.4 CALCULATION OF $\dot{M}_{SP}$

The mass of a fog droplet is much smaller than that of a spray droplet. Therefore, when a spray droplet collides with a fog droplet, the fog droplet will coalesce with the spray drop and fall to the sump. In the present study, the fog removal rate by sprays is given by Equation (4.2).

It is expected that the spray drop collection efficiency is very high, and therefore a 100 percent drop collection efficiency is assumed in the analysis. A sensitivity study was carried out to study the effect of E on the volume fraction of fog droplets and will be discussed later.

6.2 FOG INERTING PROBABILITY IN THE SEQUOYAH PLANT

To compute the fog formation rates some output data from the Sequoyah CLASIX analysis[27] are needed. These data include time histories of gas temperature, wall temperature, total pressure, and steam partial pressure in each containment subcompartment, as well as the intercompartmental and fan flow rates. The subcompartmentalization model used in the Sequoyah CLASIX analysis is shown in Figure 6.1. In this study only the S_2D accident scenario has been analyzed.

The input data for Sequoyah S_2D Case 1 are given in Tables 6.1 and 6.2, and the calculational results are shown in Figures 6.2 and 6.3. In Figure 6.2, the fog formation rate in the lower compartment is shown. For the first few hundred seconds the wall temperature is lower than the dew point corresponding to the steam partial pressure and therefore fog starts to form. After about 600 seconds, the fog formation rate becomes negligibly small since the wall temperature is only a few degrees below the dew point. There is no fog formation in the lower compartment after about 1800 seconds. The fog formation rate in the ice condenser is shown in Figure 6.3. It is seen that the fog formation rate in the ice condenser is much larger than that in the lower compartment. It increases with the ice condenser steam flow rate and reaches a peak of

FIGURE 6.1 SEQUOYAH CLASIX CONTAINMENT MODEL

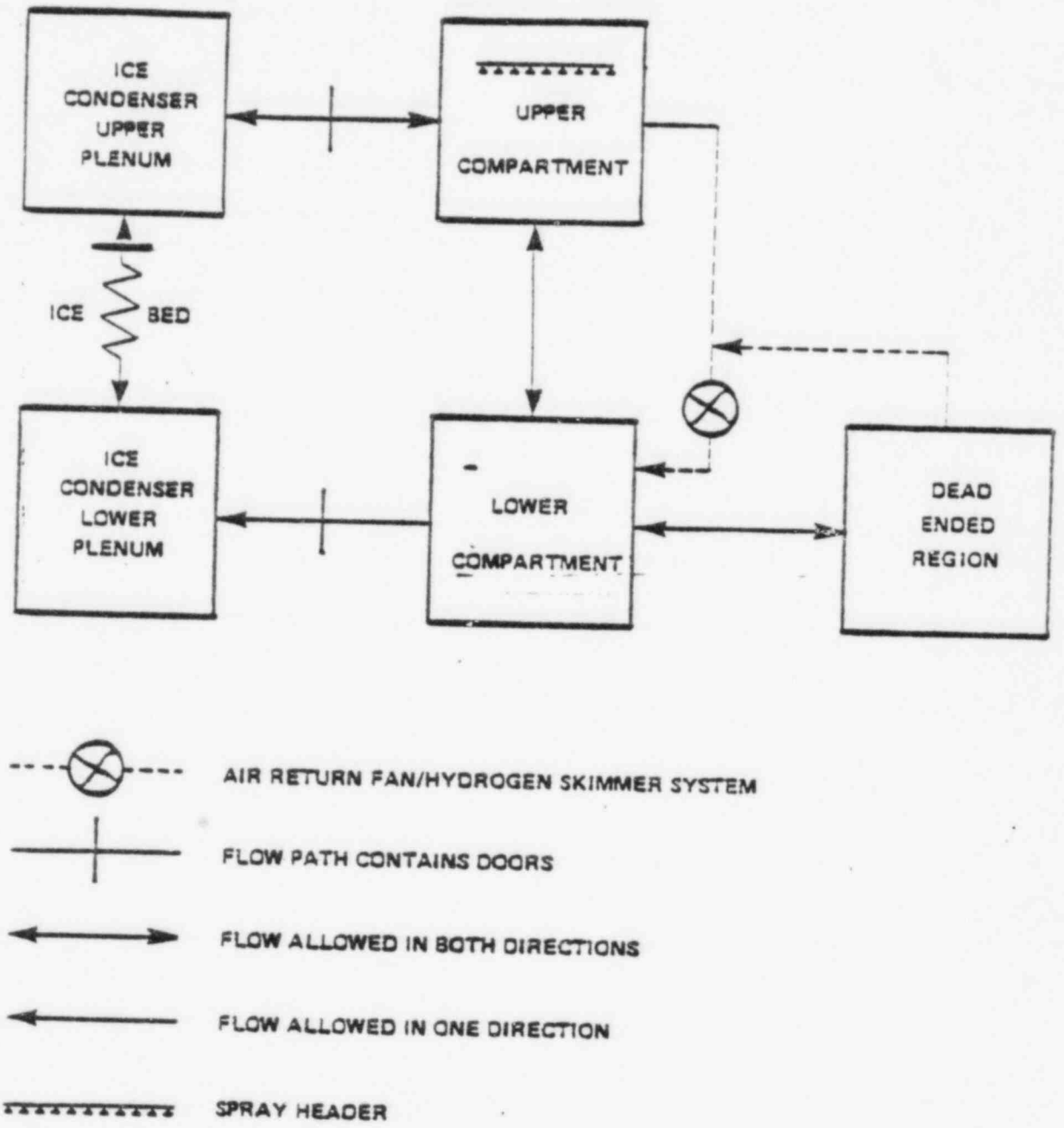

14 lb/sec at about 1800 seconds. The fog formation rate in the ice condenser then begins to decrease and is low at the time of significant hydrogen release.

The input data needed to calculate the rate of fog generation by the break flow, the fog settling rate due to gravity, and the fog removal rate due to sprays, as well as the rates of fog entrainment by inter-compartmental and fan flows are discussed as follows.

The rate of reactor coolant release to the containment and the coolant enthalpy were obtained from the MARCH output[7] for a small LOCA. The quality of the break flow was calculated using the enthalpy and the lower compartment gas temperature. According to the MARCH prediction[7] the discharge of liquid by the break flow into the lower compartment lasts for only 2172 seconds. Afterward, the water level in the reactor vessel drops below the break elevation and the fluid discharged from the break is essentially steam. Therefore, in the present study, it is assumed that no fog is generated by the break flow after 2172 seconds.

For fog removal by gravitational settling, a volume mean drop size of 10 μ was assumed. The terminal velocity of a 10 μ drop is about 1 cm/sec. Because of this low terminal velocity, gravitational settling is not an effective fog removal mechanism. The assumption of 10 μ volume mean drop size is therefore conservative, considering the fact that for a few thousand seconds the drop agglomeration mechanism would be able to increase volume mean drop size substantially. It should also be noted that a smaller volume mean drop size means that the minimum fog inerting concentration would be reduced and thus makes the present analysis conservative. Furthermore, no consideration was given to the deposition of fog on the walls and vertical surfaces of the structure, or for fog removal in the fan flows when it passes through ducts and fans. All the assumptions mentioned above make the present analysis very conservative. The containment geometric data needed in computing the settling rate are given in Table 6.3.

FOG FORMATION IN TVA SEQUOYAH LOWER COMPARTMENT
FOG FORMATION RATE (LB/SEC)
0.6000
0.5000
0.4000
0.3000
0.2000
0.1000
0.0
0.0
1000.0
2000.0
3000.0
4000.0
5000.0
TIME (SEC)

FIGURE 6.2

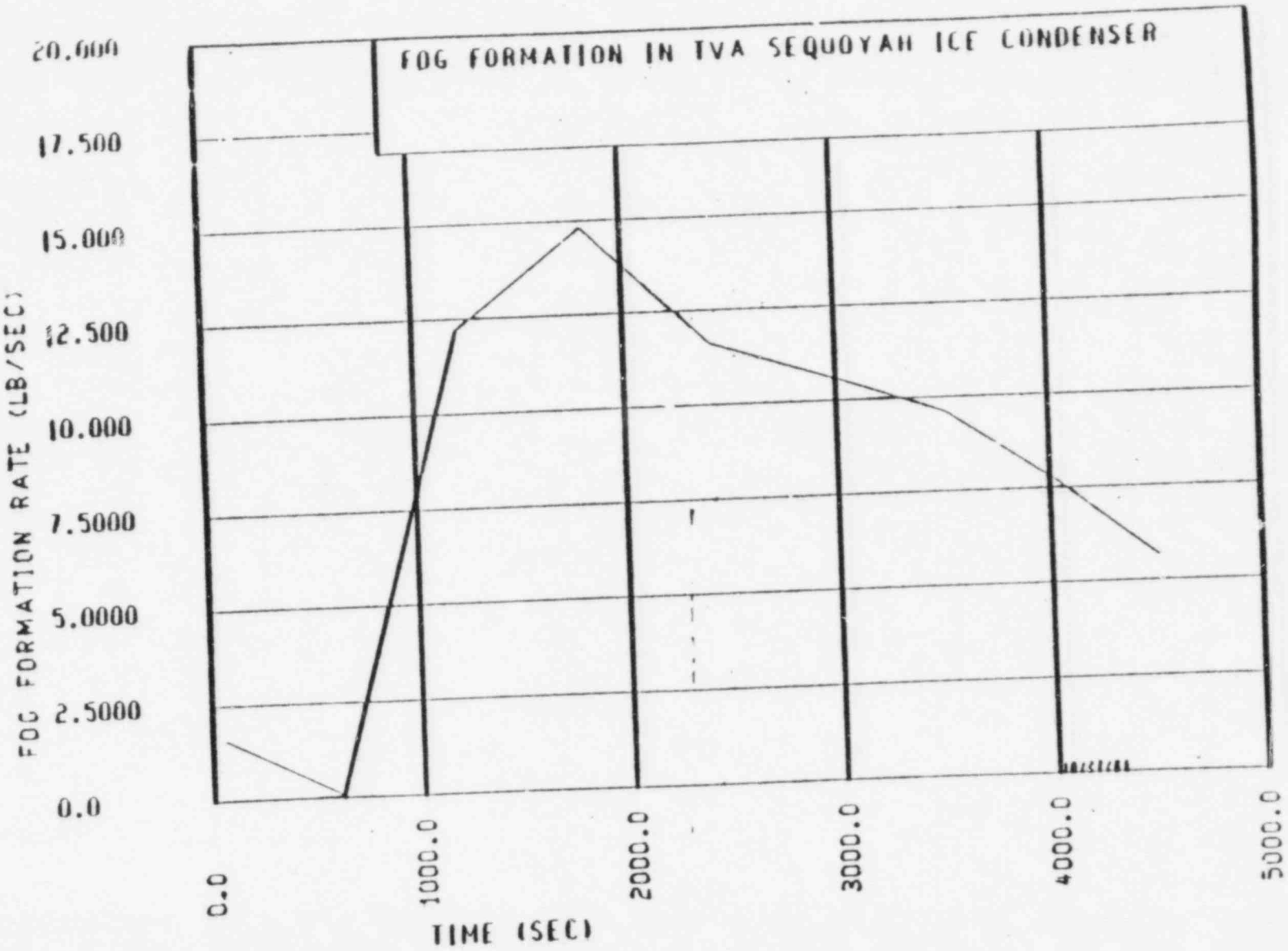

FIGURE 6.3 FOG FORMATION IN TVA SEQUOYAH ICE CONDENSER

For fog removal by sprays, a spray flow rate of 9500 gpm was used for Sequoyah. According to the Sequoyah CLASIX analysis[27], the sprays are initiated at 142 seconds. A volume fraction of sprays (volume of sprays divided by volume of the spray zone) of 3.3×10^{-4} was used, which was obtained using a spray drop fall height of 107 ft, a spray zone volume of 485,500 ft^3, and a volume mean drop size of 700 μ. As previously discussed a spray removal of a 100 percent was used.

In Figure 6.1, the directions of the intercompartmental flows are shown. The intercompartmental flow rates for the six flow paths and nine time steps were obtained from the CLASIX analysis and are given in Table 6.5. The present analysis considers the intercompartmental flows as the mechanisms of transporting fog from one compartment to another.

It is seen in Figure 6.1 that two trains of the air return fan and hydrogen skimmer system take suction from the dead ended region and from the upper compartment and discharge into the lower compartment. The fans are initiated at 712 seconds. The fan head-flow curve reported in Reference 27 was used to compute the fan flow rates. Fan flow rates of 1645 ft^3/sec and 10 ft^3/sec were used for the air return fan and the hydrogen skimmer system, respectively. These flow rates were calculated using average Δp's between the upper compartment and the lower compartment, and between the dead ended region and the lower compartment.

The results of the calculation are shown in Figure 6.4. It is seen that for the first few hundred seconds the fog concentrations in the lower compartment, ice condenser lower and upper plenums are about the same and increasing. At about 700 seconds, the lower compartment volumetric fog concentration reaches its peak of 2.2×10^{-4} ft^3 H_2O/ft^3 mix. Afterward, the intercompartmental flows transport more fog droplets out of the lower compartment than are generated by the break flow and condensation and, therefore, the lower compartment fog concentration decreases. However, the upper plenum fog concentration keeps rising until about 900 seconds, due to an increasing fog formation in the ice condenser and more fog entrained in the intercompartmental

flow into the upper plenum. The upper plenum fog concentration reaches its peak of 5.4×10^{-4} ft^3 H_2O/ft^3 mix at about 900 seconds. The lower plenum fog concentration is almost the same as the lower compartment fog concentration because of little difference in the intercompartmental flow rates into and out of the ice condenser lower plenum. Therefore, these two volumes behave as a single volume in terms of fog concentration.

At 2172 seconds, the break flow in the lower compartment stops generating fog and, therefore, the fog concentrations drop sharply thereafter. The effect is more pronounced for the lower compartment and lower plenum fog concentrations. The highest fog concentration exists in the ice condenser upper plenum while the lowest exists in the upper compartment. The effect of sprays on the upper compartment fog concentration is clearly seen in Figure 6.4. At 142 seconds, the sprays are turned on and the upper compartment fog concentration drops sharply until about 600 seconds. At about 600 seconds, the upper compartment fog concentration starts to increase again because the intercompartmental flow into the compartment increases sharply at that time. A peak concentration of 7×10^{-6} ft^3 H_2O/ft^3 mix in the upper compartment is reached at about 1200 seconds.

Hydrogen starts to release into the containment at about 3804 seconds, according to the MARCH calculation[27]. It reaches 4 volume percent at about 4300, 4400, and 4670 seconds in the lower compartment, upper plenum, and upper compartment, respectively.

At 4300 seconds, the calculated lower compartment fog concentration is 9.7×10^{-7} ft^3 H_2O/ft^3 mix, which is about an order of magnitude smaller than the minimum fog concentrations required for inerting 4 percent H_2. At 4670 seconds, the upper compartment fog concentration is 1.35×10^{-6} ft^3 H_2O/ft^3 mix, which is about a factor of five smaller than the minimum fog concentration required for inerting 4 percent H_2*. At the times of reaching 8.0 percent H_2, the fog

*The fog inerting criteria is described in Section 5.2.

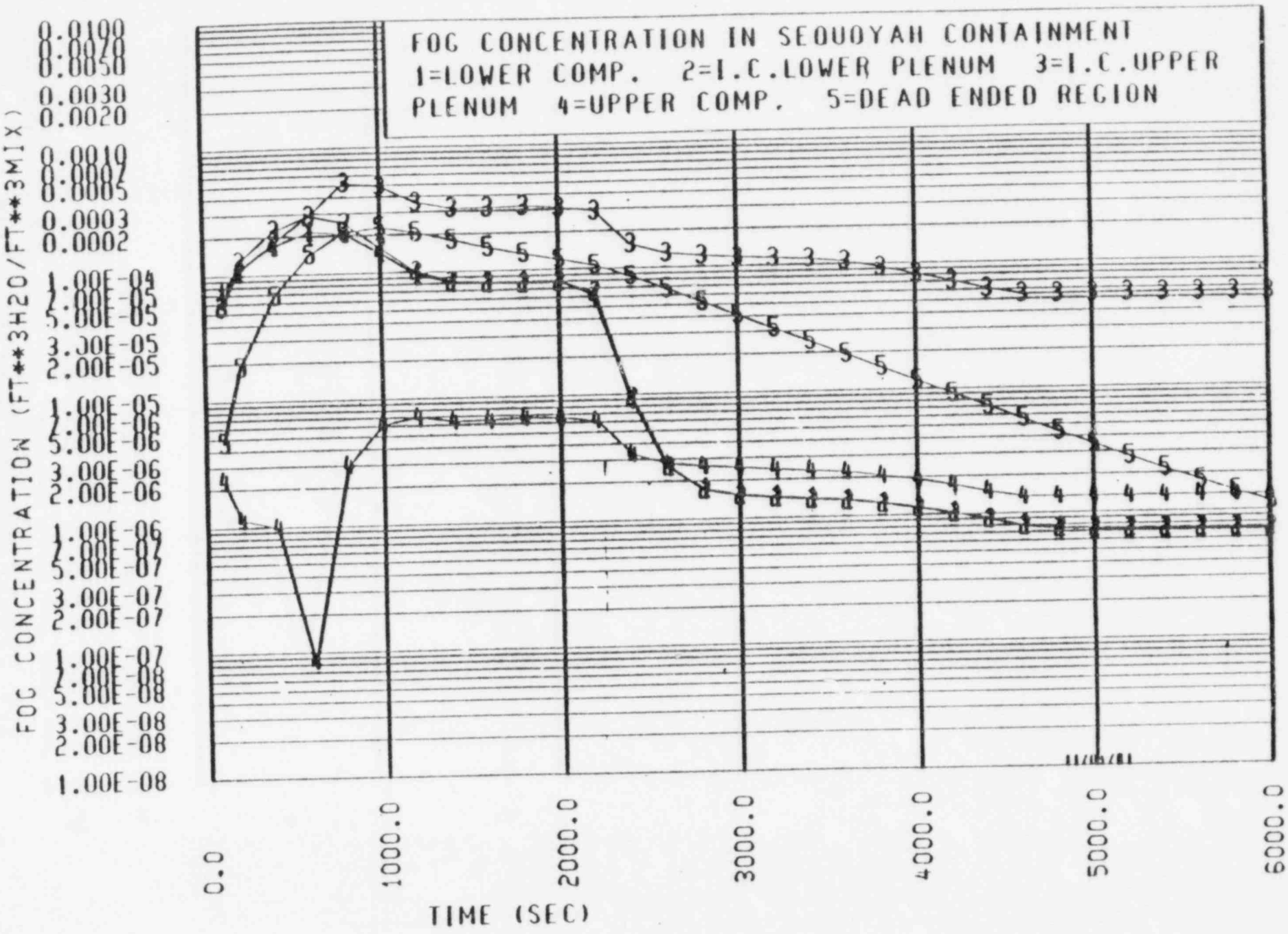
FOG CONCENTRATION IN SEQUOYAH CONTAINMENT
1=LOWER COMP. 2=I.C.LOWER PLENUM 3=I.C.UPPER PLENUM 4=UPPER COMP. 5=DEAD ENDED REGION
FOG CONCENTRATION (FT**3H2O/FT**3MIX)
0.0100
0.0070
0.0050
0.0030
0.0020
0.0010
0.0007
0.0005
0.0003
0.0002
1.00E-04
2.00E-05
5.00E-05
3.00E-05
2.00E-05
1.00E-05
2.00E-06
5.00E-06
3.00E-06
2.00E-06
1.00E-06
2.00E-07
5.00E-07
3.00E-07
2.00E-07
1.00E-07
2.00E-08
5.00E-08
3.00E-08
2.00E-08
1.00E-08
0.0
1000.0
2000.0
3000.0
4000.0
5000.0
6000.0
TIME (SEC)

FIGURE 6.4

concentrations in the lower and upper compartments are even lower than the figures given above. Therefore, it is concluded that the fog concentrations in the lower and upper compartments are too low to have any inerting effect. The use of the present theory on fog inerting also leads to the same conclusion.

However, at 4400 seconds, the calculated fog concentration in the upper plenum is 6.1×10^{-5} ft^3 H_2O/ft^3 mix which is higher than the Factory Mutual fog inerting data extrapolated to 10 μ drops and the present theoretical prediction. The data shows that in order to inert 4.76 percent H_2 the fog concentration must be 8.4×10^{-6} ft^3 H_2O/ft^3 mix or higher for 10 μ volume mean drop size. At 4600 seconds, the upper plenum hydrogen concentration reaches about 7 percent and the fog concentration is 5.5×10^{-5} ft^3 H_2O/ft^3 mix. Again, an extrapolation of the Factory Mutual data to 10 μ shows that fog concentration of 2.1×10^{-5} ft^3 H_2O/ft^3 mix or higher is required to inert 7.2 percent H_2. In comparison, the present theory on fog inerting predicts 1.02×10^{-4} ft^3 H_2O/ft^3 mix for 7.2 percent H_2.

Therefore, it appears that it is possible to inert 7 percent H_2 but unlikely. However, at 8 percent H_2 in the upper plenum, which occurs at about 4650 seconds, the fog concentration is 5.5×10^{-5} ft^3 H_2O/ft^3 mix, which is too low to inert 8 percent H_2. An extrapolation of the Factory Mutual 8 percent H_2 data to 10 μ volume mean drop size and the present prediction give 1.9×10^{-4} and 1.2×10^{-4} ft^3 H_2O/ft^3 mix for the minimum required fog inerting concentration, respectively. Therefore both the theory and the extrapolation of test data show that fog inerting will not occur in the upper plenum.

The glow plug igniters which have been installed in the Sequoyah containment were designed to burn hydrogen at the lower flammability limit. As discussed previously, no fog inerting effects will be expected in the Sequoyah lower and upper compartments. Therefore, the glow plug igniters are expected to function as designed in these two

compartments. It may be possible that fog present in the ice condenser upper plenum could prevent the glow plug igniters from igniting hydrogen below 7 percent. However, it seems very unlikely that the same igniters would fail to ignite 8.0 percent H_2 given the fact that considerable conservatism has been exercised in the present analysis. CLASIX analyses have previously been performed that showed the Sequoyah containment response to burning 8.0 percent H_2 mixtures would be acceptable.

Sensitivity studies of the spray removal efficiency and the fraction of blowdown droplets smaller than 20 μ for the Sequoyah plant have been performed. A case of 10 percent spray removal efficiency was investigated. The calculational results showed that the fog concentrations in the lower compartment, lower plenum, and upper compartment at 4600 seconds were increased approximately by a factor of 10. However, these concentrations are still too low to inert 8 percent hydrogen. In comparison, the fog concentration in the upper plenum is increased by only 20 percent because the concentration at this time is primarily determined by the fog formation rate in the ice condenser. This increase is too small to change the conclusion given previously on the inerting probability in the upper plenum. Another case in which all the blowdown droplets were assumed to be smaller than 20 μ was investigated. The calculational results showed that at 4600 seconds the fog concentrations in the lower compartment and lower plenum were increased by 15 percent while the increases in the upper plenum and upper compartment were negligibly small. The insensitivity of the fog concentrations to the parameter of the fraction of blowdown droplets smaller than 20 μ is due to the effectiveness of the spray removal. At 4600 seconds, almost all the blowdown droplets are removed by the sprays. The sensitivity studies showed that the fog concentration in the upper plenum at the time of significant hydrogen release is not sensitive to the spray removal efficiency and the fraction of blowdown droplets smaller than 20 μ.

TABLE 6.1 INPUT DATA FOR SEQUOYAH LOWER COMPARTMENT

Time (sec)	Lower Compartment Gas Flow Rate (ft^3/sec)	Gas Temp. (°F)	Wall Temp. (°F)	Total Pressure (psia)	Steam Partial Pressure (psia)
60	1404.5	150	118	16.7	5
610	646.7	215	202	21.6	15.3
1210	3157.2	188	176	20.4	8.9
1810	3115.5	188	176	20.5	8.8
2410	2913.7	180	173	20.1	7.5
3010	2871.7	179	169	19.9	7.2
3510	2739.3	178	169	19.9	6.9
4010	2755.9	175	164	19.4	5.5
4510	2848.8	197	173	19.8	4.8

TABLE 6.2 INPUT DATA FOR SEQUOYAH ICE CONDENSER

Time (sec)	Ice Condenser Gas Flow Rate (ft^3/sec)	Gas Temp. (°F)	Ice Temp. (°F)	Total Pressure (psia)	Steam Partial Pressure (psia)
60	1082	120	32	16.5	2.5
610	96.4	132	32	21.8	2.3
1210	2654	186	32	20.4	8.1
1810	2799	188	32	20.5	8.8
2410	2679	182	32	20.0	7.6
3010	2629	179	32	19.9	7.2
3510	2502	178	32	19.9	7.0
4010	2594	171	32	19.4	5.7
4510	2628	187	32	19.8	4.7

TABLE 6.3 GEOMETRIC DATA FOR SEQUOYAH CONTAINMENT

	Volume (ft^3)	Floor Area (ft^2)
Lower Compartment	289,000	5,410
Ice Condenser Lower Plenum	24,200	3,100
Ice Condenser Upper Plenum	47,000	3,200
Upper Compartment	651,000	10,390
Dead Ended Region	94,000	3,350

TABLE 6.4 MARCH PREDICTION OF REACTOR COOLANT MASS AND ENERGY RELEASE RATE FOR THE S_2D SEQUENCE

Time (seconds)	H_2O Mass Release Rate (lbm/sec)	H_2O Energy Release Rate (Btu/sec)
0.0	197.2	1.167×10^5
2172	190.5	1.097×10^5
2478	44.85	5.230×10^4
3180	53.53	6.547×10^4
3804	34.82	4.262×10^4
4428	21.40	2.842×10^4
4752	48.42	5.558×10^4
5700	19.42	2.182×10^4
6012	14.07	1.583×10^4
6960	5.253	5.989×10^3
7062	4.718	5.388×10^3
7206	4.060	4.693×10^3

TABLE 6.5 INTERCOMPARTMENTAL FLOW RATES (ft^3/sec)
PREDICTED BY CLASIX FOR SEQUOYAH

Time (sec)	Flow From LC to LP	Flow From LP to UP	Flow From UP to UC	Flow From UC to LC	Flow From DE to LC
6.001E1	1.175E3	1.082E3	7.029E2	-9.905E1	-1.304E2
6.100E2	3.580E2	9.641E1	-3.931E1	-2.113E1	-2.676E2
1.210E3	2.864E3	2.654E3	1.272E3	-1.838E2	-1.094E2
1.810E3	2.828E3	2.799E3	1.323E3	-1.793E2	-1.088E2
2.410E3	2.695E3	2.679E3	1.375E3	-1.502E2	-6.855E1
3.010E3	2.654E3	2.629E3	1.407E3	-1.634E2	-6.326E1
3.510E3	2.528E3	2.502E3	1.352E3	-1.643E2	-4.699E1
4.010E3	2.613E3	2.594E3	1.537E3	-1.095E2	-3.348E1
4.510E3	2.694E3	2.628E3	1.627E3	-1.106E2	-4.426E1

6.3 FOG INERTING PROBABILITY IN THE McGUIRE PLANT

To compute the fog formation rates some output data from the McGuire CLASIX analysis[28] are needed. These data include time histories of gas temperature, wall temperature, total pressure, and steam partial pressure in each containment subcompartment, as well as the intercompartmental and fan flow rates. The subcompartmentalization model used in the McGuire CLASIX analysis is shown in Figure 6.5. In this study only the S_2D accident scenario has been analyzed by CLASIX for McGuire.

The input data for McGuire S_2D Case 1 are given in Tables 6.6 and 6.7, and the calculational results are shown in Figures 6.6 and 6.7. In Figure 6.6, the fog formation rate in the lower compartment is shown. For the first few hundred seconds the wall temperature is lower than the dew point corresponding to the steam partial pressure and therefore fog starts to form. The fog formation rate is low because the wall temperature is only a few degrees below the dew point. Fog formation in the lower compartment becomes zero after about 600 seconds. The fog formation rate in the ice condenser is shown in Figure 6.7. It is seen that the fog formation rate in the ice condenser is much larger than that in the lower compartment. The fog formation rate increases with the ice condenser steam flow rate and reaches the first peak at about 1510 seconds. Then the rate decreases because of the decrease in the steam flow rate. The fog formation and the steam flow rates start to increase again at about 2510 seconds. The fog formation rate reaches the second peak of 10.2 lb/sec at about 3260 seconds.

The input data needed to calculate the rate of fog generation by the break flow, the fog settling rate due to gravity, and the fog removal rate due to sprays, as well as the rates of fog entrainment by intercompartmental and fan flows are discussed as follows.

The rate of reactor coolant release to the containment and the coolant enthalpy were obtained from the MARCH output[7] for a small LOCA. The quality of the break flow was calculated using the enthalpy and the

FIGURE 6.5 MCGUIRE CLASIX CONTAINMENT MODEL

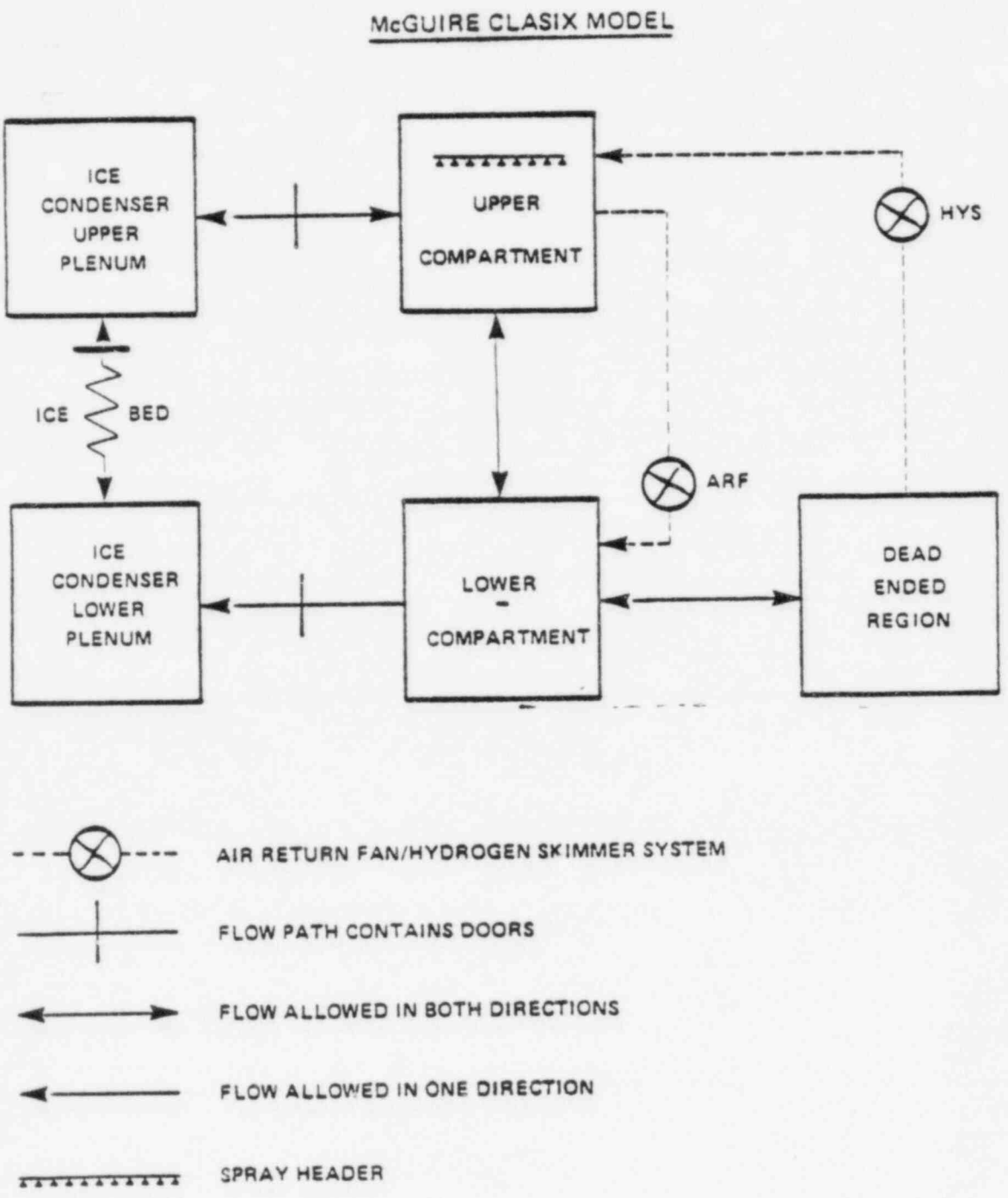

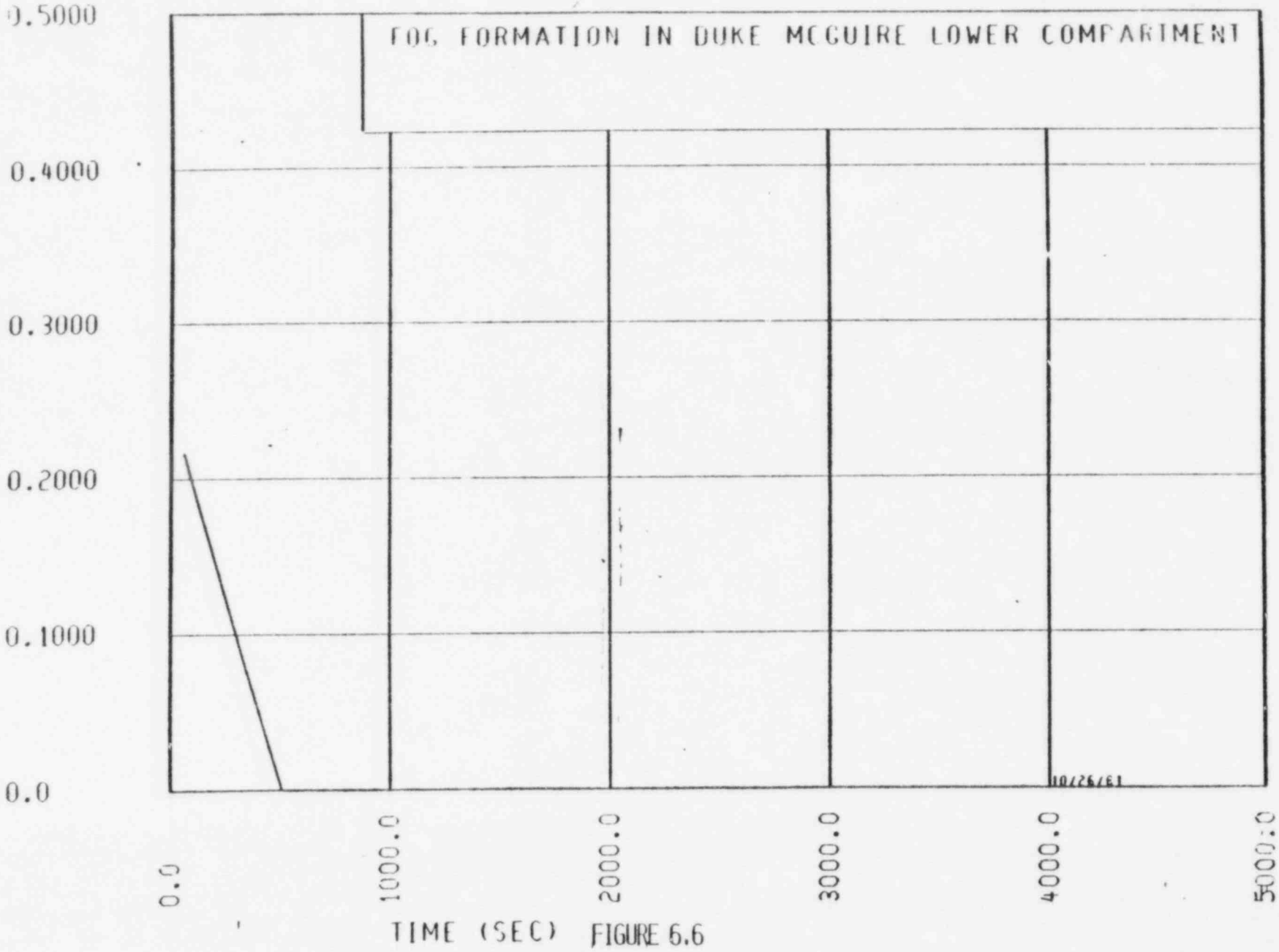
FOG FORMATION IN DUKE MCGUIRE LOWER COMPARTMENT
0.5000
0.4000
0.3000
0.2000
0.1000
0.0
FOG FORMATION RATE (LB/SEC)
0.0
1000.0
2000.0
3000.0
4000.0
5000.0
TIME (SEC)
10/26/81

FIGURE 6.6

FIGURE 6.7

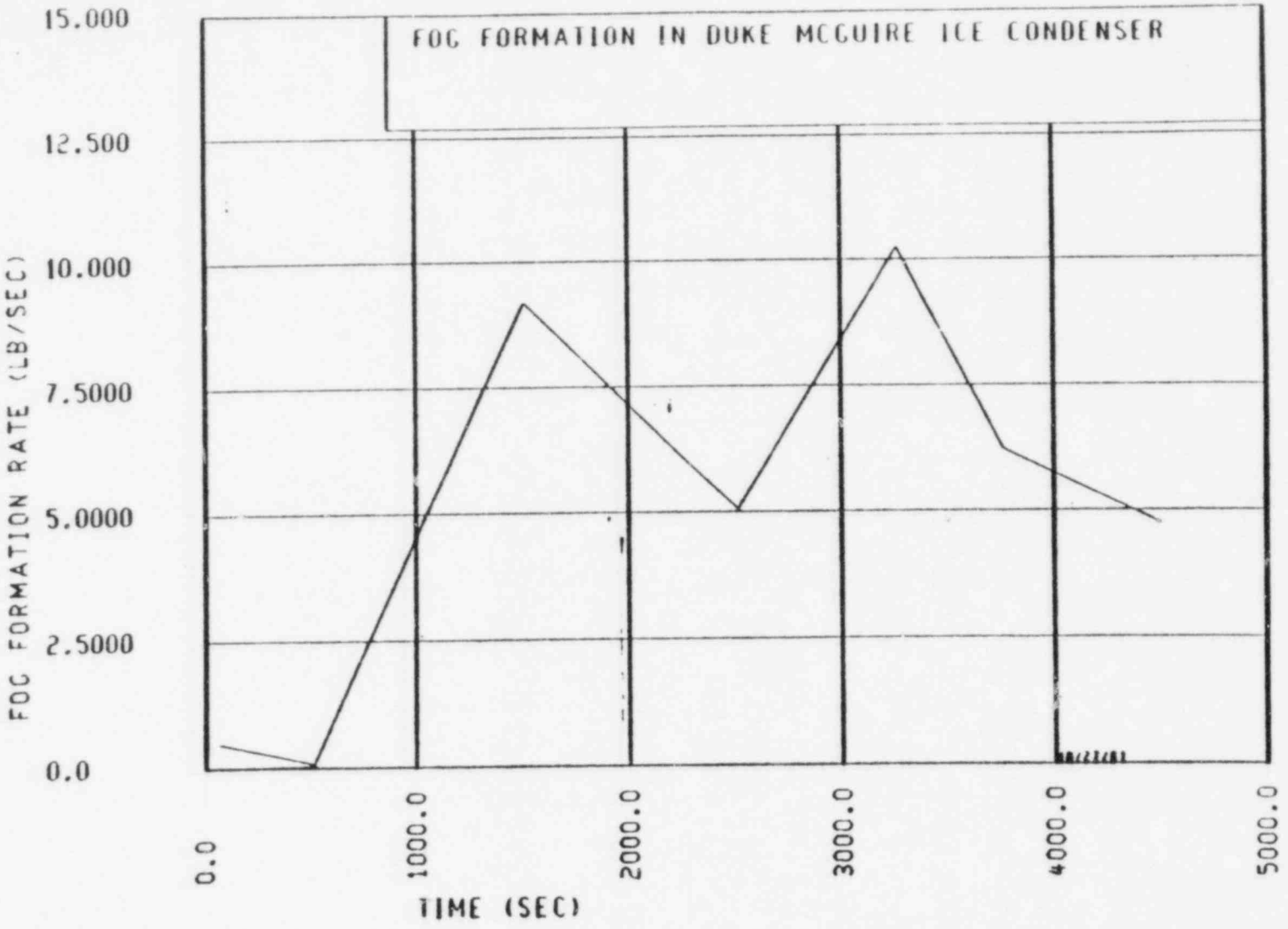
FOG FORMATION IN DUKE MCGUIRE ICE CONDENSER
FOG FORMATION RATE (LB/SEC)
15.000
12.500
10.000
7.5000
5.0000
2.5000
0.0
0.0
1000.0
2000.0
3000.0
4000.0
5000.0
TIME (SEC)

lower compartment gas temperature. According to the MARCH prediction[7] the discharge of liquid by the break flow into the lower compartment lasts for only 2172 seconds. Afterward, the water level in the reactor vessel drops below the break elevation and the fluid discharged from the break is essentially steam. Therefore, in the present study, it is assumed that no fog is generated by the break flow after 2172 seconds.

For fog removal by gravitational settling, a volume mean drop size of 10 μ was assumed. The assumption of 10 μ volume mean drop size is conservative, considering the fact that for a few thousand seconds the drop agglomeration mechanism would be able to increase volume mean drop size substantially. It should also be noted that a smaller volume mean drop size means that the minimum fog inerting concentration would be reduced and thus makes the present analysis conservative. Furthermore, no consideration was given to the deposition of fog on the walls and vertical surfaces of the structure, or for fog removal in the fan flows when it passes through ducts and fans. All the assumptions mentioned above make the present analysis very conservative. The containment geometric data needed in computing the settling rate are given in Table 6.8.

For fog removal by sprays, a spray flow rate of 6800 gpm was used for McGuire. According to the McGuire CLASIX analysis[28], the sprays are initiated at 124 seconds. A volume fraction of sprays (volume of sprays divided by volume of the spray zone) of 3.3×10^{-4} was used. As previously discussed a spray removal efficiency of a 100 percent efficiency was used.

In Figure 6.5, the directions of the intercompartmental flows are shown. The intercompartmental flow rates for the six flow paths and eight times steps were obtained from the CLASIX analysis and are given in Table 6.9. The present analysis considers the intercompartmental flows as the mechanisms of transporting fog from one compartment to another.

Figure 6.5 shows two trains of the air return fan and hydrogen skimmer system and the fan flow directions. The fans are initiated at 694 seconds. The fan head-flow curve reported in Reference 28 was used to compute the fan flow rates. Fan flow rates of 1000 ft^3/sec and 100 ft^3/sec were used for the air return fan and the hydrogen skimmer system, respectively. These flow rates were calculated using average Δp's between the upper compartment and the lower compartment, and between the dead ended region and the upper compartment.

The results of the calculation are shown in Figure 6.8. It is seen that for the first few hundred seconds the fog concentrations in the lower compartment, ice condenser lower and upper plenums are about the same and increasing. At about 600 seconds, the lower compartment volumetric fog concentration reaches its peak of 1.6×10^{-4} ft^3 H_2O/ft^3 mix. Afterward, the intercompartmental flows transport more fog droplets out of the lower compartment than are generated by the break flow and condensation and, therefore, the lower compartment fog concentration decreases. However, the upper plenum fog concentration keeps rising until about 800 seconds, due to an increasing fog formation in the ice condenser and more fog entrained in the intercompartmental flow into the upper plenum. The upper plenum fog concentration reaches its peak of 6.4×10^{-4} ft^3 H_2O/ft^3 mix at about 800 seconds. The lower plenum fog concentration is almost the same as the lower copartment fog concentration because of little difference in the intercompartmental flow rates into and out of the ice condenser lower plenum. Therefore, these two volumes behave as a single volume in terms of fog concentration.

At 2172 seconds, the break flow in the lower compartment stops generating fog and, therefore, the fog concentrations drop sharply thereafter. The effect is more pronounced for the lower compartment and lower plenum fog concentrations. The highest fog concentration exists in the ice condenser upper plenum while the lowest exists in the upper compartment. The effect of sprays on the upper compartment fog concentration is clearly seen in Figure 6.8. At 124 seconds, the sprays are turned on and the upper compartment fog concentration drops sharply

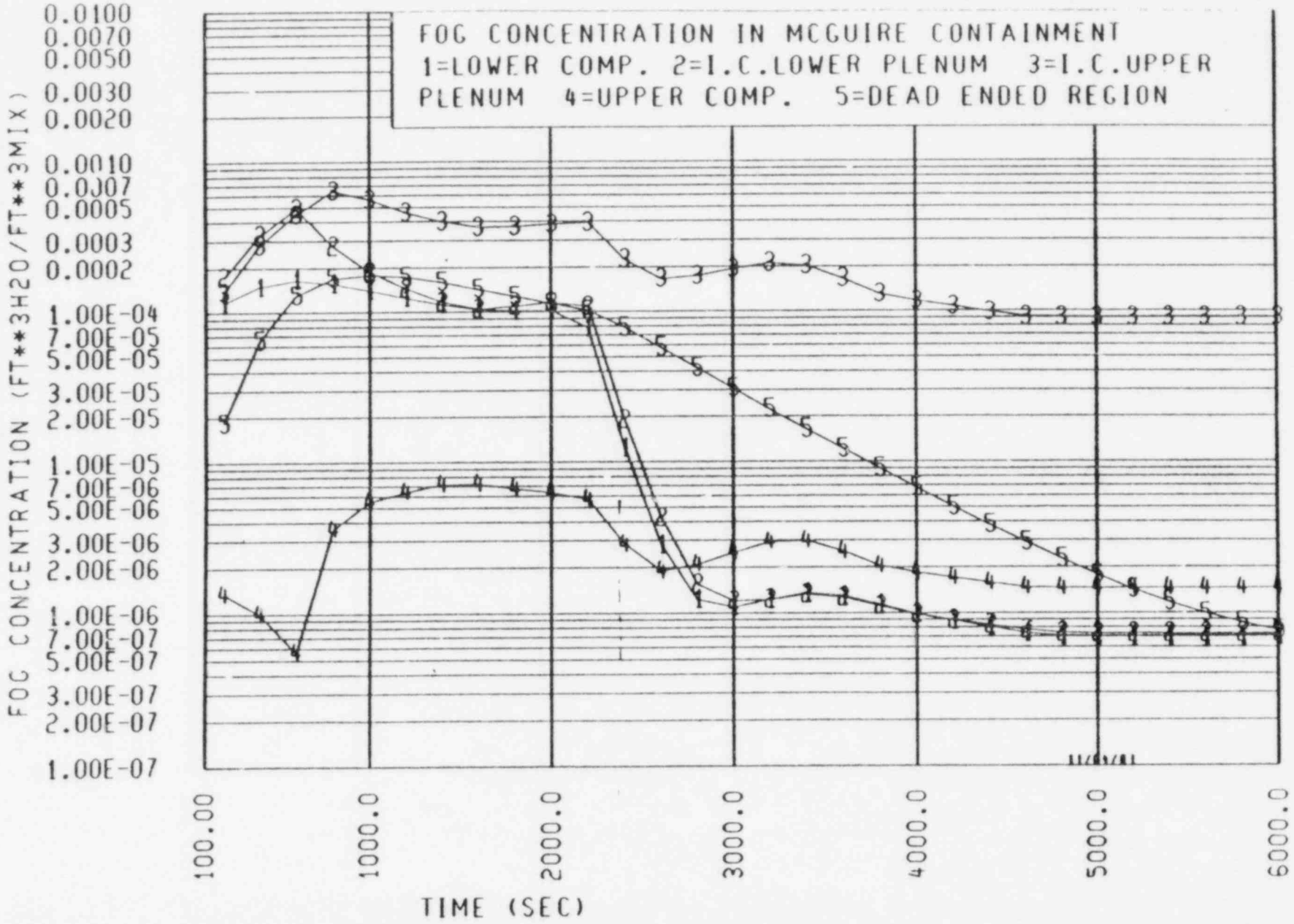
FOG CONCENTRATION IN MCGUIRE CONTAINMENT
1=LOWER COMP. 2=I.C.LOWER PLENUM 3=I.C.UPPER PLENUM 4=UPPER COMP. 5=DEAD ENDED REGION
FOG CONCENTRATION (FT**3H2O/FT**3MIX)
0.0100
0.0070
0.0050
0.0030
0.0020
0.0010
0.0007
0.0005
0.0003
0.0002
1.00E-04
7.00E-05
5.00E-05
3.00E-05
2.00E-05
1.00E-05
7.00E-06
5.00E-06
3.00E-06
2.00E-06
1.00E-06
7.00E-07
5.00E-07
3.00E-07
2.00E-07
1.00E-07
100.00
1000.0
2000.0
3000.0
4000.0
5000.0
6000.0
TIME (SEC)

FIGURE 6.8

until about 600 seconds. At about 600 seconds, the upper compartment fog concentration starts to increase again because the intercompartmental flow into the compartment increases sharply at that time. A peak concentration of 7.5×10^{-6} ft^3 H_2O/ft^3 mix in the upper compartment is reached at about 1500 seconds.

Hydrogen starts to release into the containment at about 3804 seconds, according to the MARCH calculation[28]. It reaches 4 volume percent at about 4300, 4400, and 4850 seconds in the lower compartment, upper plenum, and upper compartment, respectively.

At 4300 seconds, the calculated lower compartment fog concentration is 8.4×10^{-7} ft^3 H_2O/ft^3 mix, which is about an order of magnitude smaller than the minimum fog concentrations required for inerting 4 percent H_2. At 4850 seconds, the upper compartment fog concentration is 1.47×10^{-6} ft^3 H_2O/ft^3 mix, which is about a factor of five smaller than the minimum fog concentration required for inerting 4 percent H_2*. At the times of reaching 8.5 percent H_2, the fog concentrations in the lower and upper compartments are even lower than the figures given above. Therefore, it is concluded that the fog concentrations in the lower and upper compartments are too low to have any inerting effect. The use of the present theory on fog inerting also leads to the same conclusion.

However, at 4400 seconds, the calculated fog concentration in the upper plenum is 9.8×10^{-5} ft^3 H_2O/ft^3 mix which is higher than the Factory Mutual fog inerting data extrapolated to 10 μ drops and the present theoretical prediction. The data shows that in order to inert 4.76 percent H_2 the fog concentration must be 8.4×10^{-6} ft^3 H_2O/ft^3 mix or higher for 10 μ volume mean drop size. At 4500 seconds, the upper plenum hydrogen concentration reaches about 7 percent and the fog concentration is 9.3×10^{-5} ft^3 H_2O/ft^3 mix. Again,

---

* The fog inerting criterion used is described in Section 5.2.

an extrapolation of the Factory Mutual data to 10 μ shows that fog concentration of 2.1 x 10^{-5} ft^3 H_2O/ft^3 mix or higher is required to inert 7.2 percent H_2. In comparison, the present theory on fog inerting predicts 1.02 x 10^{-4} ft^3 H_2O/ft^3 mix for 7.2 percent H_2. Therefore, it appears that it is possible to inert 7 percent H_2, but unlikely. However, at 8 percent H_2 in the upper plenum, which occurs at about 4600 seconds, the fog concentration is 9.1 x 10^{-5} ft^3 H_2O/ft^3 mix, which is too low to inert 8 percent H_2. An extrapolation of the Factory Mutual 8 percent H_2 data to 10 μ volume mean drop size and the present prediction give 1.9 x 10^{-4} and 1.2 x 10^{-4} ft^3 H_2O/ft^3 mix for the minimum required fog inerting concentration, respectively. Therefore, both the theory and the extrapolation of the test data indicate that fog inerting will not occur.

The glow plug igniters which have been installed in the McGuire containment were designed to burn hydrogen at the lower flammability limit. As discussed previously, no fog inerting effects will be expected in the McGuire lower and upper compartments. Therefore, the glow plug igniters are expected to function as designed in these two compartments. It may be possible that fog present in the ice condenser upper plenum could prevent the glow plug igniters from igniting hydrogen below 7 percent. However, it seems very unlikely that the same igniters would fail to ignite 8.5 percent H_2 given the fact that considerable conservatism has been exercised in the present analysis. CLASIX analyses have previously been performed that showed the McGuire containment response to burning 8.5 percent H_2 mixtures would be acceptable.

TABLE 6.6 INPUT DATA FOR McGUIRE LOWER COMPARTMENT

Time (sec)	Lower Compartment Gas Flow Rate (ft^3/sec)	Gas Temp. (°F)	Wall Temp. (°F)	Total Pressure (psia)	Steam Partial Pressure (psia)
60	1624.6	160	149	16.5	7
510	1248.1	225	215	22.2	18.3
1510	2387.8	205	198	21.9	12.6
2010	2393.8	205	198	22	12.4
2510	1940.7	195	193	21.5	10.4
3260	2055.5	200	195	21.6	10.8
3760	1801.7	200	194	21	9.3
4510	1919.3	250	222	21.2	7.3

TABLE 6.7 INPUT DATA FOR McGUIRE ICE CONDENSER

Time (sec)	Ice Condenser Gas Flow Rate (ft^3/sec)	Gas Temp. (°F)	Ice Temp. (°F)	Total Pressure (psia)	Steam Partial Pressure (psia)
60	820.5	90	32	16.5	1
510	107.1	130	32	22.2	2.3
1510	1926	190	32	21.9	9.3
2010	1637	193	32	22	9
2510	1145	188	32	21.4	8.6
3260	1630	195	32	21.6	10.3
3760	1514	193	32	21.1	8.1
4510	1464	192	32	22.1	7.1

TABLE 6.8 GEOMETRIC DATA FOR McGUIRE CONTAINMENT

	Volume (ft^3)	Floor Area (ft^2)
Lower Compartment	237,400	5,410
Ice Condenser Lower Plenum	24,200	3,100
Ice Condenser Upper Plenum	47,000	3,200
Upper Compartment	670,000	10,390
Dead Ended Region	130,900	3,350

TABLE 6.9 INTERCOMPARTMENTAL FLOW RATES (ft^3/sec)
PREDICTED BY CLASIX FOR McGUIRE

Time (sec)	Flow From LC to LP	Flow From LP to UP	Flow From UP to UC	Flow From UC to LC	Flow From DE to LC
6.001E1	1.351E3	8.205E2	5.783E2	-1.198E2	-1.538E2
5.100E2	8.716E2	1.071E2	-2.269E1	-2.863E1	-3.479E2
1.510E3	2.008E3	1.926E3	8.635E2	-1.900E2	-1.898E2
2.010E3	2.010E3	1.637E3	6.869E2	-2.266E2	-1.572E2
2.510E3	1.722E3	1.145E3	4.807E2	-1.410E2	-7.767E1
3.260E3	1.713E3	1.630E3	6.666E2	-2.087E2	-1.338E2
3.760E3	1.546E3	1.514E3	7.231E2	-1.289E2	-1.268E2
4.510E3	1.634E3	1.464E3	7.640E2	-1.328E2	-1.515E2

6.4 FOG INERTING PROBABILITY IN THE D. C. COOK PLANT

To compute the fog formation rates some output data from the Cook CLASIX analysis[29] are needed. These data include time histories of gas temperature, wall temperature, total pressure, and steam partial pressure in each containment subcompartment, as well as the intercompartmental and fan flow rates. The subcompartmentalization model used in the Cook CLASIX analysis is shown in Figure 6.9. In this study only the S_2D accident scenario has been analyzed.

The input data for Cook S_2D Case 1 are given in Tables 6.10 and 6.11, and the calculational results are shown in Figures 6.10 and 6.11. In Figure 6.10, the fog formation rate in the lower compartment is shown. It is seen that the fog formation rate is negligibly small. It should be noted that the calculation of the lower compartment fog concentration in the D. C. Cook plant starts at 600 seconds instead of 60 seconds used for the other two plants. The fog formation rate in the lower compartmemt starts to increase at about 4200 seconds because of the increase in the steam partial pressure. It reaches 0.017 lb/sec at about 4590 seconds. Fog formation in the lower compartment will stop after 4700 seconds because of the hydrogen burn thereafter. The fog formation rate in the ice condenser is shown in Figure 6.11. It is seen that the fog formation rate in the ice condenser is much larger than that in the lower compartment. It increases with the ice condenser steam flow rate and reaches a peak of about 15.6 lb/sec at about 1200 seconds. The fog formation rate in the ice condenser then begins to decrease and is low at the time of significant hydrogen release.

The input data needed to calculate the rate of fog generation by the break flow, the fog settling rate due to gravity, and the fog removal rate due to sprays, as well as the rates of fog entrainment by intercompartmental and fan flows are discussed as follows.

The rate of reactor coolant release to the containment and the coolant enthalpy were obtained from the MARCH output[7] for a small LOCA. The

FIGURE 6.9
D.C. COOK CLASIX MODEL

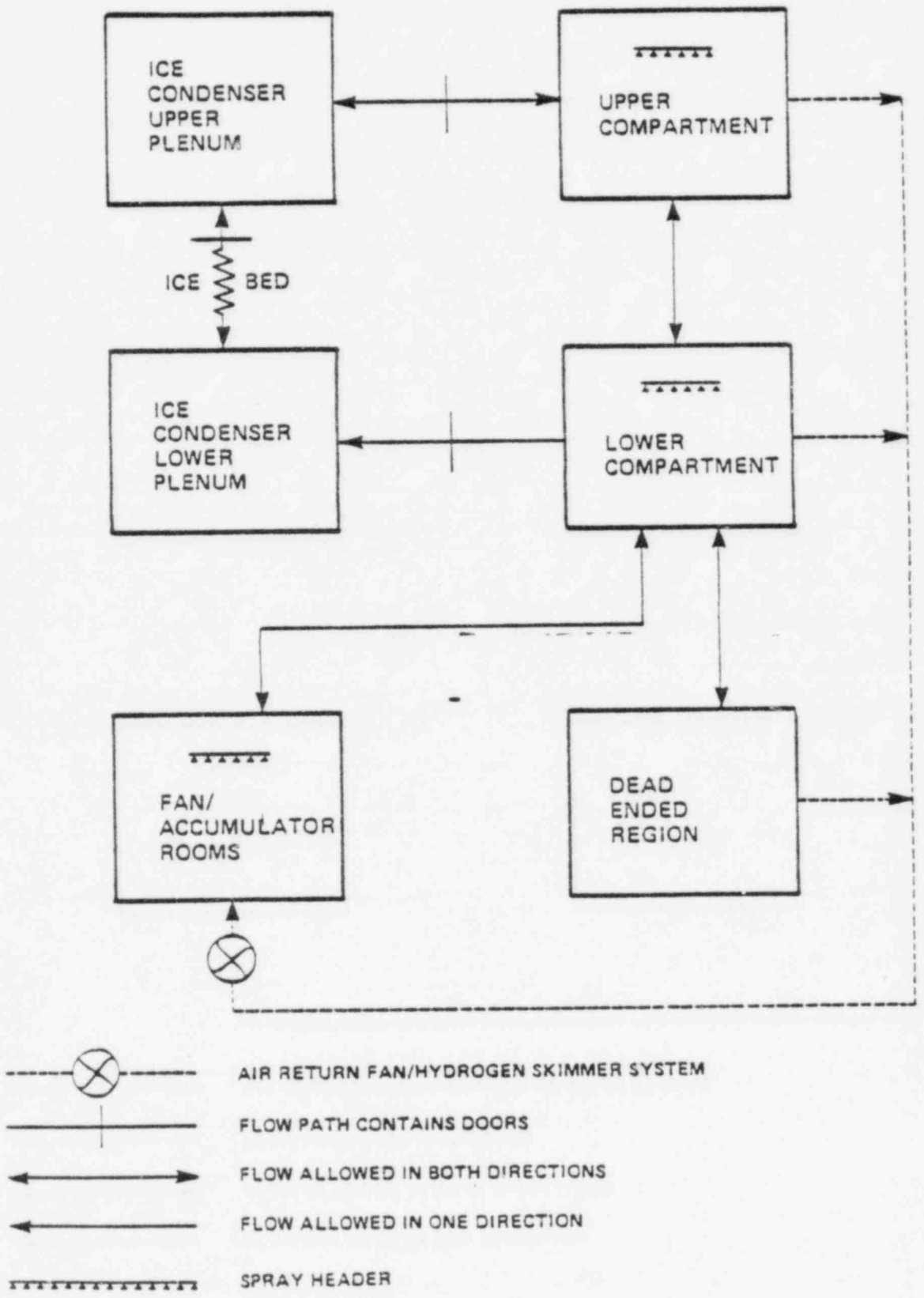

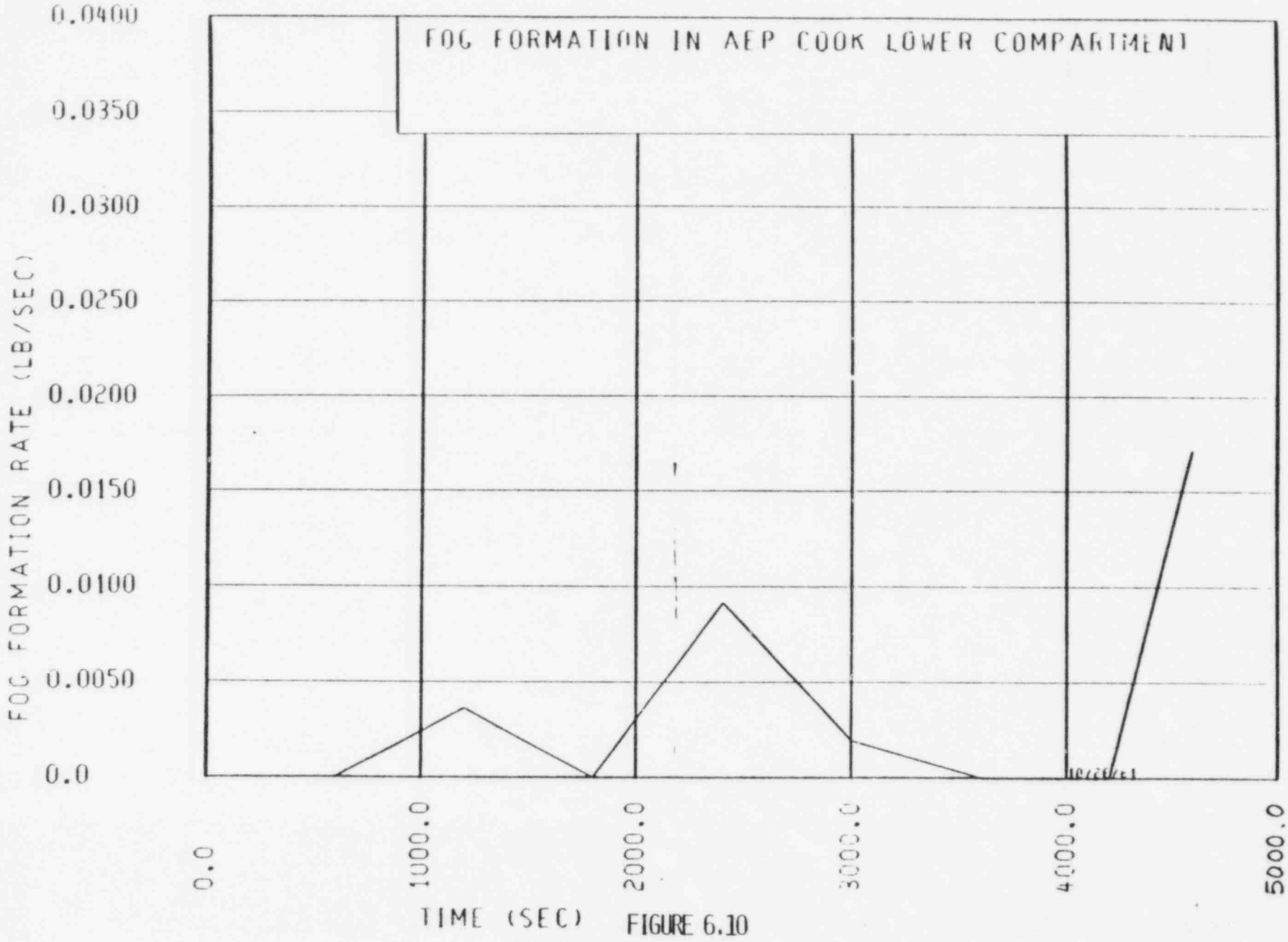
FOG FORMATION IN AEP COOK LOWER COMPARTMENT
FOG FORMATION RATE (LB/SEC)
0.0400
0.0350
0.0300
0.0250
0.0200
0.0150
0.0100
0.0050
0.0
0.0
1000.0
2000.0
3000.0
4000.0
5000.0
TIME (SEC)

FIGURE 6.10

FIGURE 6.11

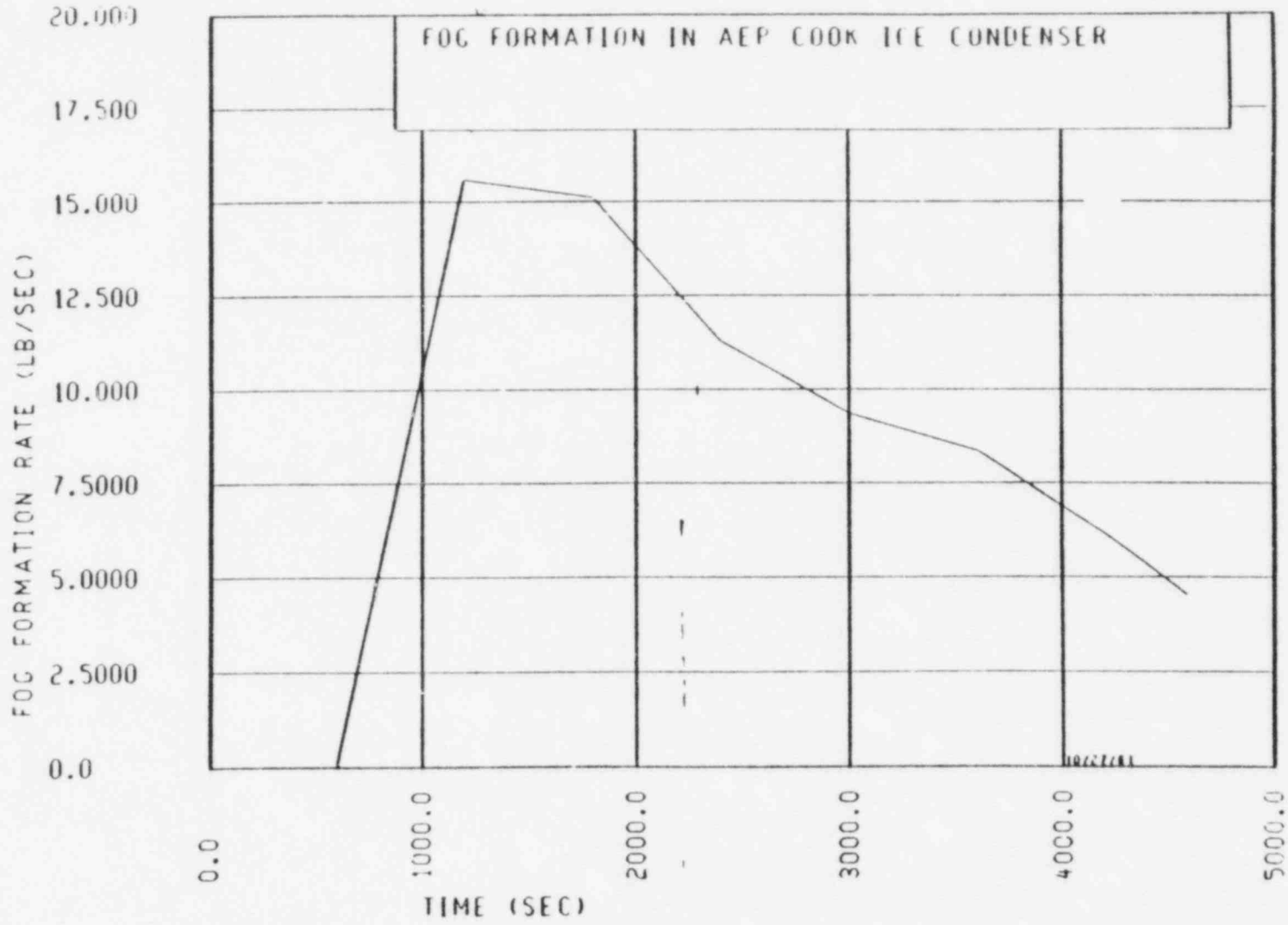
FOG FORMATION IN AEP COOK ICE CONDENSER
FOG FORMATION RATE (LB/SEC)
20.000
17.500
15.000
12.500
10.000
7.5000
5.0000
2.5000
0.0
0.0
1000.0
2000.0
3000.0
4000.0
5000.0
TIME (SEC)

quality of the break flow was calculated using the enthalpy and the lower compartment gas temperature. According to the MARCH prediction[7] the discharge of liquid by the break flow into the lower compartment lasts for only 2172 seconds. Afterward, the water level in the reactor vessel drops below the break elevation and the fluid discharged from the break is essentially steam. Therefore, in the present study, it is assumed that no fog is generated by the break flow after 2172 seconds.

For fog removal by gravitational settling, a volume mean drop size of 10 μ was assumed. The assumption of 10 μ volume mean drop size is conservative, considering the fact that for a few thousand seconds the drop agglomeration mechanism would be able to increase volume mean drop size substantially. It should also be noted that a smaller volume mean drop size means that the minimum fog inerting concentration would be reduced and thus makes the present analysis even more conservative. Furthermore, no consideration was given to the deposition of fog on the walls and vertical surfaces of the structure, or for fog removal in the fan flows when it passes through ducts and fans. All the assumptions mentioned above make the present analysis very conservative. The containment geometric data needed in computing the settling rate are given in Table 6.12.

For fog removal by sprays, spray flow rates of 4000, 1800, and 528 gpm were used for the upper compartment, lower compartment, and fan/accumulator rooms, respectively. According to the Cook CLASIX analysis[29], the sprays are initiated at 141 seconds. A volume fraction of sprays (volume of sprays divided by volume of the spray zone) of 3.3×10^{-4} was used. As previously discussed a spray removal efficiency of a 100 percent efficiency was used.

In Figure 6.9, the directions of the intercompartmental flows are shown. The intercompartmental flow rates for the six flow paths and eight time steps were obtained from the CLASIX analysis and are given in

Table 6.13. The present analysis considers the intercompartmental flows as the mechanisms of transporting fog from one compartment to another.

Figure 6.9 shows two trains of the air return fan and hydrogen skimmer system and the fan flow directions. The fans are initiated at 711 seconds. The fan head-flow curve reported in Reference 29 was used to compute the fan flow rates. Fan flow rates of 1388, 61.76, and 4.13 ft^3/sec were used for the flows from the upper compartment, lower compartment, and dead ended region to the fan/accumulator rooms, respectively. These flow rates were calculated using the Δp's between the the fan/accumulator rooms and three other compartments.

The results of the calculation are shown in Figure 6.12. It is seen that for the first few hundred seconds the fog concentrations in the lower compartment, and the ice condenser lower plenum are high. At about 140 seconds, the lower compartment volumetric fog concentration reaches its peak of 1×10^{-4} ft^3 H_2O/ft^3 mix. After the sprays are initiated at 141 seconds, the fog concentrations in the lower compartment, upper compartment, and fan/ accumulator rooms drop sharply. However, the upper plenum fog concentration keeps rising until about 1200 seconds, due to an increasing fog formation in the ice condenser and more fog entrained in the intercompartmental flow into the upper plenum. The upper plenum fog concentration reaches its peak of 2.4×10^{-4} ft^3 H_2O/ft^3 mix at about 1200 seconds. After about 1200 seconds, the lower plenum fog concentration is almost the same as the lower copartment fog concentration since the intercompartmental flows quickly make the fog concentrations in these two compartments uniform. Therefore, these two volumes behave as a single volume in terms of fog concentration.

At 2172 seconds, the break flow in the lower compartment stops generating fog and, therefore, the fog concentrations drop sharply thereafter. The effect is more pronounced for the lower compartment and lower plenum fog concentrations. The highest fog concentration exists in the ice condenser upper plenum. The effect of sprays on the upper

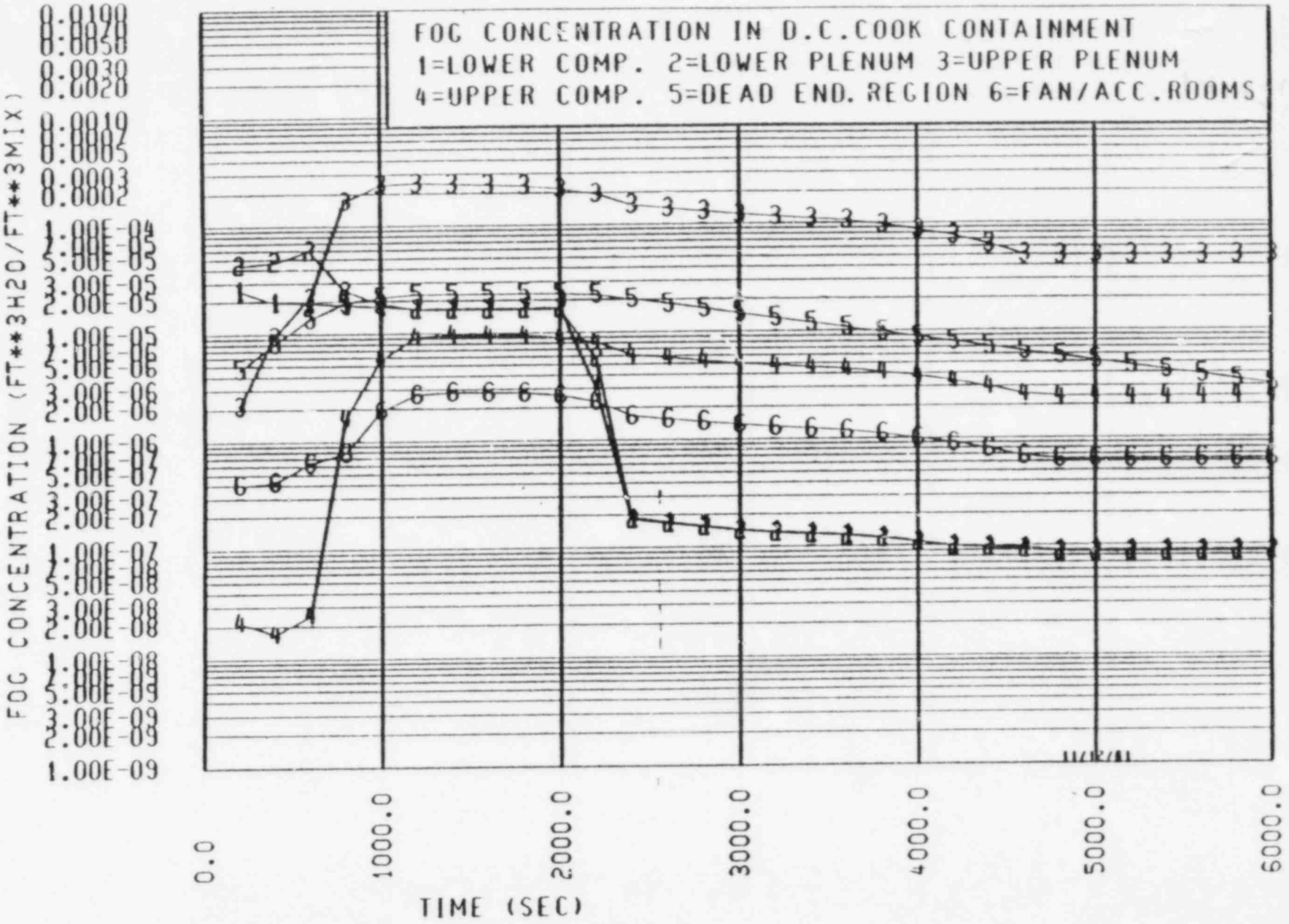
FOG CONCENTRATION IN D.C.COOK CONTAINMENT
1=LOWER COMP. 2=LOWER PLENUM 3=UPPER PLENUM
4=UPPER COMP. 5=DEAD END. REGION 6=FAN/ACC.ROOMS
FOG CONCENTRATION (FT**3H2O/FT**3MIX)
8.0190
8.0080
8.0050
8.0030
8.0020
8.0019
8.0007
8.0005
8.0003
8.0002
1.00E-04
5.00E-05
3.00E-05
2.00E-05
1.00E-05
5.00E-06
3.00E-06
2.00E-06
1.00E-06
5.00E-07
3.00E-07
2.00E-07
1.00E-07
5.00E-08
3.00E-08
2.00E-08
1.00E-08
5.00E-09
3.00E-09
2.00E-09
1.00E-09
0.0
1000.0
2000.0
3000.0
4000.0
5000.0
6000.0
TIME (SEC)

FIGURE 6.12

compartment fog concentration is clearly seen in Figure 6.12. At 141 seconds, the sprays are turned on and the upper compartment fog concentration drops sharply until about 300 seconds. At about 300 seconds, the upper compartment fog concentration starts to increase again because the intercompartmental flow into the compartment increases sharply at that time. A peak concentration of 9.5×10^{-6} ft^3 H_2O/ft^3 mix in the upper compartment is reached at about 1400 seconds.

Hydrogen starts to release into the containment at about 3804 seconds, according to the MARCH calculation[29]. It reaches 4 volume percent at about 4350, 4370, and 4700 seconds in the lower compartment, upper plenum, and upper compartment, respectively.

At 4350 seconds, the calculated lower compartment fog concentration is 10^{-7} ft^3 H_2O/ft^3 mix, which is about two orders of magnitude smaller than the minimum fog concentrations required for inerting 4 percent H_2. At 4700 seconds, the upper compartment fog concentration is 2.4×10^{-6} ft^3 H_2O/ft^3 mix, which is about a factor of two smaller than the minimum fog concentration required for inerting 4 percent H_2*. At the times of reaching 8.0 percent H_2, the fog concentrations in the lower and upper compartments are even lower than the figures given above. Therefore, it is concluded that the fog concentrations in the lower and upper compartments are too low to have any inerting effect. The use of the present theory on fog inerting also leads to the same conclusion.

However, at 4370 seconds, the calculated fog concentration in the upper plenum is 6.5×10^{-5} ft^3 H_2O/ft^3 mix which is higher than the Factory Mutual fog inerting data extrapolated to 10 μ drops and the present theoretical prediction. The data shows that in order to inert 4.76 percent H_2 the fog concentration must be 8.4×10^{-6} ft^3 H_2O/ft^3 mix or higher for 10 μ volume mean drop size. At 4530 seconds, the upper plenum hydrogen concentration

---

* The fog inerting criterion used is described in Section 5.2.

reaches about 7 percent and the fog concentration is 5.5×10^{-5} ft^3 H_2O/ft^3 mix. Again, an extrapolation of the Factory Mutual data to 10 μ shows that fog concentration of 2.1×10^{-5} ft^3 H_2O/ft^3 mix or higher is required to inert 7.2 percent H_2. In comparison the present theory of fog inerting predicts 1.02×10^{-4} ft^3 H_2O/ft^3 mix for 7.2 percent H_2. Therefore, it appears that it is possible to inert 7 percent H_2, but unlikely. However, at 8 percent H_2 in the upper plenum, which occurs at about 4600 seconds, the fog concentration is 5.1×10^{-5} ft^3 H_2O/ft^3 mix, which is too low to inert 8 percent H_2. An extrapolation of the Factory Mutual 8 percent H_2 data to 10 μ volume mean drop size and the present prediction give 1.9×10^{-4} and 1.2×10^{-4} ft^3 H_2O/ft^3 mix for the minimum required fog inerting concentration, respectively.

The glow plug igniters which have been installed in the Cook containment were designed to burn hydrogen at the lower flammability limit. As discussed previously, no fog inerting effects will be expected in the Cook lower and upper compartments. Therefore, the glow plug igniters are expected to function as designed in these two compartments. It may be possible that fog present in the ice condenser upper plenum could prevent the glow plug igniters from igniting hydrogen below 7 percent. However, it seems very unlikely that the same igniters would fail to ignite 8 percent H_2 given the fact that considerable conservatism has been exercised in the present analysis. CLASIX analyses have previously been performed that showed the Cook containment response to burning 8.0 percent H_2 mixtures would be acceptable.

TABLE 6.10 INPUT DATA FOR D. C. COOK LOWER COMPARTMENT

Time (sec)	Lower Compartment Gas Flow Rate (ft^3/sec)	Gas Temp. (°F)	Wall Temp. (°F)	Total Pressure (psia)	Steam Partial Pressure (psia)
600	799.4	222	215.2	21.8	17.4
1200	2798.2	190	183.5	20.2	9.4
1800	2805.8	190	180.3	20	9.1
2400	2513.6	180	177.2	19.6	7.6
3000	2448.5	178	170.4	19.3	7.2
3600	2359.7	175	169.3	19.2	6.4
4200	2272.3	165	161.9	18.8	5.3
4590	2482.7	168	161	19.5	5.8

TABLE 6.11 INPUT DATA FOR D. C. COOK ICE CONDENSER

Time (sec)	Ice Condenser Gas Flow Rate (ft^3/sec)	Gas Temp. (°F)	Ice Temp. (°F)	Total Pressure (psia)	Steam Partial Pressure (psia)
600	76	147	32	21.8	3.4
1200	2548	190	32	20.1	9.3
1800	2572	188	32	19.9	9.0
2400	2359	184	32	19.7	7.9
3000	2256	187	32	19.3	7.1
3600	2199	175	32	19.2	6.6
4200	2126	166	32	18.8	5.3
4590	2312	163	32	19.8	4.3

TABLE 6.12 GEOMETRIC DATA FOR D. C. COOK CONTAINMENT

	Volume (ft^3)	Floor Area (ft^2)
Lower Compartment	249,681	5,410
Ice Condenser Lower Plenum	24,700	3,100
Ice Condenser Upper Plenum	47,010	3,200
Upper Compartment	681,283	10,390
Dead Ended Region	61,105	853
Fan/Accumulator Rooms	54,828	2,500

TABLE 6.13 INTERCOMPARTMENTAL FLOW RATES (ft^3/sec)
PREDICTED BY CLASIX FOR D. C. COOK

Time (sec)	Flow From LC to LP	Flow From LP to UP	Flow From UP to UC	Flow From UC to LC	Flow From DE to LC	Flow From F/A to LC
600	6.387E2	7.600E1	-4.410E1	-3.746E1	-1.232E2	-1.229E2
1200	2.577E3	2.548E3	1.106E3	-1.740E2	-4.720E1	1.509E3
1800	2.600E3	2.572E3	1.155E3	-1.620E2	-4.381E1	1.529E3
2400	2.356E3	2.359E3	1.145E3	-1.325E2	-2.512E1	1.595E3
3000	2.273E3	2.256E3	1.178E3	-1.463E2	-2.923E1	1.553E3
3600	2.202E3	2.199E3	1.190E3	-1.334E2	-2.333E1	1.603E3
4200	2.136E3	2.126E3	1.258E3	-1.183E2	-1.802E1	1.642E3
4590	2.346E3	2.312E3	1.400E3	-1.130E2	-2.371E1	1.650E3

7.0 SUMMARY AND CONCLUSIONS

The present study has developed a systematic methodology to study the potential fog inerting problem for the PWR ice condenser plants. In the present investigation, major fog formation and removal mechanisms are identified and quantified. Theoretical models are developed to predict the fog formation rate due to boundary layer and bulk stream condensation, the fog removal rates due to gravitational settling and containment sprays. The mass conservation equations for the fog droplets in each of the containment subcompertments are solved simultaneously in order to obtain time histories of fog concentration. These equations incorporate fog formation due to condensation, fog generation due to break flow, fog removal due to gravitational settling and sprays, transport of fog by the intercompartmental flows and fan flows. These equations have been used to analyze an S_2D accident sequence for the Sequoyah, McGuire, and D.C. Cook plants. The analyses employed output data from the respective CLASIX analyses. Specifically, time histories of gas temperature, wall temperature, total pressure, and steam partial pressure in each containment subcompartment, as well as the intercompartmental and fan flow rates were used in the present analysis.

A fog inerting criterion has been developed to predict the minimum fog concentration for a particular volume mean fog drop size required to inert a given hydrogen concentration. The present fog inerting criterion has been shown to be in general agreement with the Factory Mutual data. The criterion shows that the minimum fog inerting concentration varies with the square of the volume mean fog drop size.

The present study shows that the fog concentrations in the upper and lower compartments of the three plants analyzed are too low to have any inerting effect on hydrogen mixtures. Therefore, the glow plug igniters are expected to function as designed in these two compartments. It may be possible that fog present in the ice condenser upper plenum could

prevent the glow plug igniters from igniting hydrogen below 7 percent. However, it seems very unlikely that the same igniters would fail to ignite 8-8.5 percent H_2, given the fact that considerable conservatism has been exercised in the present anlysis. CLASIX analyses have previously been performed that showed the containment responses to burning 8.0-8.5 percent H_2 mixtures would be acceptable.

ACKNOWLEDGMENTS

The author wishes to express his sincere gratitude to Mr. N.J. Liparulo, Drs. V. Srinivas, B. Lewis, and B. Karlovitz for assistance, suggestions, and helpful discussions, particularly in the area of the fog inerting criteria and the flame temperature criteria for fog, to Messrs. [illegible]eford, R. Bryan, F. G. Hudson, and K. Shiu for valuable comments, to Mr. K. C. Perry, Mr. S. J. Reiser, and Ms. R. M. Mariner for providing data on the three ice condenser plants, and to Mr. T. J. Miele for providing programming assistance.

He also would like to thank TVA, Duke Power, and AEP for providing the financial support.

REFERENCES

1. B. Lowry, "Preliminary Results: A Study of Hydrogen Igniters," ENN80-45, Lawrence Livermore National Laboratory, November 17, 1980.

2. "Additional Questions on Hydrogen Control System for Ice Condenser Plants," NRC memo from L. Rubenstein to R. Tedesco, dated June 26, 1981.

3. "The Marvikken Full Scale Containment Experiments," MXB-301 AB Atomenergi, March, 1977.

4. T. F. Kanzleiter, "LOCA Experiments With a PWR Multi-Compartment Model Containment," Trans. 1977 LWR Safety Conf., Idaho Falls, Idaho, 1977.

5. G. M. Fuls, "The CLASIX Computer Program for the Hydrogen Release and Degradation", OPS-07A35, Offshore Power Systems, 1981.

6. K. K. Almenas, "The Physical State of Post-Loss-of-Coolant Accident Containment Atmospheres," Vol. 44, Nuclear Technology, pp. 411-427, August, 1979.

7. "Summary of Analysis of Ice Condenser Containment Response to Hydrogen Transients," Offshore Power Systems report No. RP-28A52, September, 1980.

8. R. Brown and J. L. York, "Sprays Formed by Flashing Liquid Jets," Vol. 8, No. 2, AICh.E Journal, p. 149, May, 1962.

9. R. G. Gido, and A. Koestel, "LOCA-Generated Drop Size Prediction - A Thermal Framentation Model," Trans. Am. Nucl. Soc., 30, p. 371, 1978.

10. P. G. Hill, H. Witting, and E. P. Demetri, "Condensation of Metal Vapors During Rapid Expansion," Journal of Heat Transfer, p. 303, November, 1963.

11. M. Volmer and H. Flood, Z. Physik Chemie, A170, p. 273, 1934.

12. C. E. Junge, Advan. Geophys., H. Landsberg and J. Van Mieghem, ed., 4.1, Academic Press, New York, 1958.

13. K. Almenas, and J. Marchello, "On the Creaction and Persistence of Mist-Laden Post-LOCA Containment Atmospheres," Trans. Am. Nucl. Soc., 30, P. 370, 1978.

14. R. K. Hilliard and L. F. Coleman, "Natural Transport Effects on Fission Product Behavior in the Containment Systems Experiment," BNWL-7457, Battelle-Northwest, Richland, Washington, 1970.

15. N. H. Fletcher, J. Chem. Phys., 29, p. 572; 31, p. 1136, 1958.

16. D. E. Rosner and M. Epstein, "Fog Formation Conditions Near Cold Surfaces," Vol. 28, No. 1, J. of Colloid and Interface Sci., September, 1968.

17. K. Hijikata, and Y. Mori, "Forced Convective Heat Transfer of a Gas With Condensing Vapor Around a Flat Plate," Vol. 2, No. 1, Heat Transfer - Jap. Res., pp. 81-101, January, 1973.

18. M. Neiburger and C. W. Chien, "Computation of the Growth of Cloud Drops by Condensation Using an Electronic Digital Computer," Geophys. Monograph No. 5, pp. 191-209, 1960.

19. R. M. Kemper, "Iodine Removal by Spray in the Salem Station Containment," WCAP-7952, Westinghouse Electric Corp., August, 1972.

20. N. J. Liparulo, J. E. Olhoeft and D. F. Paddleford, "Glow Plug Ignitor Tests in H_2 Mixtures," WCAP-5909, Westinghouse Electric Corp., March 6, 1981.

21. R. G. Zalosh and S. N. Bajpai, "Water Fog Inerting of Hydrogen - Air Mixtures," EPRI Project Preliminary Rp. 1932-1, September, 1981.

22. J. M. Marchello, "Control of Air Pollution Source," Marcel Dekker, Inc., New York, 1976.

23. Letter from B. Lewis and B. Karlovitz to L. E. Hochreiter, dated may 5, 1980.

24. M. Berman, et al., "Analysis of Hydrogen Mitigation for Degraded Core Accidents in the Sequoyah Nuclear Power Plant," Sandia draft report, December 1, 1980.

25. T. von Karman, Unpublished notes, 1956.

26. S. S. Tsai, "Flame Temperature Criteria Tests," NS-CCA-81-039, Westinghouse internal memo, dated June 17, 1981.

27. Attachment to Offshore Power System letter PST-NE-109, dated May 22, 1981.

28. Attachment to Offshore Power System letter PST-NE-106, dated May 14, 1981.

29. Attachment to Offshore Power System letter PST-NE-218, dated August 6, 1981.

30. M. L. Corrin, J. R. Connel, and A. J. Gero, "An Assessment of Warm Fog - Nucleation, Control, and Recommended Research," NASACR-2477, November, 1974.

APPENDIX A

COMPUTATION OF Y_o AND ξ IN EQUATION (3.12)

The Hijikata-Mori fog formation theory[17] used the boundary layer approximation for the continuity, momentum, and energy equations. The fog concentration and velocity profiles in the boundary layer are assumed in Eqs. (3.7) and (3.8). Substituting Eqs. (3.7) through (3.10) into the conservation equations, we have

$$-\frac{3}{16}+\frac{3}{16}\xi+\frac{7}{120}Y_o+v'_\infty=0 \tag{A-1}$$

$$-(1+Y_o)\frac{V_o}{R}-\frac{3}{16}+\frac{3}{16}\xi+\frac{7}{120}V+\frac{1}{20}\xi V_\infty+v'_\infty=0 \tag{A-2}$$

$$\frac{9}{35}+\frac{9}{35}\xi+\frac{311}{10080}Y_o+v'_\infty=-\frac{3}{2}(1+\xi)\frac{1}{R} \tag{A-3}$$

$$A(n)+B(n)\xi+\left\{C(n)+\frac{7}{120}E\right\}Y_o=\frac{1}{R}\left\{\frac{n}{Pr}-V_o-V_o(1+E)Y_o\right\} \tag{A-4}$$

where $A(n)=\dfrac{3(n+5)}{4(n+1)(n+3)(n+4)}$

$B(n)=\dfrac{3(n+6)}{4(n+2)(n+3)(n+4)}$

$C(n)=\dfrac{3(n+7)}{4(n+3)(n+5)(n+6)}$

$V_\infty=\dfrac{\Delta W}{1-W_\infty}$

$V_o=\dfrac{2\Delta W}{(1-W_o)S_c}$

$E=\dfrac{h_{fg}}{C_{pg}\Delta T}$

$$R = \frac{a^2 U_\infty}{\nu}$$

$$v'_\infty = \frac{\delta v_\infty}{a U_\infty}$$

W_∞ = weight fraction of vapor at free stream
W_0 = weight fraction of vapor at wall
ΔW = $W_\infty - W_0$
S_c = Schmidt number
ν = kinetic viscosity
v_∞ = component of the free stream velocity perpendicular to the wall
h_{fg} = heat of vaporization
C_{pg} = specific heat of non-condensible gas
ΔT = $T_\infty - T_0$
T_∞ = gas temperature at free stream
T_0 = gas temperature at wall

Equations (A-1) through (A-4) are four algebraic equations for four unknowns, Y_0, ξ , R, and v'_∞ . These equations have been solved by the computer program FOG. In FOG, the values of Y_0, ξ, and R are computed and used in Eq. (3.12) to compute the fog formation rate.

APPENDIX B

DERIVATION OF EQUATION (5.5)

This appendix gives detailed procedures to derive Eq. (5.5), starting from Eq. (5.4)

$$(K)_{crit}\,\theta_i = f\left((Y_u - Y_f)/\theta_i\right) \tag{5.4}$$

where the ratio of heat loss rate per unit volume to the heat release rate by chemical reaction per unit volume, $(K)_{crit}$, is defined as

$$K_{crit} = S/C_p w \tag{B-1}$$

and the ratio of sensible heat to heat of combustion, θ_i, is defined as

$$\theta_i = C_p\,(T_i - T_u)/q \tag{B-2}$$

To arrive at Eq. (5.5), it is necesary to assume that all the heat loss is attributed to convection heat transfer to fog droplets of only one drop size. Under this assumption, the rate of heat loss per unit volume per degree, S, may be expressed as

$$S = n\pi d^2 h$$

where n = number of drops per unit volume
d = volume mean drop size
h = heat transfer coefficient

It is further assumed that the relative velocity between the droplets and the mixture flow is so small that heat transfer coefficient, h, can be approximated by the conduction limit. Under this assumption, Eq. (B-3) reduces to

$$S = \frac{12n\bar{\lambda}}{d^2} \tag{B-4}$$

where λ = mean heat conductivity

n = volume fraction of mist droplets ($\frac{n}{6} \pi d^3$)

The rate of heat generation per unit volume, w, is related to he laminar burning velocity, S_u, and the thickness of the reaction zone, ℓ, by

$$w = \frac{\rho_u S_u (Y_u - Y_f)}{\ell} \tag{B-5}$$

The thickness of the reaction zone may be approximated by

$$\ell = \frac{\bar{\lambda}}{\rho_u S_u \bar{C}_p} \tag{B-6}$$

Combining Eqs. (B-1), (B-4), (B-5), and (B-6), we have

$$K_{crit} = \frac{12 n \bar{\lambda}^2}{\rho_u^2 S_u^2 \bar{C}_p^2 (Y_u - Y_f) d^2} \tag{B-7}$$

Substituting Eqs. (B-2) and (B-7) into Eq. (5.4), we have

$$\frac{n}{d^2} = \frac{q \bar{C}_p \rho_u^2 S_u^2}{12 \bar{\lambda}^2 (T_i - T_u)} (Y_u - Y_f) f \left(\frac{Y_u - Y_f}{\theta_i}\right) \tag{5.5}$$

Q.E.D.